NORSAR

ROYAL NORWEGIAN COUNCIL FOR SCIENTIFIC AND INDUSTRIAL RESEARCH

Scientific Report No. 2-80/81

SEMIANNUAL TECHNICAL SUMMARY 1 October 1980—31 March 1981

By
Alf Kr. Nilsen (ed.)

Kjeller, June 1981

SECURITY CLASSIFICATION OF THIS PAGE *(When Data Entered)*

REPORT DOCUMENTATION PAGE		READ INSTRUCTIONS BEFORE COMPLETING FORM
1. REPORT NUMBER F08606-79-C-0001	2. GOVT ACCESSION NO.	3. RECIPIENT'S CATALOG NUMBER
4. TITLE *(and Subtitle)* SEMIANNUAL TECHNICAL SUMMARY 1 October 1980 - 30 March 1981		5. TYPE OF REPORT & PERIOD COVERED 1 Oct 80 - 30 Mar 1981 6. PERFORMING ORG. REPORT NUMBER Sci. Report 2/80-81
7. AUTHOR*(s)* A.K. Nilsen (ed.)		8. CONTRACT OR GRANT NUMBER*(s)*
9. PERFORMING ORGANIZATION NAME AND ADDRESS NTNF/NORSAR Post Box 51 N-2007 Kjeller, Norway		10. PROGRAM ELEMENT, PROJECT, TASK AREA & WORK UNIT NUMBERS NORSAR Phase 3
11. CONTROLLING OFFICE NAME AND ADDRESS		12. REPORT DATE May 1981 13. NUMBER OF PAGES 98
14. MONITORING AGENCY NAME & ADDRESS*(if different from Controlling Office)* VELA Seismological Center 312 Montgomery Street Alexandria, VA 22314 USA		15. SECURITY CLASS. *(of this report)* 15a. DECLASSIFICATION/DOWNGRADING SCHEDULE
16. DISTRIBUTION STATEMENT *(of this Report)* APPROVED FOR PUBLIC RELEASE; DISTRIBUTION UNLIMITED.		
17. DISTRIBUTION STATEMENT *(of the abstract entered in Block 20, if different from Report)*		
18. SUPPLEMENTARY NOTES		
19. KEY WORDS *(Continue on reverse side if necessary and identify by block number)*		
20. ABSTRACT *(Continue on reverse side if necessary and identify by block number)* The operation, maintenance and research activities of the Norwegian Seismic Array (NORSAR) for the period 1 October 1980 to 31 March 1981 are described in this report. The detection processor operation has shown improvements as compared with previous reporting period with uptime percentage of 91.2 and 0.8 days mean-		

DD FORM 1 JAN 73 1473 EDITION OF 1 NOV 65 IS OBSOLETE

SECURITY CLASSIFICATION OF THIS PAGE *(When Data Entered)*

time-between-failures as compared with 71.1% and 0.6 days. Still the special processing system (SPS) counts for most of the downtime. The MODCOMP is approaching the final implementation; presently the MODCOMP-to-IBM communication is performed on one subarray.

NORSAR has reported a total of 1873 events in the period with a daily average of 10.3 events, the number of events per month varying from 211 in December to 328 in February. The event processor program package is now implemented in the new IBM 4341 computer, giving many advantages, i.e., operator interactive analysis and large disk storage capacity.

Due to a shortage of tapes, a new long period data retention program has been accomplished for the period 10/01/76 to 12/31/80 giving 897 tapes back for recirculation.

A new NORSAR SP analog station has been installed utilizing an existing data line by use of a voltage controlled oscillator.

The ten subsections of the last chapter give brief summaries of the research activities, including analysis results from the new 12-channel NORESS (NORSAR Experimental Small-Aperture Subarray), investigation of intraplate seismicity from earthquake zones in Svalbard and microearthquake monitoring of the Nansen Ridge during the FRAM I expedition in the first three subsections. One subsection describes a new method used in NORSAR event processor for automatic determination of event characteristics. The last subsection lists the proceedings from the NATO Advanced Study Institute held in Oslo in September 1980.

AFTAC Project Authorization No.	:	VELA VT/0702/B/PMP, Amendment 1
ARPA Order No.	:	2551
Program Code No.	:	0F10
Name of Contractor	:	Royal Norwegian Council for Scientific and Industrial Research
Effective Date of Contract	:	1 October 1979
Contract Expiration Date	:	30 September 1981
Project Manager	:	Frode Ringdal (02) 71 69 15
Title of Work	:	The Norwegian Seismic Array (NORSAR) Phase 3
Amount of Contract	:	$2.119.000
Contract Period Covered by the Report	:	1 April - 30 September 1980

This research was supported by the Advanced Research Projects Agency of the Department of Defense and was monitored by AFTAC, Patrick AFB FL 32925, under contract no.

NORSAR Contribution No. 294

TABLE OF CONTENTS

I. SUMMARY

The operation, maintenance and research activities of the Norwegian Seismic Array (NORSAR) for the period 1 October 1980 to 31 March 1981 are described in this report.

The detection processor operation has shown improvements as compared with previous reporting period with uptime percentage of 91.2 and 0.8 days mean-time-between-failures as compared with 71.1% and 0.6 days. Still the special processing system (SPS) counts for most of the downtime. The MODCOMP is approaching the final implementation; presently the MODCOMP-to-IBM communication is performed on one subarray.

NORSAR has reported a total of 1873 events in the period with a daily average of 10.3 events, the number of events per month varying from 211 in December to 328 in February. The event processor program package is now implemented in the new IBM 4341 computer, giving many advantages, i.e., operator interactive analysis and large disk storage capacity.

Due to a shortage of tapes, a new long period data retention program has been accomplished for the period 10/01/76 to 12/31/80 giving 897 tapes back for recirculation.

A new NORSAR SP analog station has been installed utilizing an existing data line by use of a voltage controlled oscillator.

The ten subsections of the last chapter give brief summaries of the research activities, including analysis results from the new 12-channel NORESS (NORSAR Experimental Small-Aperture Subarray), investigation of intraplate seismicity from earthquake zones in Svalbard and microearthquake monitoring of the Nansen Ridge during the FRAM I expedition in the first three subsections. One subsection describes a new method used in NORSAR event processor for automatic determination of event characteristics. The last subsection lists the proceedings from the NATO Advanced Study Institute held in Oslo in September 1980.

A. Kr. Nilsen

II. OPERATION OF ALL SYSTEMS

II.1 Detection Processor (DP) Operation

There have been 220 breaks in the otherwise continuous operation of the NORSAR online system within the current 6-month reporting interval. The SPS had no major breakdowns in the period, but the numbers of stops, 203 out of 220, show that it is still the main problem in DP operation. The uptime percentage is 91.2 as compared to 71.1 for the previous period (April-September 1980). Of the downtime of 8.8% only 0.4% is due to other reasons than SPS failure.

Fig. II.1.1 and the accompanying Table II.1.1 both show the daily DP downtime for the days between 1 October 1980 and 31 March 1981. The monthly recording times and percentages are given in Table II.1.2.

The breaks can be grouped as follows:

a)	SPS malfunction	203
b)	Error on the multiplexor channel	0
c)	Stops related to possible program errors	0
d)	Maintenance stops	2
e)	Power jumps and breaks	2
f)	Hardware problems	9
g)	Magnetic tape and disk drive problems	1
h)	Stops related to system operation	3
i)	TOD error stops	0

The total downtime for the period was 385 hours and 17 minutes. The mean-time-between-failures (MTBF) was 0.8 days as compared with 0.6 days for the previous period.

J. Torstveit

LIST OF BREAKS IN CP PROCESSING THE LAST HALF-YEAR

DAY	START		STOP		COMMENTS.....
275	22	16	23	2	SPS ERROR
283	7	45	8	0	SPS ERROR
284	9	30	9	39	SPS ERROR
284	10	11	10	25	SPS ERROR
291	12	19	12	25	SPS ERROR
295	7	44	8	2	SPS ERROR
295	16	45	16	57	SPS ERROR
298	2	28	2	38	SPS ERROR
298	21	35	22	51	SPS ERROR
299	0	17	13	52	SPS ERROR
299	17	35	18	58	CPU ERROR
300	18	32	19	21	SPS ERROR
301	13	4	13	14	SPS ERROR
302	12	34	13	42	SPS ERROR
303	8	21	9	0	SPS ERROR
303	16	39	17	53	SPS ERROR
303	18	42	21	29	SPS ERROR
303	22	44	24	0	SPS ERROR
304	0	0	8	39	SPS ERROR
304	9	29	12	16	SPS ERROR
304	19	37	20	16	SPS ERROR
306	11	4	12	48	SPS ERROR
306	16	20	17	31	SPS ERROR
307	4	7	5	16	SPS ERROR
309	7	47	7	58	MT ERROR
311	5	26	8	37	SPS ERROR
311	21	9	22	9	SPS ERROR
312	1	55	2	43	SPS ERROR
312	7	0	7	52	SPS ERROR
312	15	14	15	27	SPS ERROR
313	7	35	8	27	SPS ERROR
313	22	3	22	43	SPS ERROR
314	4	50	5	44	SPS ERROR
314	6	18	9	0	SPS ERROR
314	20	32	21	20	SPS ERROR
314	23	55	24	0	SPS ERROR
315	5	0	6	59	SPS ERROR
316	13	7	13	18	SPS ERROR
317	2	4	7	20	SPS ERROR
318	1	48	2	26	SPS ERROR
318	10	28	10	36	SPS ERROR
318	12	59	13	7	SPS ERROR
319	8	14	8	24	SPS ERROR
319	21	36	22	18	SPS ERROR
320	1	43	5	25	SPS ERROR
320	7	59	10	29	SPS ERROR
321	6	10	9	2	SPS ERROR
321	9	53	10	4	SPS ERROR
321	20	4	20	52	SPS ERROR
322	23	18	24	0	SPS ERROR
323	0	0	0	15	SPS ERROR
323	10	43	12	47	SPS ERROR
323	16	21	17	4	SPS ERROR
325	8	28	8	37	SPS ERROR
326	2	16	3	32	SPS ERROR
326	6	55	7	5	SPS ERROR
326	14	35	14	49	SPS ERROR
326	21	58	22	6	SPS ERROR
327	0	32	7	45	SPS ERROR
329	15	37	17	5	SPS ERROR
329	21	11	22	33	SPS ERROR
330	10	34	10	52	SPS ERROR
330	19	43	19	56	CPU ERROR
331	16	32	17	42	SPS ERROR
332	7	59	8	31	SPS ERROR
336	6	14	7	24	SPS ERROR
336	19	45	20	4	SPS ERROR
339	1	1	1	54	SPS ERROR
341	15	22	17	29	SPS ERROR
341	22	19	23	37	SPS ERROR
342	3	9	7	22	SPS ERROR
342	7	27	7	44	SPS ERROR
343	12	4	12	18	SPS ERROR
343	14	35	14	49	SPS ERROR
344	3	35	5	18	SPS ERROR
344	10	51	11	3	SPS ERROR
344	11	22	12	49	SPS ERROR
344	15	12	15	39	SPS ERROR
345	6	42	7	24	SPS ERROR
345	7	36	10	32	SPS ERROR
348	12	34	12	43	PROG ERROR
349	1	31	2	12	SPS ERROR
350	15	47	17	5	SPS ERROR
351	12	37	13	2	SPS ERROR
352	7	5	7	31	CPU ERROR
352	16	47	18	0	SPS ERROR
353	14	45	14	54	SPS ERROR
353	15	0	15	28	SPS ERROR
353	21	48	22	24	SPS ERROR
354	11	23	11	38	SPS ERROR
354	17	8	17	16	SPS ERROR
354	20	27	20	35	SPS ERROR
356	0	3	12	31	SPS ERROR
356	19	46	21	55	SPS ERROR
357	1	49	8	30	SPS ERROR
358	1	13	1	37	SPS ERROR
358	11	20	11	44	SPS ERROR
358	12	46	14	0	SPS ERROR
359	3	5	4	2	SPS ERROR
359	17	13	20	16	SPS ERROR
360	9	37	11	23	SPS ERROR
360	23	34	24	2	SPS ERROR
361	0	0	2	2	SPS ERROR
361	10	1	11	32	CPU ERROR
362	13	23	17	20	SPS ERROR
363	0	59	8	47	SPS ERROR
363	13	45	14	43	SPS ERROR
363	15	1	16	32	SPS ERROR
364	22	31	23	41	SPS ERROR
366	7	38	9	22	SPS ERROR
366	12	37	12	55	SPS ERROR
366	18	44	24	0	SPS ERROR
1	0	0	0	19	SPS ERROR
1	1	13	1	53	SPS ERROR

Table II.1.1 (page 1 of 2)

LIST OF BREAKS IN DP PROCESSING THE LAST HALF-YEAR

DAY	START		STOP		COMMENTS.....
11	13	19			SPS ERROR
34	6	38			SPS ERROR
57	21	27			SPS ERROR
1	9	42			CE MAINTENANCE
49	18	30			SPS ERROR
49	14	3			SPS ERROR
43	8	8			SPS ERROR
19	10	26			SPS ERROR
3	7	4			SPS ERROR
50	5	21			SPS ERROR
29	9	40			SPS ERROR
54	21	44			SPS ERROR
36	10	10			SPS ERROR
26	14	22			SPS ERROR
35	5	38			SPS ERROR
24	14	37			SPS ERROR
52	5	32			SPS ERROR
37	16	14			SPS ERROR
27	21	14			SPS ERROR
35	24	0			SPS ERROR
0	6	16			SPS ERROR
45	6	27			SPS ERROR
45	1	28			SPS ERROR
45	19	30			SPS ERROR
22	22	29			SPS ERROR
10	24	0			SPS ERROR
0	8	1			SPS ERROR
0	9	47			SPS ERROR
30	12	38			SPS ERROR
34	9	45			SPS ERROR
49	18	40			SPS ERROR
22	7	30			SPS ERROR
23	20	47			SPS ERROR
49	5	57			SPS ERROR
46	11	34			SPS ERROR
16	24	0			SPS ERROR
0	1	28			SPS ERROR
53	16	40			SPS ERROR
34	14	31	14	41	SPS ERROR
36	5	42	7	2	SPS ERROR
36	10	50	10	58	SPS ERROR
37	4	50	7	14	SPS ERROR
37	14	34	14	43	SPS ERROR
39	2	15	3	1	SPS ERROR
39	23	40	24	0	SPS ERROR
40	0	0	0	38	SPS ERROR
41	8	2	8	8	SPS ERROR
43	3	8	5	6	SPS ERROR
44	16	16	17	10	SPS ERROR
45	8	26	9	11	SPS ERROR
48	10	40	10	50	SPS ERROR
48	16	3	16	18	SPS ERROR
48	18	53	19	28	POWER FAILURE CPU
49	7	23	7	33	POWER FAILURE CPU
49	15	35	17	23	CPU ERROR
49	17	40	20	57	SPS ERROR
50	0	23	8	40	SPS ERROR
50	9	43	10	22	SPS ERROR
50	21	32	22	20	SPS ERROR
51	8	7	8	40	SPS ERROR
52	0	46	6	35	SPS ERROR
52	11	19	12	33	SPS ERROR
52	13	18	13	24	SPS ERROR
53	17	37	18	35	SPS ERROR
54	8	0	8	23	POWER BREAK
54	9	43	9	54	MAINTENANCE
55	14	4	14	16	SPS ERROR
56	8	1	8	34	CPU ERROR
59	11	26	20	39	CPU ERROR
61	23	41	24	0	SPS ERROR
62	0	0	6	46	SPS ERROR
62	6	55	7	3	SPS ERROR
62	12	43	13	0	SPS ERROR
62	13	17	13	43	SPS ERROR
65	8	8	8	31	SPS ERROR
66	7	11	12	49	SPS ERROR
66	13	7	13	18	SPS ERROR
66	14	3	14	19	SPS ERROR
66	16	19	24	0	SPS ERROR
67	0	0	7	41	SPS ERROR
67	8	41	13	21	SPS ERROR
67	16	21	18	49	SPS ERROR
67	19	22	21	45	SPS ERROR
68	9	29	9	58	SPS ERROR
69	0	47	1	37	SPS ERROR
69	13	50	14	7	SPS ERROR
70	10	40	10	50	SPS ERROR
70	14	24	14	34	SPS ERROR
72	16	23	16	56	SPS ERROR
74	12	12	15	24	SPS ERROR
74	21	56	22	32	SPS ERROR
75	2	42	7	25	SPS ERROR
77	19	30	20	48	SPS ERROR
78	8	16	8	30	SPS ERROR
78	13	53	14	41	SPS ERROR
78	19	6	20	46	SPS ERROR
79	5	39	5	54	SPS ERROR
79	6	5	7	45	SPS ERROR
79	8	7	12	5	SPS ERROR
79	14	40	14	53	SPS ERROR
79	17	0	19	48	SPS ERROR
81	10	13	14	36	SPS ERROR
81	17	7	17	16	SPS ERROR
82	1	32	2	23	SPS ERROR
82	11	40	11	54	POWER BREAK
82	13	35	13	40	SPS ERROR
82	14	38	14	55	SPS ERROR
83	10	13	10	30	SPS ERROR
83	14	13	18	43	SPS ERROR
84	14	55	15	5	SPS ERROR
86	14	12	15	9	SPS ERROR
86	15	57	16	40	SPS ERROR
87	13	44	14	45	SPS ERROR
88	18	52	19	58	SPS ERROR
89	13	45	13	52	SPS ERROR

Table II.1.1 (page 2 of 2)

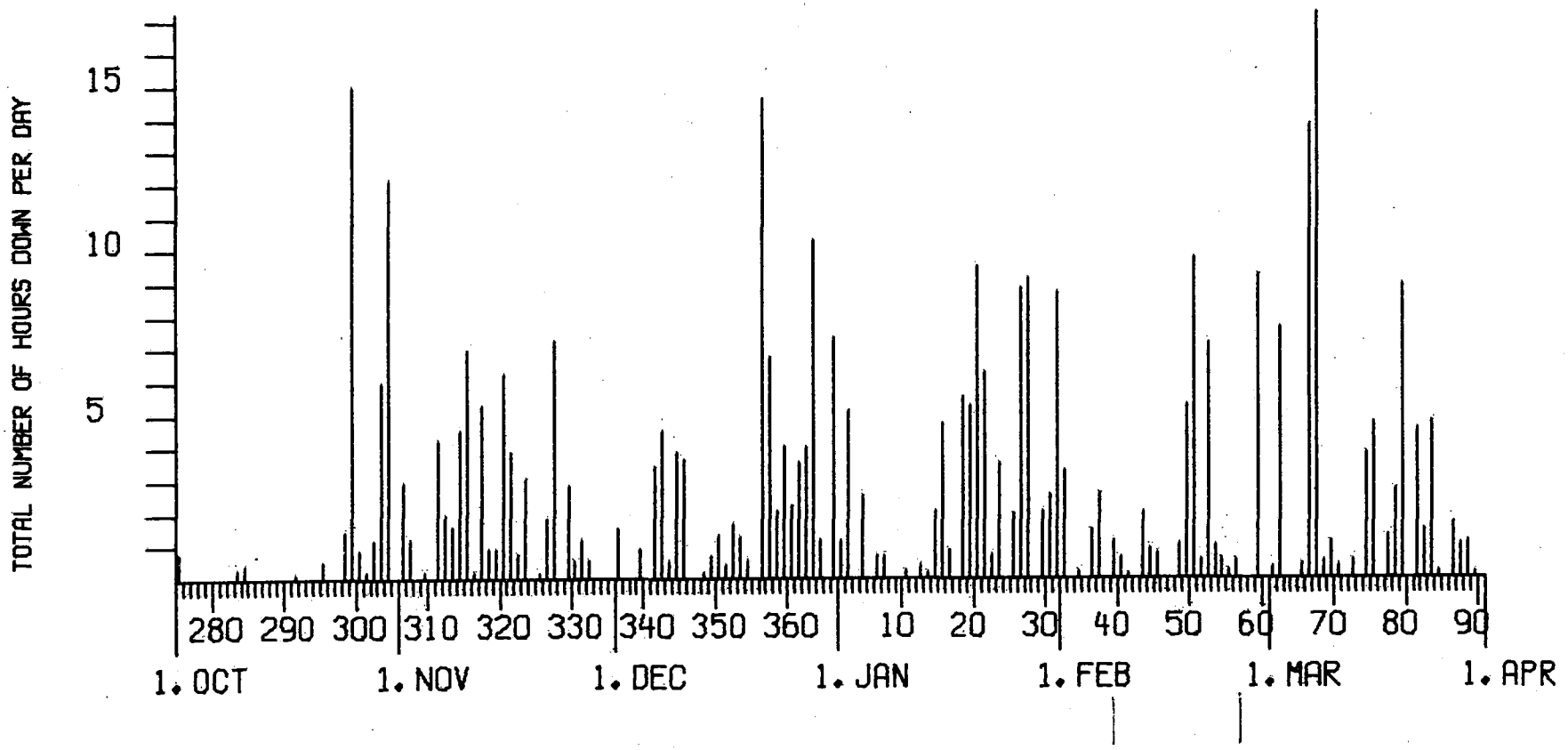

Fig. II.1.1 Detection Processor downtime in the period 1 October 1980 - 31 March 1981.

Month	DP Uptime (hrs)	DP Uptime (%)	No. of DP Breaks	No. of Days with Breaks	DP MTBF* (days)
Oct	705.48	94.8	20	12	1.4
Nov	661.47	91.9	42	23	0.6
Dec	664.08	89.3	46	24	0.6
Jan	661.77	88.9	36	23	0.7
Feb	623.93	92.8	32	20	0.8
Mar	665.98	89.5	44	22	0.6
	3982.71	91.2	220	124	0.8

*Mean-time-between-failures = Total uptime/No. of up intervals)

TABLE II.1.2

Online System Performance
1 October 1980 - 31 March 1981

II.2 Event Processor Operation

In Table II.2.1 some monthly statistics of the Event Processor operation are given:

	Teleseismic	Core Phases	Sum	Daily
Oct 80	241	60	301	9.7
Nov 80	244	52	296	9.9
Dec 80	211	42	253	8.2
Jan 81	229	44	273	8.8
Feb 81	328	54	382	13.6
Mar 81	308	60	368	11.9
	1561	312	1873	10.3

TABLE II.2.1

B. Kr. Hokland

II.3 NORSAR Data Processing Center (NDPC) Operation

Data Center

Two new computers were installed at the end of 1980. The MODCOMP was upgraded to a MODCOMP Classic and an IBM 4341 was installed. To make room for the IBM 4341 the IBM 2260 with its controller IBM 4828 was removed; in addition, the remaining equipment was rearranged. The operation was just slightly hampered by this activity; DP operation was not affected at all. Almost all jobs apart from DP online now run on the new computers, the IBM 4331 and IBM 4341.

J. Torstveit

II.4 Array Communication

Table II.4.1 reflects the performance of the communications system throughout the reporting period.

Besides conditions caused by elements directly related to the communications channels, the table aslo reflects other sources which may be interpreted as errors in the communications system itself. Such 'other sources' may be

- CTV power failure
- SLEM failures (such as incorrect A/D conversion)
- Line switching between the SPS and the Modcomp processor
- Maintenance visits.

On 21 October NTA had to break the communications a few hours in connection with cable work (01B). Also 03C had cable problems; NTA worked in the field on 21 October. 06C was frequently visited this month, mainly in connection with maintenance.

On 26 November 01A and 01B were switched to the Modcomp processor. 03C was out of operation for periods on 19 and 26 November.

On 12 and 19 December 01A and 01B were again used for test purposes (Modcomp). 04C ICU errors were reported to the NTA on 22 December.

Sub-Array	OCT (5) (29.9-2.11)		NOV (4) (3.11-30.11)		DEC (5) (1.12-4.1.81)		JAN (4) (5.1-1.2)		FEB (4) (2.2-1.3)		MAR (4) (1.-29.3)		AVERAGE ½ YEAR	
	>20	>200	>20	>200	>20	>200	>20	>200	>20	>200	>20	>200	>20	>200
01A	0.2	0.3	-	0.8	-	3.0	-	0.5	0.3	0.2	0.1	6.2	0.1	1.8
01B	-	6.3	-	15.0	-	4.8	-	4.4	5.4	14.0	1.4	18.6	1.1	10.5
02B	6.4	0.4	0.2	0.1	0.1	0.8	0.2	0.7	0.2	4.1	0.1	0.2	1.2	1.0
02C	0.3	0.5	0.3	0.5	-	0.5	0.2	0.3	0.3	3.4	0.5	0.3	0.3	0.9
03C	0.1	0.6	0.2	7.5	-	-	-	7.8	0.1	0.4	0.1	2.0	0.1	3.0
04C	1.0	0.4	1.7	0.2	0.2	11.8	-	0.2	0.1	0.3	0.2	0.2	0.5	2.2
06C	0.1	0.7	0.2	0.2	-	-	0.2	1.0	-	0.2	1.0	19.2	0.2	3.5
AVER	1.2	1.3	0.4	3.5	-	3.0	0.1	2.1	0.9	3.2	0.5	6.7	0.5	3.3
LESS	02B	01B		01B 03C		01B 04C		01B 03C	01B	01B	01B	01A,01B 06C		
	0.3	0.5		0.4		0.9		0.5	0.1	1.4	0.3	0.7		

TABLE II.4.1

Communications (degraded performance >20/outages >200)

Figures in per cent of total time. Month four or five weeks, as indicated.

In January 03C was affected by outages, probably caused by cable problems in the Rena area.

On 16 February 02B had an outage of unknown origin. NTA checked the communications path toward 04C in connection with low level (-27.0 dBm) to Kjeller. The low level was found to be due to the CTV equipment. On 16 March the separation filter (AHS-card) in the CTV modem was replaced and the line level became normal. In March 01A and 01B again were frequently switched to Modcomp. 03C was out of function due to 'cross-talk' and varying line level to Kjeller on 18 and 19 March.

Table II.4.2 indicates distribution of outages with respect to the individual subarrays. The table also indicates (by asterisks) weeks when some or all subarrays have been affected simultaneously. Although week 10 also is preceded by an asterisk, only two figures are quoted (01B, 02C). In this case the number or errors was less than 200 (and not considered as outages), but all subarrays were involved.

II.5 The ARPA Subnetwork

The SDAC communications circuit via Germany may also this period be characterized as less reliable, although good periods have been observed. However, too often the 'Marginal Circuit Indicator' showed deteriorated data. 'Loss of carrier' has also quite often been observed. The input level seems to be rather stable.

The sequence of problems can be summarized as follows:

On 2 Oct a line test between Kjeller and Germany was requested (by Germany). On 9 Oct there was 'Deriorated data' and had to have the TIP in 'Wait State'. Germany was engaged. On 24 October there was again 'Deteriorated data'. Germany requested NTA support. From 7-14 November the ciruit was out of operation. The NCC called the night between 7 and 8 November and reported serious trouble and that it was impossible to get the system back in operation. In the above-mentioned period tests and measurements went on more or less continuously on both sides, and finally (14 Nov) it was stated that there was too low level between Fort Dietrich and the SDAC.

Week/ Year	Subarray/per cent outage						
	01A	01B	02B	02C	03C	04C	06C
* 40/80	0.2	2.6	0.2	0.2	0.2	0.2	0.4
* 41	0.7	6.0	1.2	1.4	0.7	1.3	0.7
* 42	0.4	7.7	0.4	0.5	0.5	0.4	0.5
43	0.2	6.5	0.2	-	1.2	0.2	0.7
44	-	8.5	-	0.2	0.2	-	1.1
45	0.4	6.7	0.4	1.1	0.7	0.4	-
46	-	39.5	-	-	0.2	-	-
47	-	10.1	0.2	0.2	15.1	-	0.7
48	3.0	3.6	-	0.7	14.2	0.4	-
* 49	1.0	3.5	0.5	0.2	0.2	0.2	-
50	11.0	8.1	0.5	-	-	0.2	-
51	3.0	8.2	2.7	1.8	-	23.2	0.4
52	-	4.1	0.7	-	-	35.1	-
01/81	-	3.5	0.7	0.4	-	0.4	-
02	0.9	5.5	0.6	0.2	30.5	-	-
03	0.4	3.7	1.2	0.7	0.4	0.4	-
04	-	2.0	0.7	-	-	-	-
* 05	0.2	8.5	0.2	0.5	0.2	0.4	4.2
* 06	0.2	2.7	1.3	-	0.2	0.2	0.2
* 07	0.5	12.8	2.5	13.0	0.5	0.5	0.5
* 08	-	17.0	12.5	0.4	0.7	0.5	-
09	-	13.5	14.6	0.2	-	-	-
* 10	-	7.4	-	0.2	-	-	-
11	1.8	19.6	-	0.4	-	-	3.0
* 12	14.9	21.2	0.7	0.2	8.0	0.7	0.2
* 13	8.0	17.0	0.2	0.4	0.2	0.2	73.7

TABLE II.4.2

The circuit became more reliable afterwards, and apart from 'Carrier Loss' (24 Nov) we had no really bad condition until 24 February, when Germany requested line loops, etc. On 26 November 'Carrier Loss' was again observed and both Fort Dietrich and Germany were engaged. Later we observed 'Carrier Loss' 3, 12, 17 and 18 March. On 20 March we found the TIP down, and line difficulties.

Finally, 23 March the NCC wanted a TIP status. The machine was running, but line problems observed. Input level -42.0 dBm, therefore the circuit was inoperative. NORSAR requested NTA support, and later the level was -15.0 dBm and the circuit in operation for a short period before it went down again. The TIP also went down, but in a 'Wait state', ready to take load dependent on the line.

No data exchange took place the following day (24 March), but during the night between 24-25 March the system resumed operation. Later the same day (25 March) the line again went down. NCC called and requested support by NTA and Germany. When brought back in operation again the same day, the system remained up for the rest of the period.

II.6 The Terminal Interface Message Processor (TIP)

We have also this period had a few incidents with TIP outages. They started 9 October, when it was impossible to start the machine. We found memory voltage +14.3 volt (nominal +15.0 volt). We were advised by Bolt, Beranek & Newman (BBN) to adjust to +15.0 volt. Although correct after adjustment, the machine would not start. Voltage adjusted back to +14.3 volt. Ran IMPLOAD and started the machine. Left it in 'Wait state' as the SDAC line was down.

27 Jan	A BBN representative arrived from Tanum, Sweden. Replaced defective cooling fan in a power unit. TIP down for about 1.5 hours.
22 Mar	Found the TIP down, probably caused by line trouble.
23 Mar	TIP went down, but was in 'Wait state' ready to take load.

TIP Port Connections - No change since last report.

O.A. Hansen

III. IMPROVEMENTS AND MODIFICATIONS

III.1 NORSAR On-line System

Fig. III.1.1 gives a schematic overview of the current NORSAR on-line computer configuration. Presently the MODCOMP to IBM communication is performed on one subarray. Using the Virtual Machine system, one 'machine' will communicate with MODCOMP and place the data in a sharable part of memory. Another virtual machine will pick up the data and do the disk filing. Detection Processing and disk-to-tape logging will also be performed by separate virtual machines.

III.2 NORSAR Event Processor

The new IBM 4331 and 4341 with the VM/CMS has turned out to be an easy-to-use system. AUTOEP is running with temporary output on the Tektronix graphics screen. Here the operator interactively determines arrival time, amplitude and period by cross-hair cursor control. The user group has established a great number of disk files with NORSAR, SRO and Southern Norway Network data for easily performed multianalysis.

J. Fyen

III.3 Retention of Long Period Data (Low Rate Tapes)

Up to now, we have saved permanently all Low Rate Tapes since 03/01/71, giving the following number of tapes:

1.	03/01/71 - 12/31/73	505
2.	01/01/74 - 09/30/76	2284
3.	10/01/76 - 12/31/80	1989
	1971 - 1980:	4778

The first of these intervals, up to the end of 1973, consists of stacked tapes, i.e., all the tapes are filled up with data. For interval 2, the tapes are all generated on-line, and consequently contain empty intervals for each time the system has stopped or been stopped. The same applies to the last interval, which covers the time period after the array was reduced from 22 to 7 subarrays.

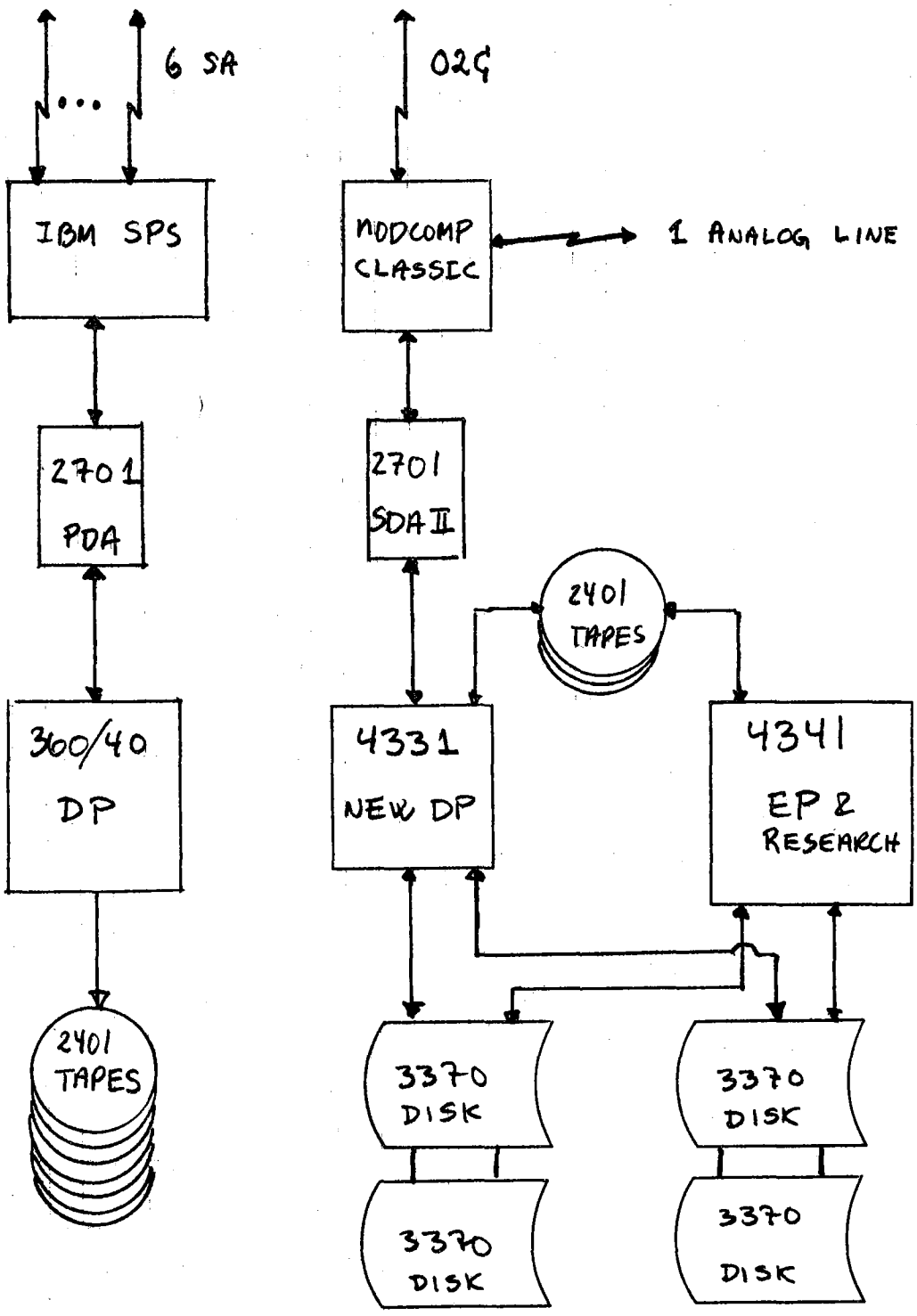

Fig. III.1.1 Schematic figure of current NORSAR on-line systems.

Because we are now running short of tapes, and because we feel that there is, after ten years of recording, a good amount of redundancy in the long period data, we have decided to recirculate the tapes with the presumably least interesting data (we do not have processing capacity to run all Low Rate Tapes through a retention procedure).

Starting with interval 3 we have used the PDE and NORSAR bulletins to generate a list of time intervals worth saving permanently. The interval lengths are

L1 = P arrival - 5 min to LR arrival + 30 min

L2 = L1 + 30 min

L3 = L2 + 60 min

and the criteria are:

Seismically active areas:

$m_b \geq 6.5$, $\Delta < 180^o$	L3
$m_b \geq 6.0$, $\Delta < 135^o$	L3
$m_b \geq 5.5$, $\Delta < 90^o$	L2
$m_b \geq 5.0$, $\Delta < 60^o$	L2
$m_b \geq 4.0$, $\Delta < 20^o$	L1
$m_b \geq 3.0$, $\Delta < 10^o$	L1

Seismically inactive areas:

Same as above, except for using 35^o instead of 20^o.

Special interest (test site) areas:

$m_b \geq 6.5$, $\Delta < 180^o$	L3
$m_b \geq 5.0$, $\Delta < 180^o$	L2
$m_b \geq 4.0$, $\Delta < 90^o$	L1
$m_b \geq 3.0$, $\Delta < 35^o$	L1

All tapes containing one of these intervals, or part of one, are saved. However, if a tape contains less than 16 hrs of data (a full tape covers 34 hrs), it is recirculated nevertheless except when containing data from presumed explosions or local events ($\Delta < 15^o$).

Using these criteria (implemented in computer programs) for interval 3 up to the end of 1979, we have flagged 897 tapes out of 1424 (or 63%) for recirculation. The data for 1980 will be processed as soon as 1981 is completed, etc. If the need for more tapes arises, we may also later consider a similar retention process for interval 2, but since that interval covers full array data, the criteria will be in case less strict. The tapes from interval 1 will be kept untouched for the foreseeable future.

H. Bungum
B.K. Hokland

III.4 Array Instrumentation and Facilities

As of 29 January 1981 a new experimental NORSAR SP Analog Station - 06C01 - was installed and operating. The unfiltered output from the short period line terminating amplifier (SP-LTA) is applied to a voltage controlled oscillator (VCO). The VCO center frequency is 340 Hz ±125 Hz deviation, and its dynamic range is 60 dB, DC to 25 Hz bandwidth. The frequency modulated (FM) signal is multiplexed with the output data word (ODW) signal in a summing function on the modem filter card. This setup allows real-time transmission of analog data from the seismometer vault to NDPC for no extra charge since the FM signal is being transmitted over already existing modem-line-modem link.

At NDPC an FM discriminator inputs the frequency modulated carrier, demodulates the carrier and outputs signal equivalent to the transmit input of the telemetry system. The discriminator has a 12,5 Hz 3-pole Butterworth lowpass output filter and after passing a 2 Hz 6-pole Chebychev highpass filter the analog signal is recorded on a Helicorder system as shown in Figure III.4.1.

P.W. Larsen

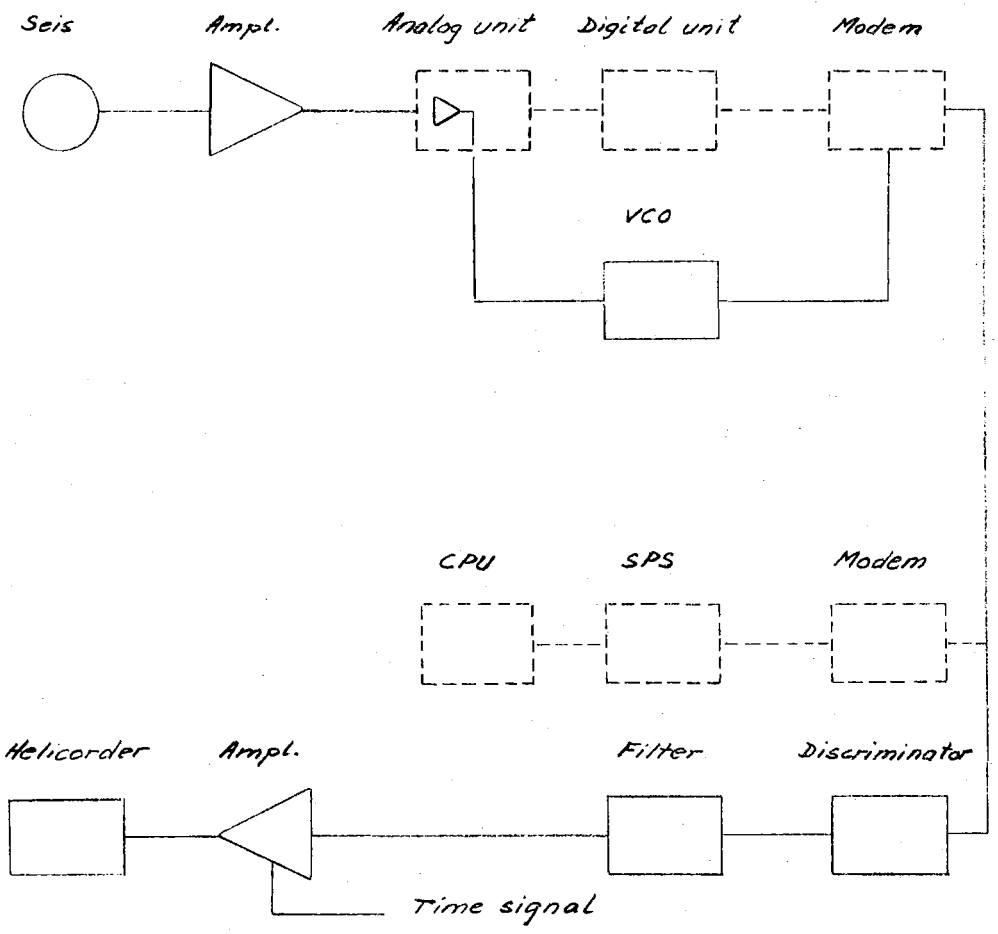

Fig. III.4.1 Signal path of analog channel 06C01 transmitted on ODW data line to NDPC, from 29 January 1981.

As of 8 January this year (refer to Table III.4.1) five SP 06 channels were modified from 4.75 Hz lowpass analog filters to 8 Hz. An additional 6 channels of NORESS were set in operation 31 October 1980 (ref. Table III.4.1).

Operation of the Southern Norway Seismic Network has continued satisfactorily throughout the period. Besides digital recording from five of the stations with 40 Hz sampling rate, one or two of the channels have been continuously recorded on analog recorders. Interesting events are selected from the analog records for plotting of all channels on graphics screen including hard copy of the events and power spectra. The geographical coordinates are as follows:

Sørum	11°15'25"E	60°03'47"N
Sarpsborg	11°20'25"E	59°21'10"N
Drangedal	09°05'50"E	59°06'15"N
Evje	07°57'38"E	58°35'00"N
Seljord	08°36'50"E	59°33'20"N
Norefjell	09°33'40"E	60°22'45"N

The frequency response is given in Table III.4.2 and III.4.3, response curve in Figure III.4.2.

Alf K. Nilsen

Subarray Normally	Instr. within SA	No. Ch. No. on NORSAR Data Tape	Time of Change 80/10/28	80/10/31	80/12/04	81/01/08
01A	1	1				-
(1)	2	2				-
	3	3				-
	4	4				-
	5	5				-
	6	6				8 Hz filter
01B	1	7	'New' NORESS(1)	'Old' NORESS(1)		
(2)	2	8	'Old' (2)	'New' (2)		
	3	9	'New' (3)	'Old' (3)		
	4	10	" (4)	" (4)		
	5	11	" (5)	" (5)		
	6	12	" (6)	" (6)		
02B	1	13				-
(3)	2	14				-
	3	15				-
	4	16				-
	5	17				-
	6	18				8 Hz filter (01/05)
02C	1	19			-	
(4)	2	20			-	
	3	21			-	
	4	22			-	
	5	23			-	
	6	24			8 Hz filter	

TABLE III.4.1

Status of NORSAR SP instruments recorded on data tape.
(Page 1)

Subarray Normally	Instr. No. within SA	Ch. No. on NORSAR Data Tape	Time of Change			
			80/10/28	80/10/31	80/11/12	81/01/07
03C	1	25				-
(5)	2	26				-
	3	27				-
	4	28				-
	5	29				-
	6	30				8 Hz filter
04C	1	31			-	
(6)	2	32			-	
	3	33			-	
	4	34			-	
	5	35			-	
	6	36			8 Hz filter	
06C	1	37	'Old' NORESS (1)	'New' NORESS (1)		
(7)	2	38	'New' (2)	'Old' NORESS (2)		
	3	39	'Old' (3)	'New' NORESS (3)		
	4	40	" (4)	" (4)		
	5	41	" (5)	" (5)		
	6	42	" (6)	" (6)		

TABLE III.4.1
(Page 2)

SOUTHERN NORWAY SEISMIC NETWORK

DIGITAL MAGNIFICATION (NM/QU AT 1 HZ) = 0.1890

PERIOD	FREQUENCY	ABS-RESP	REL-RESP
0.1	10.000	0.0095	0.0503
0.2	5.000	0.0210	0.1111
0.3	3.333	0.0341	0.1803
0.4	2.500	0.0480	0.2540
0.5	2.000	0.0620	0.3280
0.6	1.667	0.0799	0.4225
0.7	1.429	0.1002	0.5303
0.8	1.250	0.1241	0.6565
0.9	1.111	0.1559	0.8248
1.0	1.000	0.1890	1.0000
1.1	0.909	0.2315	1.2248
1.2	0.833	0.2807	1.4850
1.3	0.769	0.3384	1.7906
1.4	0.714	0.4063	2.1495
1.5	0.667	0.4801	2.5400
1.6	0.625	0.5676	3.0033
1.7	0.588	0.6710	3.5505
1.8	0.556	0.7759	4.1053
1.9	0.526	0.9079	4.8037
2.0	0.500	1.0720	5.6719
2.2	0.455	1.3744	7.2720
2.4	0.417	1.7978	9.5120
2.6	0.385	2.1778	11.5226
2.8	0.357	2.4857	13.1521
3.0	0.333	3.0211	15.9848
3.2	0.313	3.8304	20.2665
3.4	0.294	4.9001	25.9262
3.6	0.278	6.1536	32.5588
3.8	0.263	7.4794	39.5733
4.0	0.250	8.8064	46.5948
4.2	0.238	10.0937	53.4059
4.4	0.227	11.3184	59.8857
4.6	0.217	12.4691	65.9740
4.8	0.208	13.5413	71.6473
5.0	0.200	14.5350	76.9046

Table III.4.2

SOUTHERN NORWAY SEISMIC NETWORK

DIGITAL MAGNIFICATION (NM/QU AT 1 HZ) = 0.1890

INDEX	FREQUENCY	PERIOD	REL-RESP	LOG-RESP
1	0.251	3.98	45.9369	1.6622
2	0.316	3.16	19.3488	1.2867
3	0.398	2.51	10.9806	1.0406
4	0.501	2.00	5.6269	0.7503
5	0.631	1.58	2.9252	0.4662
6	0.794	1.26	1.6661	0.2217
7	1.000	1.00	1.0000	0.0
8	1.259	0.79	0.6483	-0.1882
9	1.585	0.63	0.4564	-0.3407
10	1.995	0.50	0.3290	-0.4828
11	2.512	0.40	0.2525	-0.5977
12	3.162	0.32	0.1930	-0.7145
13	3.981	0.25	0.1437	-0.8426
14	5.012	0.20	0.1108	-0.9555
15	6.310	0.16	0.0844	-1.0739
16	7.943	0.13	0.0640	-1.1939
17	10.000	0.10	0.0503	-1.2987
18	12.589	0.08	0.0521	-1.2835
19	15.849	0.06	0.0674	-1.1712
20	19.953	0.05	0.0845	-1.0730

Table III.4.3

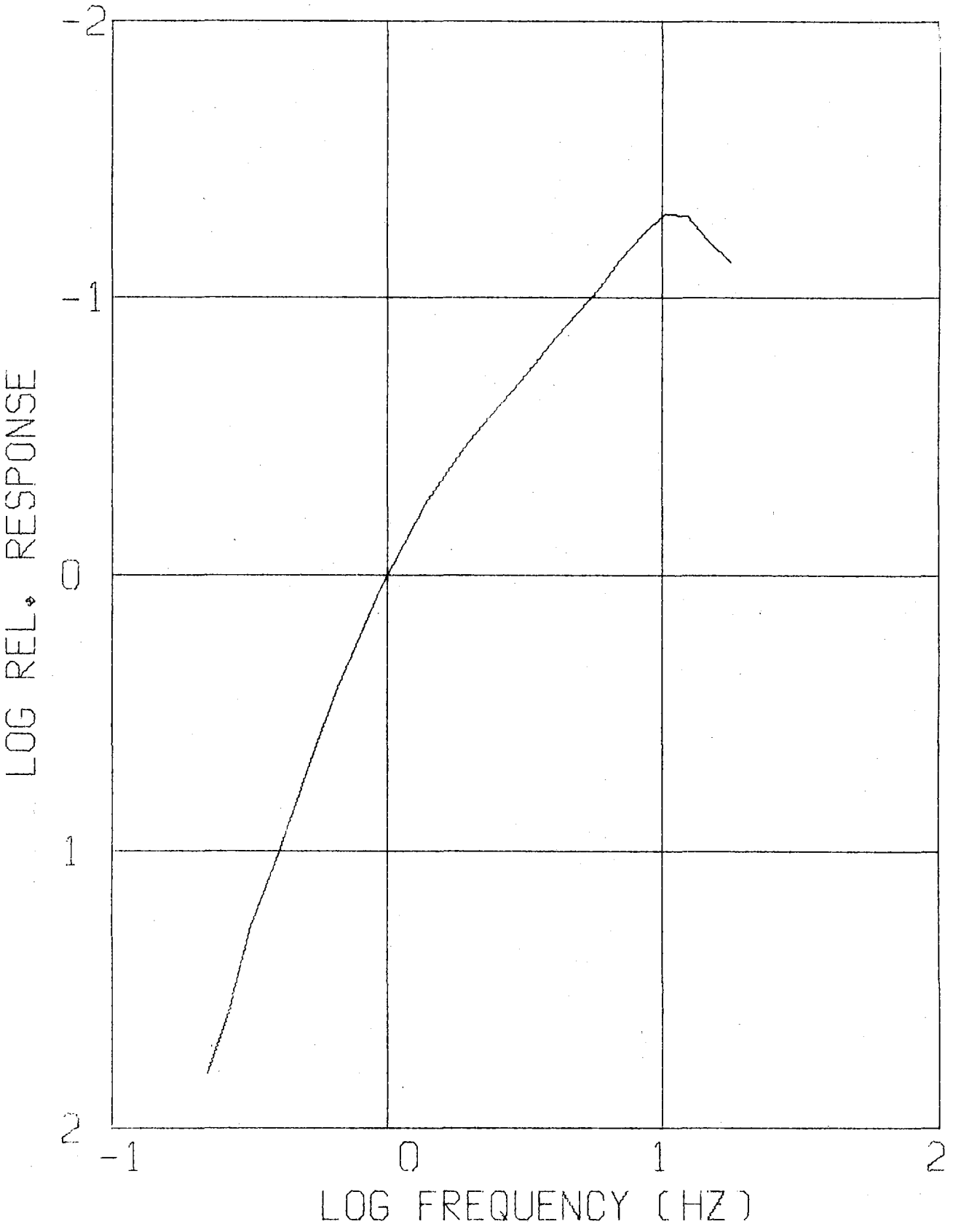

Fig. III.4.2 Southern Norway Seismic Network relative response.

III.5 Future NORSAR Data Processing Center

The dual 4300 system has had one major breakdown each since they were installed. Both errors were in the processor boards (the unit holding the cards). IBM repaired the errors in 12-20 hours. Three minor 'card errors' were fixed in an hour. A more serious problem occurred when one of the disks crashed. 570 Mbyte was lost. Our backup procedures guarantee tape backup not older than 7 days. The replacement of a disk module is a 15-minute job. These cases excepted, the system has been very reliable. Both computers may be upgraded to group 2 with higher speeds, and moreover 4331 may be exchanged with 4341. We feel that the 4300 computers cover NORSAR's present needs for computing capacity, but most important, should NORSAR need to increase the capacity, we may triple the system's CPU capacities without any software changes. Disk capacity may be increased from 2000 Mbyte to 40 000 Mbyte.

The most obvious need for upgrade today is the tape systems. With 6250 bpi density, one tape would cover approximately 14 hours of NORSAR data, such that all data may be saved permanently.

J. Fyen

IV. FIELD MAINTENANCE ACTIVITY

The field instrumentation has operated satisfactorily also in this period and the field maintenance activity has been low. Two stations (02C01 and 02) not easily accessible during the summer season were visited by snowvehicle for replacement of seismometer amplifiers. Otherwise the main workload has been on NORESS (NORSAR Experimental Small-Aperture Subarray). One field technician visited Stiegler's Gorge Seismic Network in Tanzania for maintenance in December.

Maintenance Visits

Table IV.1 gives the number of visits to the NORSAR subarrays. The average number of visits to each subarray is 5.9; excluding NORESS/06C the number is 2.5.

Subarrays	01A	01B	02B	02C	03C	04C	06C/NORESS	Total
No. of Visits	3	5	2	2	2	1	26	41

TABLE IV.1

Number of visits to the NORSAR subarrays including NORESS in the period 1 October 1980-31 March 1981

Preventive Maintenance Projects

The preventive maintenance activity of the NORSAR array instrumentation is listed in Table IV.2. The adjustments are corrections of characteristics before they drift outside the tolerance limits.

Unit	Action	No. of Actions
Seismometer	MP adjust (in field)	21
Line Termination Amplifier	Adjustment of channel gain (SP)	4
	-"- DC Offset (SP)	1
	-"- CMR (SP)	4
Emergency Power	Battery and charger check	8

TABLE IV.2

Preventive maintenance work in the period
1 October 1980 - 31 March 1981

Corrective Maintenance

The corrective maintenance is listed in Table IV.3. These are required adjustments and replacements.

Unit	Characteristics	SP		LP	
		Repl.	Adj.	Repl.	Adj.
Seismometer	Damping		3		1
	MP/FP (at NDPC)				50
	MP (in field)				4
	RCD			2	
Seismometer Ampl. RA/5, Ithaco	Distortion	1			
	Gain	1			
Line Termination Amplifier	Time constant	1			
	Channel gain		6		4
	DCO		9	1	
	CMR		2		
	Ripple	1			
SLEM RSA/ADC	Missing numbers		1		
	Spikes on data	1			

TABLE IV.3

Total number of required adjustments and replacements of NORSAR field equipment in the period 1 October 1980 - 31 March 1981

Power Breaks, Cable Breakages, Communications Faults

There has been one power break requiring action of our field technicians, namely, at 06C 24-26 March. Two cables have been repaired, 01B03 cable and 'New' NORESS channel 04. The cable to 01B03 required 5 days' work.

Only one communication fault was repaired by our staff; at 04C 16 March.

Array Status

The status of the array instrumentation is comparable with previous periods. As of 31 March 1981 two channels were out-of-tolerance (01A03, 02C01). Channels with nonstandard conditions are:

01A	02,03	NS and EW horizontal SP (since April 1978)
01A	04	Attenuated 30 dB channel 01A06 data
01B	01-06	'Old' NORESS
	LP	Disconnected
06C	01-06	'New' NORESS (02 as before).

A.K. Nilsen

ABBREVIATIONS

ADC	-	Analog-to-digital converter
CMR	-	Common mode rejection
CPU	-	Central Processor Unit
DC	-	Direct current
FP	-	Free period
LP	-	Long period
LTA	-	Line Terminating Amplifier
MP	-	Mass position
NDPC	-	NORSAR Data Processing Center
NORESS	-	NORSAR Experimental Small-Aperture Subarray
ODW	-	Output data word
RCD	-	Remote centering device
RSA	-	Range switching amplifier
SLEM	-	Seismic short and long period electronics module
SP	-	Short period
SPS	-	Special Processing System
VCO	-	Voltage controlled oscillator

V. DOCUMENTATION DEVELOPED

Bungum, H., Y. Kristoffersen & E.S. Husebye (1981): The seismicity of the Bouvet Island region, Norsk Polarinst. Skrifter, in press.

Bungum, H., B.J. Mitchell & Y. Kristoffersen (1981): Concentrated earthquake zones in Svalbard, Tectonophysics, in press.

Bungum, H., S. Vaage & E.S. Husebye (1981): The Meløy earthquake sequence, N. Norway; Source parameters and their scaling relations. Bull. Seism. Soc. Am., in press

Christoffersson, A. & F. Ringdal (1981): Optimum approaches to magnitude measurements, in: 'Identification of Seismic Sources - Earthquake or Underground Explosion' E.S. Husebye & S. Mykkeltveit (eds.), D. Reidel Publ. Co., Dordrecht, The Netherlands, in press.

Doornbos, D.J. (1981): Seismic Moment Tensors, in 'Identification of Seismic Sources - Earthquake or Underground Explosion' E.S. Husebye & S. Mykkeltveit (eds.), D. Reidel Publ. Co., Dordrecht, The Netherlands, in press.

Hovland, J. & E.S. Husebye (1981): Three-dimensional seismic velocity image of the upper mantle beneath southeastern Europe, in: 'Identification of Seismic Sources - Earthquake or Underground Explosion' E.S. Husebye & S. Mykkeltveit (eds.), D. Reidel Publ. Co., Dordrecht, The Netherlands, in press.

Husebye, E.S. & S. Mykkeltveit (1981): Identification of Seismic Sources - Earthquake or Underground Explosion, Proceedings of the NATO ASI held in Oslo, September 1980, D. Reidel Publ. Co., Dordrecht, The Netherlands, in press.

Kristoffersen, Y., E.S. Husebye, H. Bungum & S. Gregersen (1981): Seismic investigations of the Nansen Ridge during the FRAM 1 experiment, Tectonophysics in press.

Krisftoffersen, Y. & H. Bungum (1981): A microearthquake survey of Bouvet Island, South Atlantic, Tectonophysics, in press.

Mykkeltveit, S. & E.S. Husebye (1981): Lg wave propagation in Eurasia, in: 'Identification of Seismic Sources - Earthquake or Underground Explosion' E.S. Husebye & S. Mykkeltveit (eds.), D. Reidel Publ. Co., Dordrecht, The Netherlands, in press.

Mykkeltveit, S. & F. Ringdal (1981): Phase identification and event location at regional distance using small-aperture array data, in: 'Identification of Seismic Sources - Earthquake or Underground Explosion' E.S. Husebye & S. Mykkeltveit (eds.), D. Reidel Publ. Co., Dordrecht, The Netherlands,

Nilsen, A.K. (ed.) (1980): Semiannual Technical Summary, 1 Apr - 30 Sep 1980, Scientific Report No. 1-80/81, NTNF/NORSAR, Kjeller, Norway.

Ringdal, F. (1981): Automatic processing methods in the analysis of data from a global seismic network, in: 'Identification of Seismic Sources - Earthquake or Underground Explosion' E.S. Husebye & S. Mykkeltveit (eds.), D. Reidel Publ. Co., Dordrecht, The Netherlands, in press.

L.B. Tronrud

VI. SUMMARY OF TECHNICAL REPORTS/PAPERS PREPARED

VI.1 NORESS Data Analysis

Extensive analysis of noise and signal recordings from the new 12-sensor NORESS miniarray of Fig. VI.1.1 is continuing. The research on this subject comprises the following items:

i) Coherence, correlation and dynamic structure of noise as a function of frequency and sensor separation
ii) Signal correlation as a function of frequency and sensor separation
iii) Redundancy sampling in order to avoid excessive beamsteering losses
iv) Automated signal parameter extraction
v) Event location.

As regards point iv), some simplified algorithms for reading onset time and amplitude of first-arriving phases have been developed and implemented in the routine analysis of conventional NORSAR data and have so far worked very satisfactorily (see Chapter VI.4). The location capability of the NORESS array is deemed good as local events in general are within 30 km of agency announced epicenter locations, see Mykkeltveit and Ringdal (1981).

Results on noise coherence are shown in Fig. VI.1.2. It can be seen that noise coherence at frequencies around 2 Hz reaches the random level for a distance of about 0.6 km, while the same level is reached at 0.3 km for 4 Hz.

The dynamic structure of the noise is of importance for the design of miniarrays, and in this regard high resolution wave number spectral analyses have been undertaken on NORESS noise records. Some of the results obtained here are displayed in Fig. VI.1.3, and the following comments apply: At lower frequencies in the range 0.25 to 0.40 Hz the noise has a clearly propagational character with observed velocities typical of fundamental and higher mode Rayleigh wave phase velocities. In the frequency range 0.50 to 1.00 Hz the noise appears to be more unorganized with broad peaks which also show frequency instability, and there are sometimes large differences between conventional and high resolution wave number spectra. However, for higher frequencies, in the range 1.5-4.0 Hz, the wave number spectra become rather peaked and at velocities indicating P waves travelling in the mantle. These results are

somewhat unexpected on two accounts, namely: i) the noise correlation falls off rapidly with sensor separation (see Fig. VI.1.2) and ii) for teleseismic events mantle attenuation would efficiently remove the higher frequencies. As regards the first problem an explanation could be tied to the fact that noise coherency estimation is based on the so-called block averaging approach which means that a multitude of coherent wavelets but with widely different phase shifts would not give significant coherency, but on the other hand could appear 'coherent' in the frequency wave number analysis. In case of the second problem, it seems difficult not to accept that mantle attenuation removes the higher frequencies of teleseismic P wave efficiently. Then unless the results are some artefact of the processing method itself, some sort of instrumental noise prior to the digitation in the field could be an explanation. However, as instrumental noise, based on previous experience, is significantly lower than the seismic noise even at 4.0 Hz, we have not a satisfactory explanation at present of the observation presented in Fig. VI.1.3.

In the following we present results bearing on noise and signal correlation across the NORESS sensors. Fig. VI.1.4 shows the recording at the 12 NORESS channels of a local event about 140 km away (6 Nov 1980, 14.53.02.2 G.M.T., 59.54°N 10.68°E, local magnitude M_L=2.1), and the time segments marked for noise, P and Lg phases were subjected to correlation analysis. The data were resampled at 100 Hz to achieve more precise shifts in the beamforming. Also, the correlation studies were performed on filtered data, using 5 different filters defined as follows:

Filter 1:	0.8-2.8 Hz	Butterworth bandpass (3rd order)
Filter 2:	1.2-3.2 Hz	-"-
Filter 3:	1.6-4.0 Hz	-"-
Filter 4:	2.0-4.8 Hz	-"-
Filter 5:	2.4-4.8 Hz	-"-

Noise suppression results are given in Fig. VI.1.5. This figure is derived as follows: For each filter, the noise suppression is first computed for a beam that includes all 12 channels. Then one channel is removed from the beam so as to have optimum noise suppression for the beam constructed from the

remaining 11 channels. This process is continued by removing one channel at a time. Generally at each stage in this process this results in removing the one channel that has the minimal average distance to the others. We see that the number of sensors required for optimum noise suppression increases with increasing frequency, but also that the noise suppression generally deteriorates from putting more sensors into the central part of the array. The results in Fig. VI.1.5 represent averages over the three consecutive noise time windows in Fig. VI.1.4, and all correlations were computed with zero lags.

Average noise correlation as a function of sensor separation up to 1500 m is given in Fig. VI.1.6 for the five frequency bands. Averaging is performed over all inter-sensor distances that fall within segments of 100 m each. In addition, averaging is done over the three noise time windows of Fig. VI.1.4.

Signal correlations are given in Figs. VI.1.7 and VI.1.8 for the phases denoted P and Lg in Fig. VI.1.4. For each phase, two consecutive time windows were analyzed, the first one containing the main arrival. For each phase, time shifts were introduced corresponding to the phase velocity and azimuth value that gave the best signal gain. The same set of time shifts was retained for the coda window correlation analysis. Relatively high correlation values are found throughout the range of NORESS sensor separations for the phase onsets. Noteworthy is the higher degree of organization in the Lg coda relative to the P coda.

The NORESS data analysis now proceeds with a study of SNR gains as a function of array layout, utilizing the above results on noise and signal correlations.

S. Mykkeltveit
E.S. Husebye
H. Bungum
K. Åstebøl, Univ. of Oslo

Reference

Mykkeltveit, S. and F. Ringdal (1981): Phase identification and event location at regional distance using small-aperture array data, in: 'Identification of Seismic Sources - Earthquake or Underground Explosion', E.S. Husebye and S. Mykkeltveit (eds.), D. Reidel Publ. Co., in press.

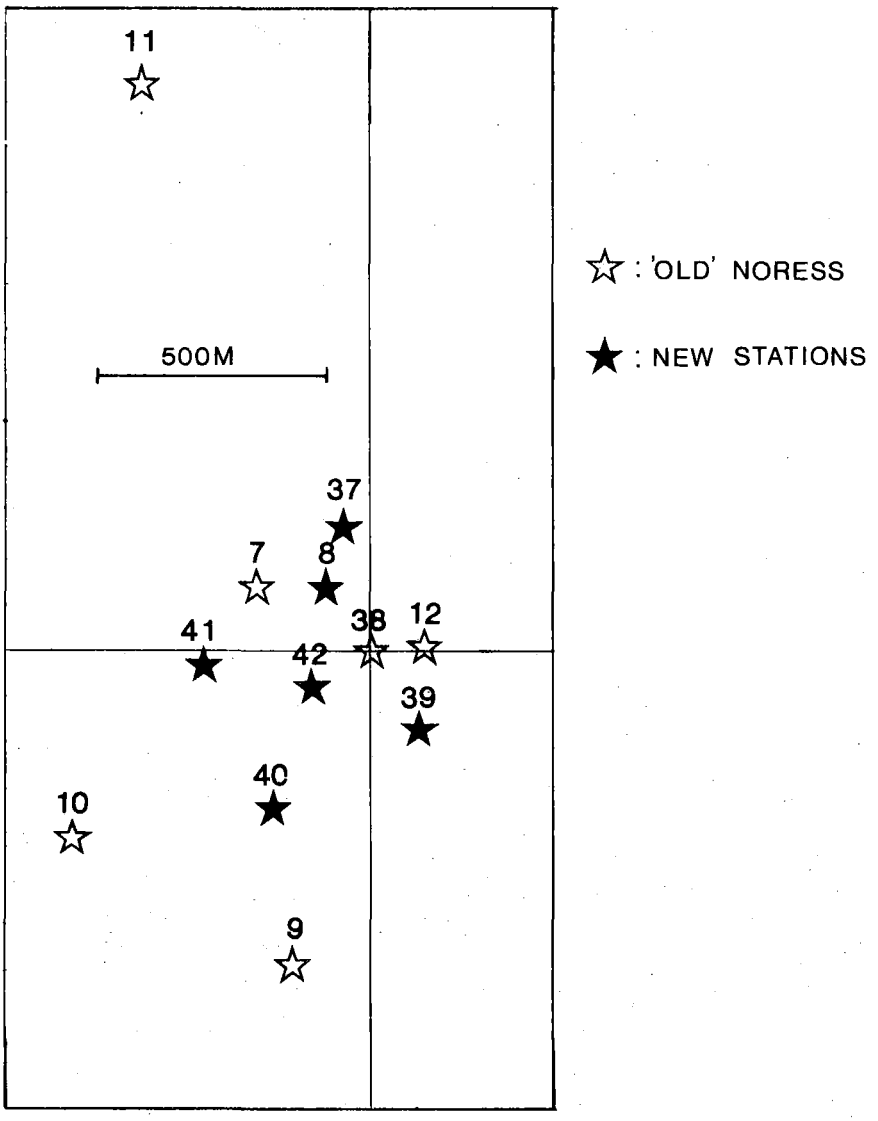

Fig. VI.1.1 Geometry of the new 12-channel NORESS array, which became operational on 28 October 1980.

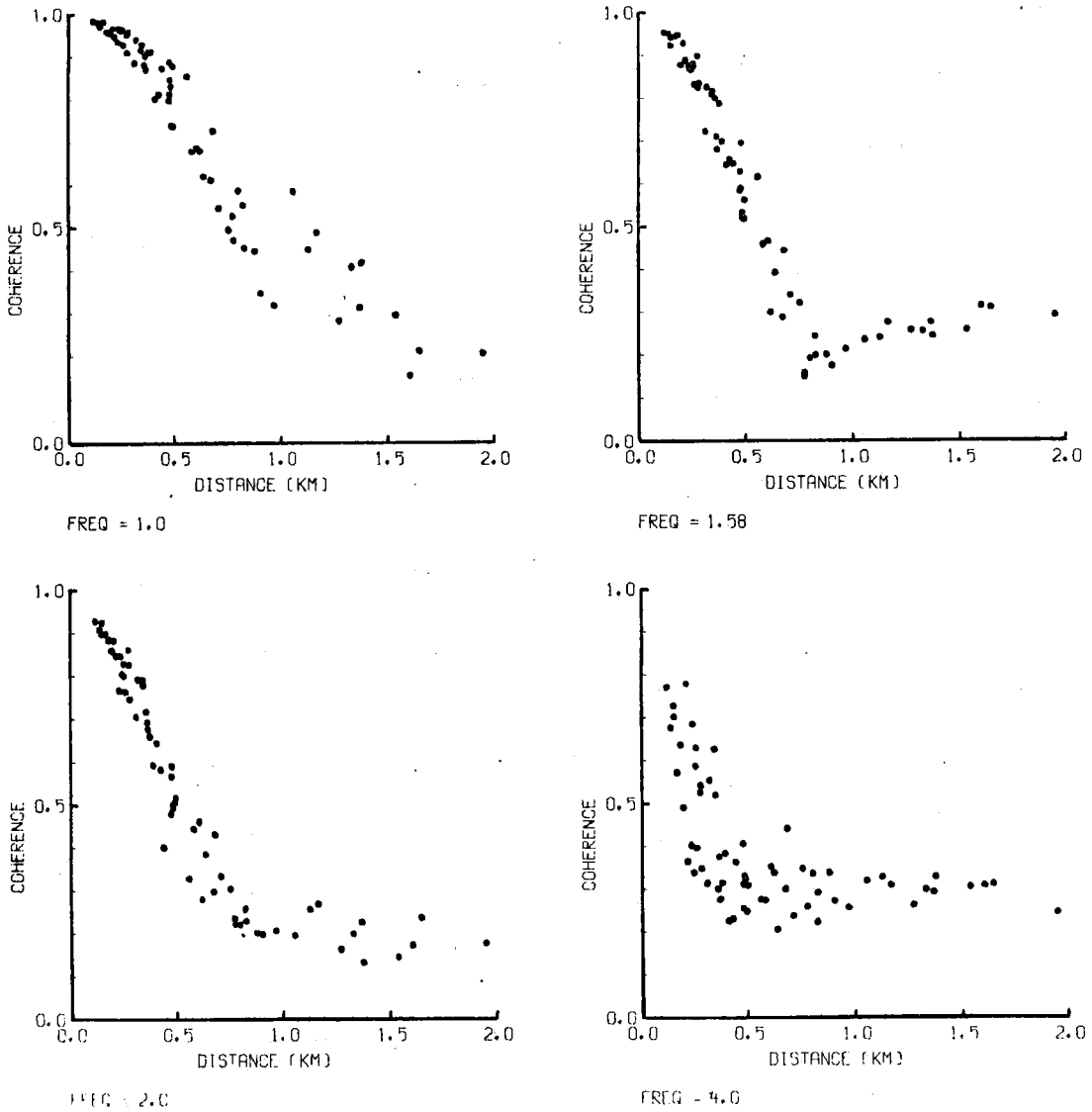

Fig. VI.1.2 NORESS noise coherence vs distance for a noise interval from day 310/80, for frequencies of 1.0, 1.5, 2.0 and 4.0 Hz. All combinations of the 12-channel array are used, and the estimates are based on averaging of 18 blocks each of 256 samples, with an additional smoothing around each of the analyzed frequencies.

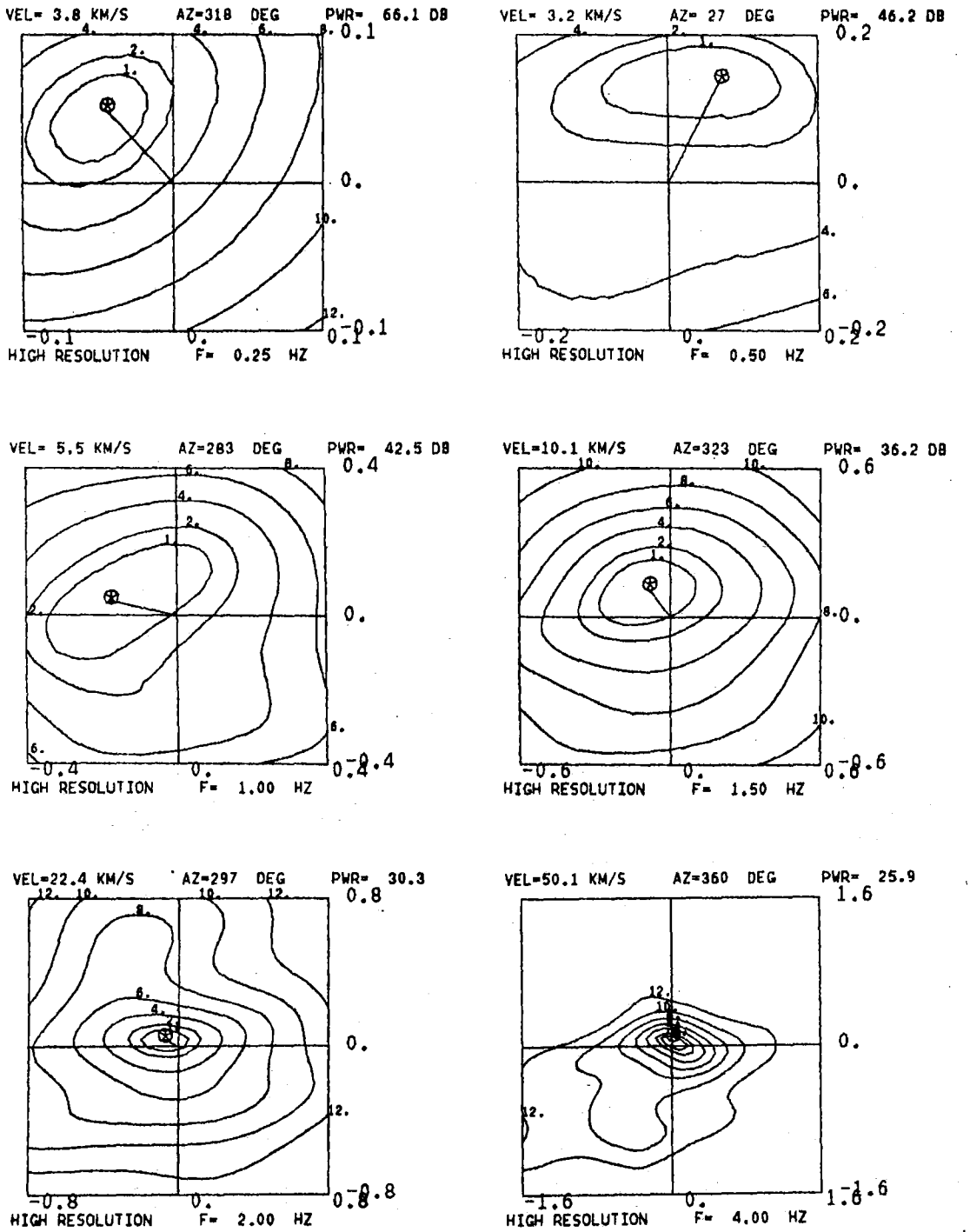

Fig. VI.1.3 High resolution wave number spectra for the data used in Fig. VI.1.2, and for the frequencies 0.25, 0.50, 1.0, 1.5, 2.0 and 4.0 Hz (the last four as in Fig. VI.1.2). The frames are scaled such that velocities down to 2.5 km/s are covered in each case, and the estimates are based on 16 blocks each of 250 samples of short period data sampled at 20 samples/sec.

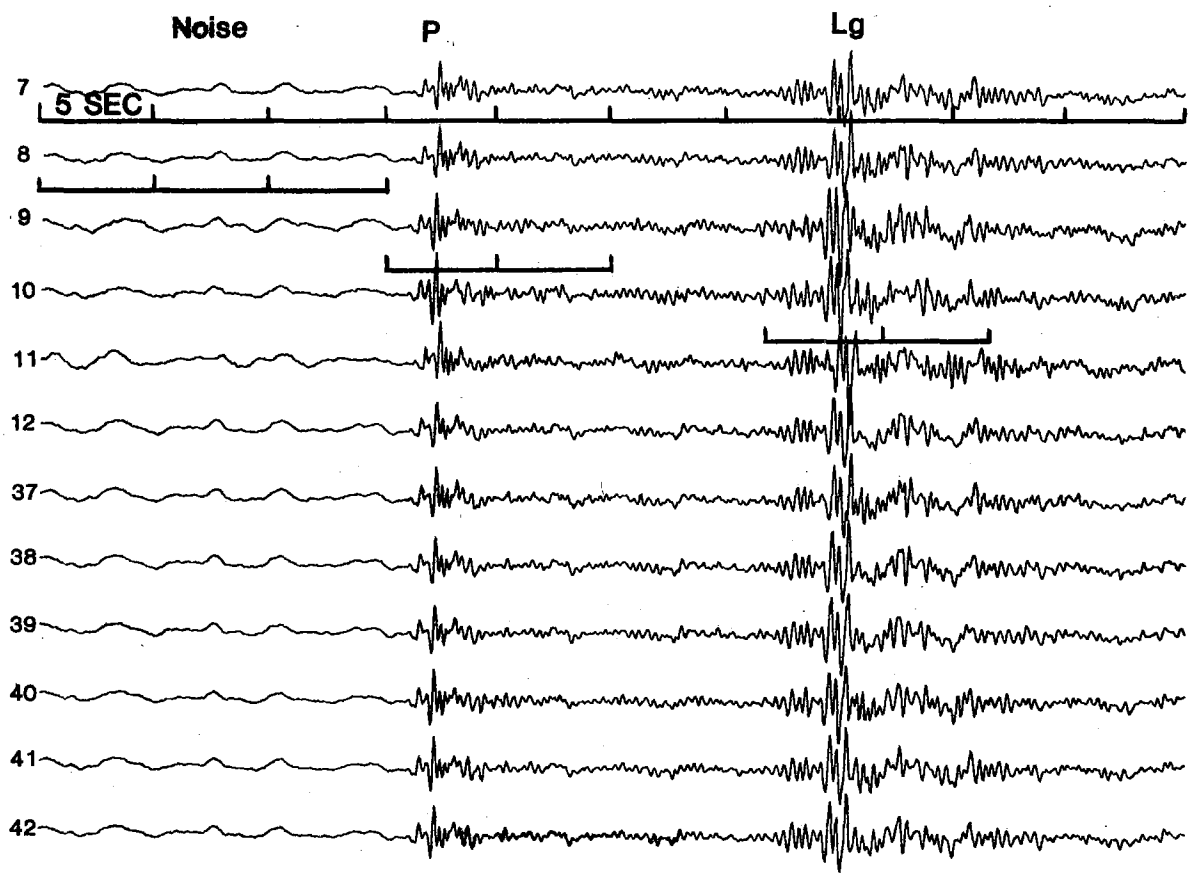

Fig. VI.1.4 Unfiltered data from the 12 NORESS stations. Channel numbers refer to Fig. VI.1.1. Epicentral distance is about 140 km. The marked time windows for noise, P and Lg phases were subjected to correlation analysis.

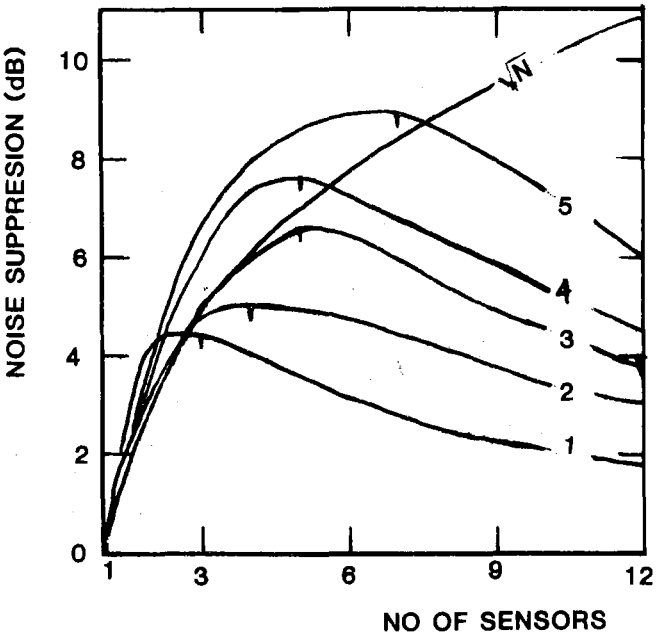

Fig. VI.1.5 Noise suppression for five different bandpass filters as a function of sensor number included in the beam (see text).

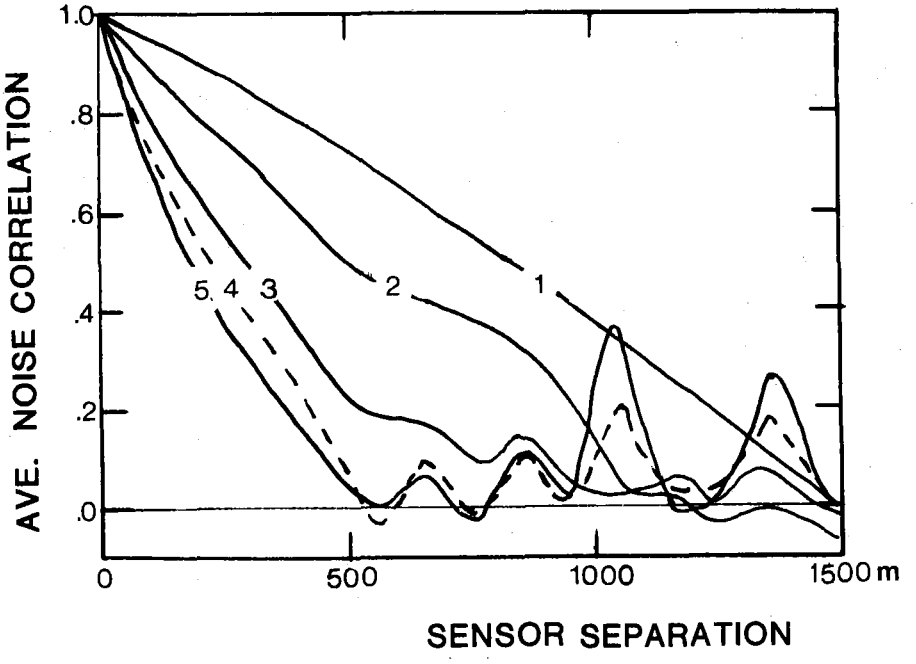

Fig. VI.1.6 Noise correlation as a function of sensor separation up to 1500 m. Averaging is performed over all sensor combinations that fall within segments of 100 m.

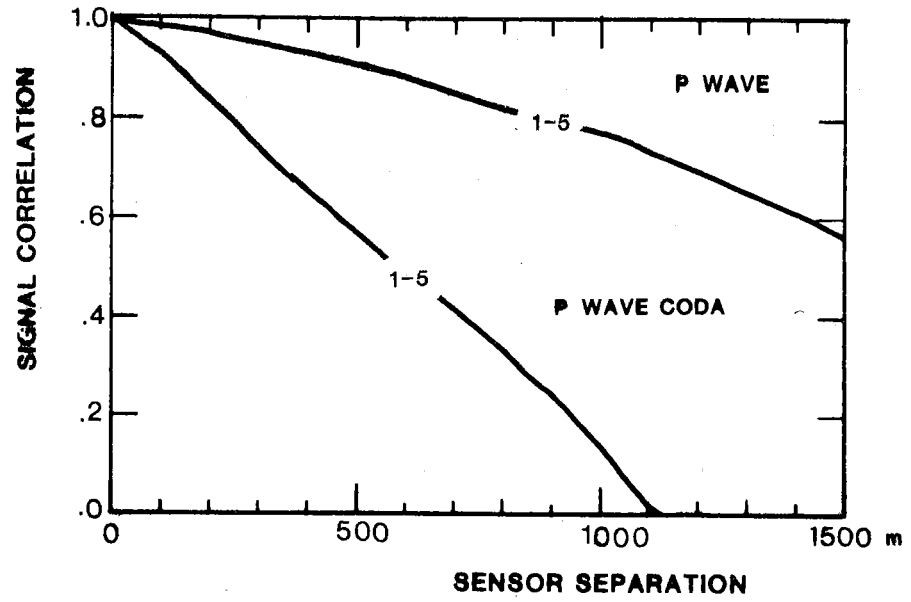

Fig. VI.1.7 P wave and P wave coda correlations as a function of sensor separation. The results are averaged over all five filters.

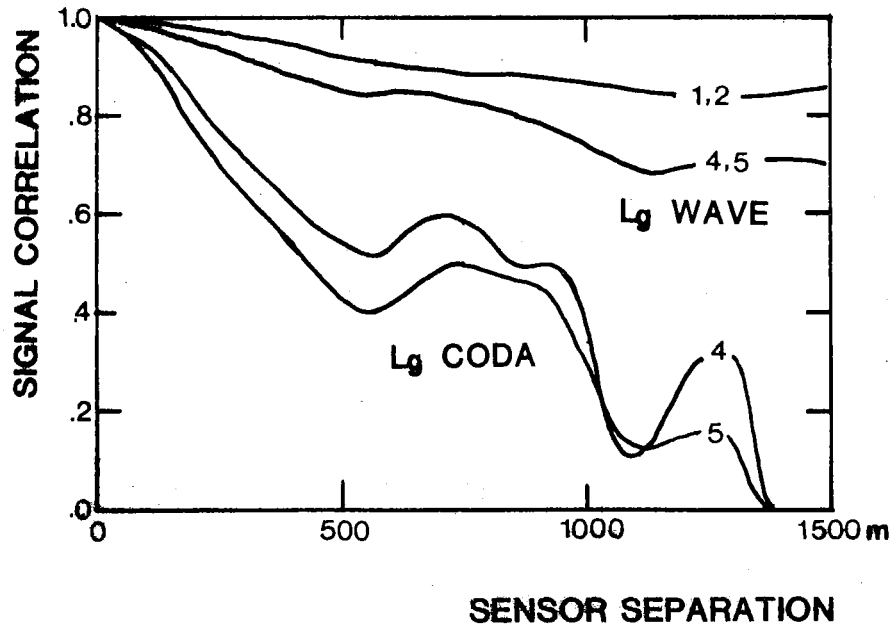

Fig. VI.1.8 Lg wave and Lg wave coda correlations as a function of sensor separation for the filters indicated.

VI.2 Concentrated Earthquake Zones in Svalbard

An interesting area for the investigation of intraplate seismicity is the Svalbard archipelago. The tectonic setting of this area is unique in that an active spreading ridge (the Knipovich Ridge) lies very near the passive continental margin, and also because the archipelago, as well as the surrounding oceanic areas have a very complex tectonic history. Since 1976, several temporary seismic arrays have been in operation in the area, with the best coverage being obtained in 1979 when a seven-station telemetered network became operational, supplemented by three portable microearthquake stations. The results reported here are based on data recorded between ultimo July and medio September 1979.

Earthquake locations using teleseismic data (Husebye et al, 1975) suggest a diffuse pattern of earthquakes near the east coast of Spitsbergen. Mitchell et al (1979), using data from temporary microearthquake networks, found that the earthquakes are centered in Heer Land and that the active zone, trending east-west, is quite concentrated in extent. Using a network of four stations located in Spitsbergen mining towns, and observing over a period of nine months (Dec 1977 - Oct 1978), Bungum and Kristoffersen (1980) reported an average of several earthquakes a day from the same area, although with considerable variation in the level of activity. The only reliable fault-plane solution for the Heer Land region is for an earthquake in January 1976, with a mainly vertical strike-slip solution in which the planes strike N108°E and N17°E (Bungum and Kristoffersen, 1980). The new data set (shown in Figs. VI.2.1 and VI.2.2) confirms the previously obtained results inasmuch as the lineation of epicenters shown in Fig. VI.2.2 coincides well with the strike direction from the fault-plane solution for the 1976 event. The ISC location for the 1976 earthquake is slightly outside the area of main activity in the Heer Land zone, a difference which probably reflects a bias in the teleseismic location.

In addition to the Heer Land events, Fig. VI.2.1 shows that one earthquake occurred near the west coast and three occurred in Storfjorden. Events in both of

those areas were reported by Bungum and Kristoffersen (1980) as isolated shocks with no sign of clustering in time or space, and they also observed seismic activity along the northern slope of the Barents shelf, with indications of a rough east-west trend from the shelf north of Spitsbergen to the Analysis of the new data set indicates that a relatively large proportion of the recorded earthquakes occurred in Nordaustlandet, spatially concentrated as the Heer Land seismic zone (Fig. VI.2.3). Because the zone is well outside the array, location uncertainties are of course larger than those for the Heer Land events. The Nordaustlandet sequence is quite different from the Heer Land zone in its time-magnitude pattern. Following a 15 day period of complete quiescence, there was an outburst of activity, but without a distinctive main shock. Some decrease in frequency of occurrence seems to occur during the last part of the recording period, and the last shock in the sequence was the largest one, with magnitude 3.9. Before that event, the recorded seismicity had a slope in its frequency-magnitude distribution (b-value) of about 0.5, a value usually associated with a swarm. In contrast the b-value for the Heer Land zone was around 1.4, which is a more typical value.

The Svalbard archipelago is cut by several major Paleozoic faults (Fig. VI.2.1) which trend in a NNW-SSE direction, and these faults were reactivated during Mesozoic and Tertiary times. A fold belt developed along the western coast of Spitsbergen as a part of an extensive early and middle Tertiary deformation. There is little evidence in the surface geology of fracture trends aligned with the strike of the seismic zone in Heer Land. Lineament analysis of Landsat images (Otha, in prep.) show that surface lineaments longer than 2.5 km have dominant strike directions in the sector NW to ENE. In Nordaustlandet late Paleozoic and older rocks are exposed around its north and northwestern perimeter, the rest of the island being covered by a glacier. In the northwest the structure is dominated by a NNW-SSE striking fold system, while farther east a large WNW trending fault extends eastward under the glacier. We therefore find that the activity in Nordaustlandet is aligned with old fault trends, while the correlation is less obvious for the Heer Land area.

The dimensions and orientation of the Nordaustlandet and Heer Land zones are the same, but this does not necessarily imply a similar regional stress field. Although scattered earthquake activity is observed throughout much of Svalbard, the most obvious features are the two concentrated earthquake zones. These intraplate earthquake zones lie only 200-300 km from the obliquely spreading Knipovich Ridge, and somewhere between these two areas a transition from oceanic to continental crust occurs (Sundvor and Eldholm, 1979). Because of the complex tectonic history of the area, it seems reasonable to attribute most of the seismic activity to an interaction between the present tectonic stress field and older zones of weakness (Bungum et al, 1981).

H. Bungum
B.J. Mitchell, Saint Louis Univ.
Y. Kristoffersen, Norwegian Polar Research Institute

References

Bungum, H. and Y. Kristoffersen (1980): A microearthquake survey of the Svalbard region. Final Report, Phase I. NORSAR Tech. Rep. No. 1/80, NTNF/NORSAR, Kjeller, Norway.

Bungum, H., B.J. Mitchell and Y. Kristoffersen (1981): Concentrated earthquake zones in Svalbard. Tectonophysics, in press.

Husebye, E.S., H. Gjoystdal, H. Bungum and O. Eldholm (1975): The seismicity of the Norwegian and Greenland Seas and adjacent continental shelf areas. Tectonophysics, 26:55-70.

Mitchell, B.J., J.E. Zollweg, J.J. Kohsman, C.-C. Cheng. and E. Haug (1979): Intraplate earthquakes in the Svalbard archipelago. J. Geophys. Res., 84: 5620-5626.

Otha, Y., in prep. Fracture and lineament studies in central eastern Spitsbergen.

Sundvor, E. and O. Eldholm (1979): The western and northern margin off Svalbard. Tectonophysics, 59:239-250.

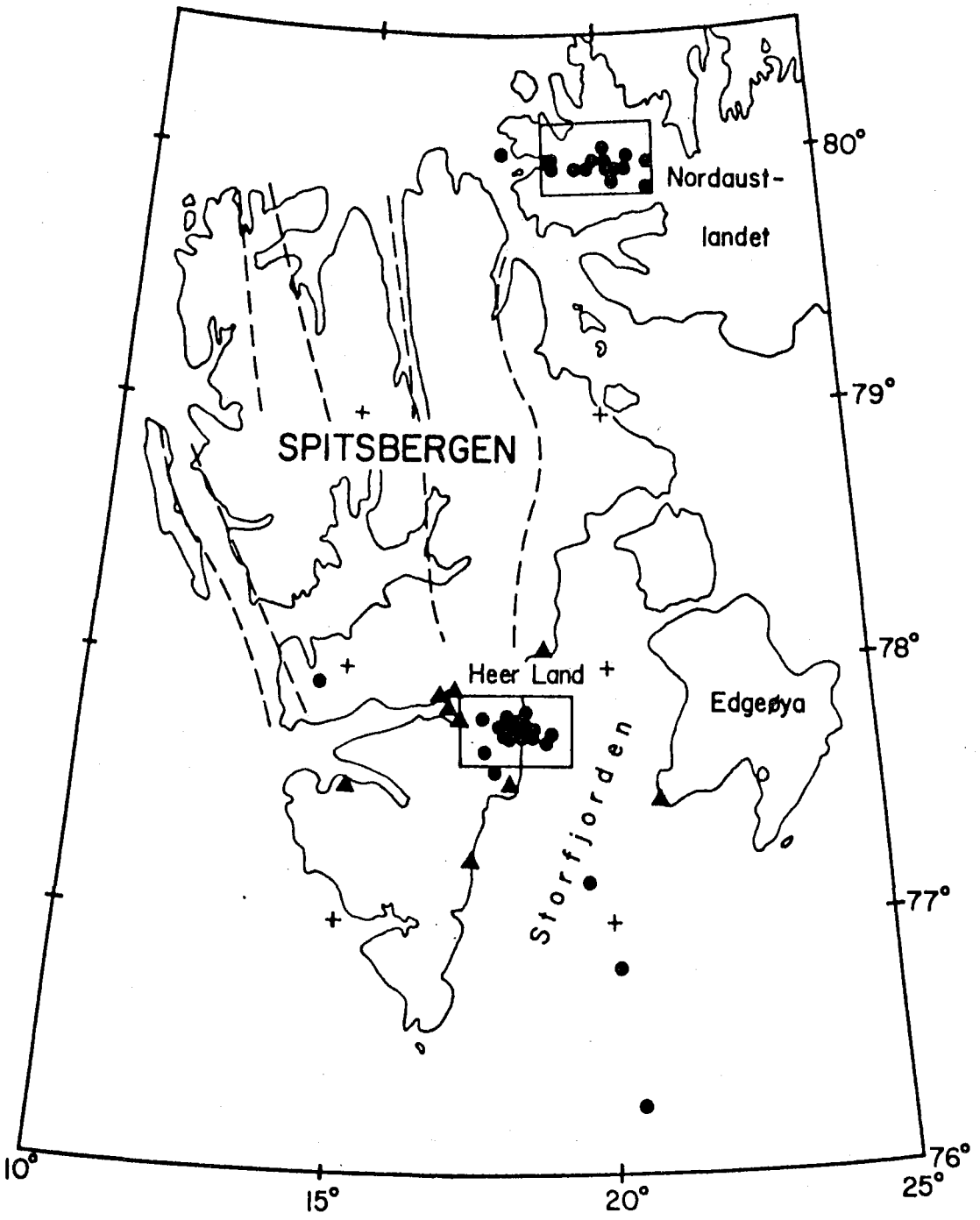

Fig. VI.2.1 Map of Svalbard with locations of recording stations (triangles) and epicenters. One station symbol has been covered by earthquake symbols in the Heer Land zone. The two inserted boxes correspond in size to the areas covered by Figs. VI.2.2 and VI.2.3.

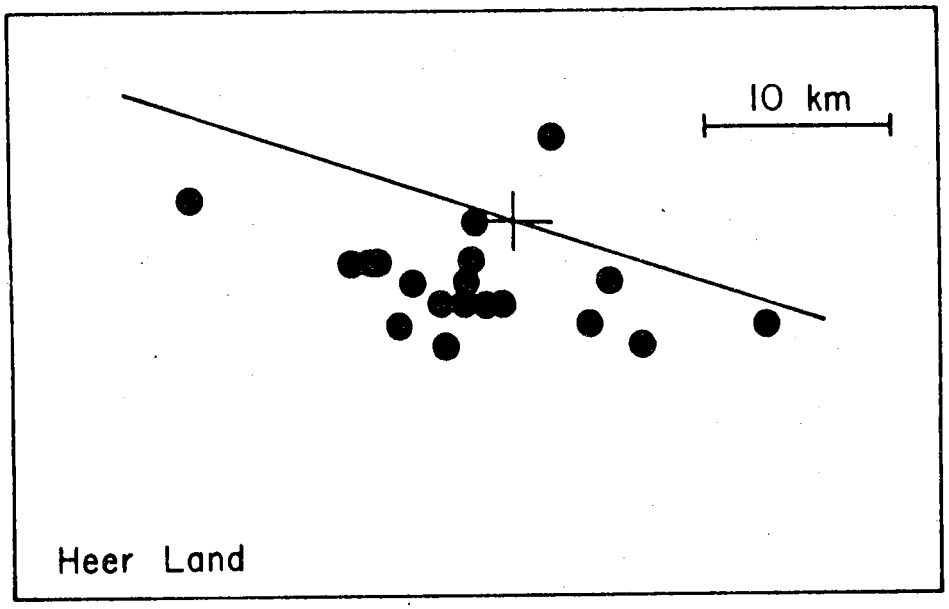

Fig. VI.2.2 Epicenter map for the Heer Land region, covering the area within the southernmost box in Fig. VI.2.1. Also shown is the ISC solution for the epicenter of the January 18, 1976, earthquake (with standard error base), as well as the direction of one of the nodal planes for the same event.

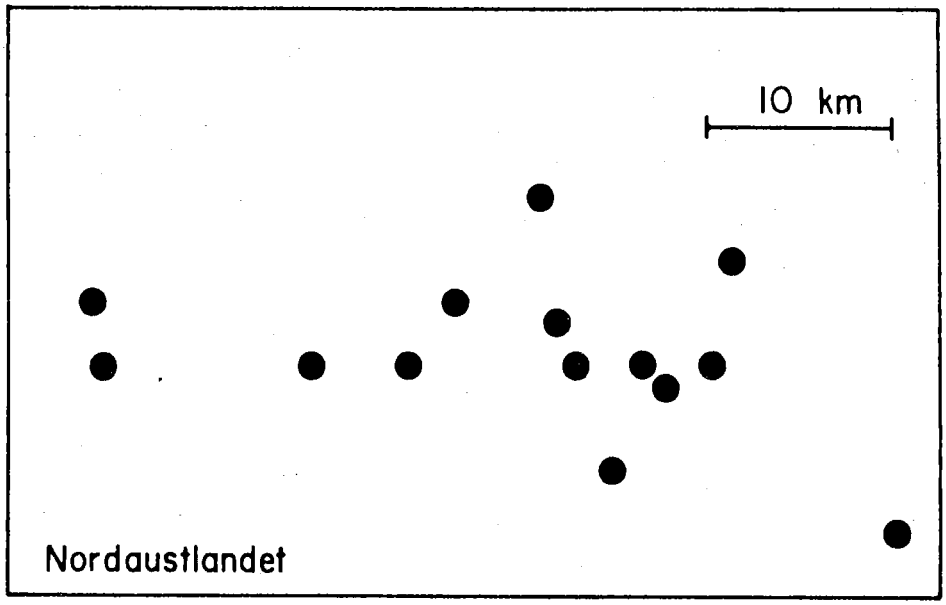

Fig. VI.2.3 Epicenter map for the Nordaustlandet region, covering the area within the northernmost box in Fig. VI.2.1.

VI.3 Microearthquake Monitoring of the Nansen Ridge during the FRAM I Experiment

As part of a long term effort to improve our knowledge of the Eurasian part of the Arctic, US station FRAM I was deployed on an ice floe in the Arctic Ocean north of Greenland from 11 March - 15 May 1979. The geophysics program on FRAM I encompassed besides microearthquake monitoring bathymetry, gravity, seismic reflection profiling, refraction measurements, and underwater acoustics.

Six slightly modified AN-SSW/41A sonobuoys were deployed on ice floes out to 4 km away from the FRAM I main camp in the beginning of April 1979. The sonobuoy array was operational for 6 weeks, and during the final days of manned operation FRAM I drifted along the northwestern crest of Nansen Ridge to within 25 km of the median valley, and 69 events were recorded. 21 of these could be located (Fig. VI.3.1), with location errors estimated to be about 1-2 km in the radial direction and 4-10 km in the tangential direction from the array. The majority of epicenters appear to lineup closely with the location of the median valley as outlined from spot soundings. It is interesting to note that several events with significantly shorter epicenter distances occurred on the northwestern flank of the rift valley.

The microearthquake locations on the Nansen Ridge show two parallel linear trends separated by about 10 km (Fig. VI.3.1). Assuming a focal depth of 1 km for all events, one epicenter trend appears to coincide with the median valley and the other as a sequence of events located along the northwestern rift valley wall. If however the hypocenters of the trend aligned with the median valley were 5 km or deeper, their locations would be closer to the southeastern rift valley wall. The seismic activity can in the case of shallow events be attributed to movement of a fault block about 10 km wide being uplifted from the median valley to the rift valley wall. The greater number of events occurring in the median valley may indicate differential movement between the two sides of the block or be related to intrusive and/or extrusive events in the median valley. If however the events occurred at a greater depth (5 km), they would have been associated with motion on fault systems on both sides of the median valley (Kristoffersen et al, 1981).

Ice station FRAM I was funded by the Office of Naval Research, Arlington, Va., and the Norwegian scientific programs were coordinated and funded by the Norwegian Polar Research Institute, Oslo.

Y. Kristoffersen, Norwegian Polar Research Institute
E.S. Husebye
H. Bungum

References

Kristoffersen, Y., E.S. Husebye, H. Bungum and S. Gregersen: Seismic investigations of the Nansen Ridge during the FRAM I experiment. Tectonophysics, in press.

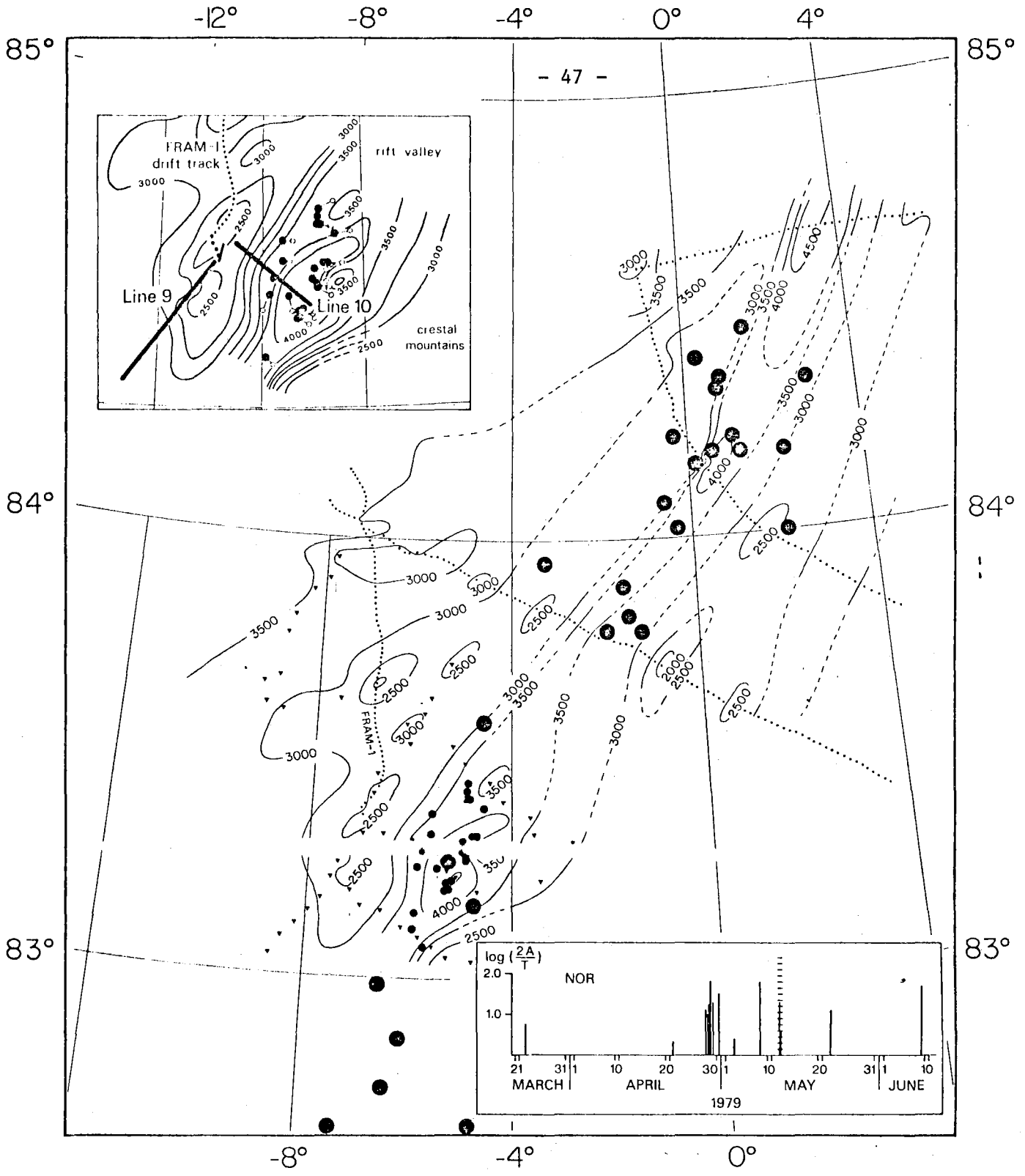

Fig. VI.3.1 Locations of microearthquakes recorded by FRAM I sonobuoy array (small dots) and teleseismically located earthquakes 1961-1979 (large dots).

Upper Left: Microearthquake locations for two assumed focal depths, 1 km (dots) and 5 km (open circles). The drift of the array during the recording interval is indicated by heavier dots, and the line at the end of the track indicates the array dimension. Heavy lines show locations of seimsic refraction lines and triangles mark points where spot soundings were made.

Lower Right: Time sequence of earthquakes occurring in the southern part of the Nansen Ridge with signal amplitude (A) recorded at NOR, northeastern Greenland illustrated by vertical bars. Shaded area indicates 36 hour recording interval at the ridge crest by sonobuoy array.

VI.4 Automatic Determination of Arrival Time, Amplitude and Period for Teleseismic Events

In our Semiannual Technical Summary for 1 Oct 79 - 31 Mar 80 we published a chapter on automated arrival time determination for local and regional P and S waves. That approach was based upon computation of signal envelopes, and the procedure has now for some time been included in our routine analysis of data from Stiegler's Gorge Seismic Network. (For other approaches to this problem, see for example Stevenson, 1976; Stewart, 1977; and Anderson, 1978.)

Our work in this area has now been extended to include teleseismic events, and we have here found it necessary to develop a completely new procedure, where also signal amplitude and period are computed. The procedure is as follows:

1. Initial arrival time. Compute STA/LTA on a filtered trace, after defining window lengths for STA and LTA. Declare a detection if P out Q successive STA/LTA values exceed a given threshold. If no detection is obtained, try again with a different (lower) threshold. The end of a detection is declared whenever the criterion fails, and several detections can be obtained for one particular event. The start of the first detection is used as the initial estimate of arrival time.

2. Signal amplitude, initial signal period. Define a window around the initial estimate of arrival time, and search for maximum absolute amplitude within this window. Then find the maximum opposite deflection by searching both ways in time until two zero crossings are observed. This search is done on a time series which has been smoothed by sliding a 5-point interpolation window through the data (using a least squares fit of a 2nd degree curve), and the exact locations of the two peaks are obtained by a similar interpolation. Signal amplitude (zero-peak) is then taken as half the difference between the two extreme deflections, and first estimate of signal period is twice the time difference between the peaks.

3. Refined signal period. Starting at the point of maximum signal amplitude, a number of peaks or troughs are found on each side. This is done by using the 5-point smoothing procedure, combined with certain criteria for defining a peak. The time differences between the peaks are then arranged in increasing order, and a refined estimate of the signal period is defined as twice the average of the median and its two neighboring values. However, if the scatter among these exceeds a certain value, the initial estimate of signal period is used (point 2 above).

4. Refined arrival time. Compute noise RMS from two successive time intervals and use the lowest of the two. Start at the point of maximum absolute amplitude and move forward one peak/trough at a time with the object of finding the first one that belongs to the signal. Any of these criteria can stop the search: i) having moved forward more than a specified distance (presently three full signal periods), ii) the last peak having fallen below a certain level as compared to the RMS noise level, iii) the last peak having fallen below a certain level as compared to the maximum amplitude. When the first peak has been identified in this way, the refined arrival time on the filtered trace is taken as the position of the peak minus one quarter period. The filter phase shift is finally compensated for by calling a subroutine with filter characteristics and signal period as input values, and phase shift in seconds as output.

Performance

The procedure outlined above has been implemented in the routine NORSAR processing of teleseismic events. The performance has been very good both with respect to arrival time and amplitude/period, even though some work still remains in determining the parameter values.

The performance with respect to arrival time determination is shown in Figs. VI.4.1-2, using 8 events from May 5-7, 1981. The two uppermost traces are unfiltered beams (scaled differently), and the bottom trace is the filtered beam on which the parameter extraction has been done. As seen from the figures all of the events are of intermediate or poor quality, which is where the challenge is in this respect. The two main problems here are

(i) To find a correct initial estimate of arrival time. Even though we have succeeded there for all the examples given, it is evident that there must be a tradeoff between detecting weak precursors and not detecting in the noise preceding the signal. If an incorrect initial estimate is obtained, the procedure will not get on the right track again.

(ii) Once a correct initial arrival time estimate is obtained, to be able to follow an emergent signal into the noise without going too far ahead. We feel that our procedure works quite well in this respect, and good examples here are events 3, 5 and 6 in Figs. VI.4.1-2.

The performance with respect to signal amplitude and period still remains to be numerically evaluated (as compared to analyst decisions), but it is evident that the performance in both cases is very good. The main problem here is to find the right window, where we have used guide lines for m_b computations. It is of course more difficult to estimate signal period than amplitude, and the key to the good performance here is that the period is estimated from the distribution of values obtained over several cycles on the seismogram. In this way we avoid the large errors that can occur if only one cycle is used (superimposed wavelets), and it has so far been very rare that the analyst has measured a signal period differing more than 0.1 sec from the automatic determination.

H. Bungum

References

Anderson, K.R. (1978): Automatic analysis of microearthquake network data. Geoexploration, 16, 159-175.

Stevenson, P.R. (1976): Microearthquakes at Flathead Lake, Montana: A study using automatic earthquake processing. Bull. Seism. Soc. Am., 66, 61-80.

Stewart, S.W. (1977): Real-time detection and location of local seismic events in Central California. Bull. Seism. Soc. Am., 67, 433-452.

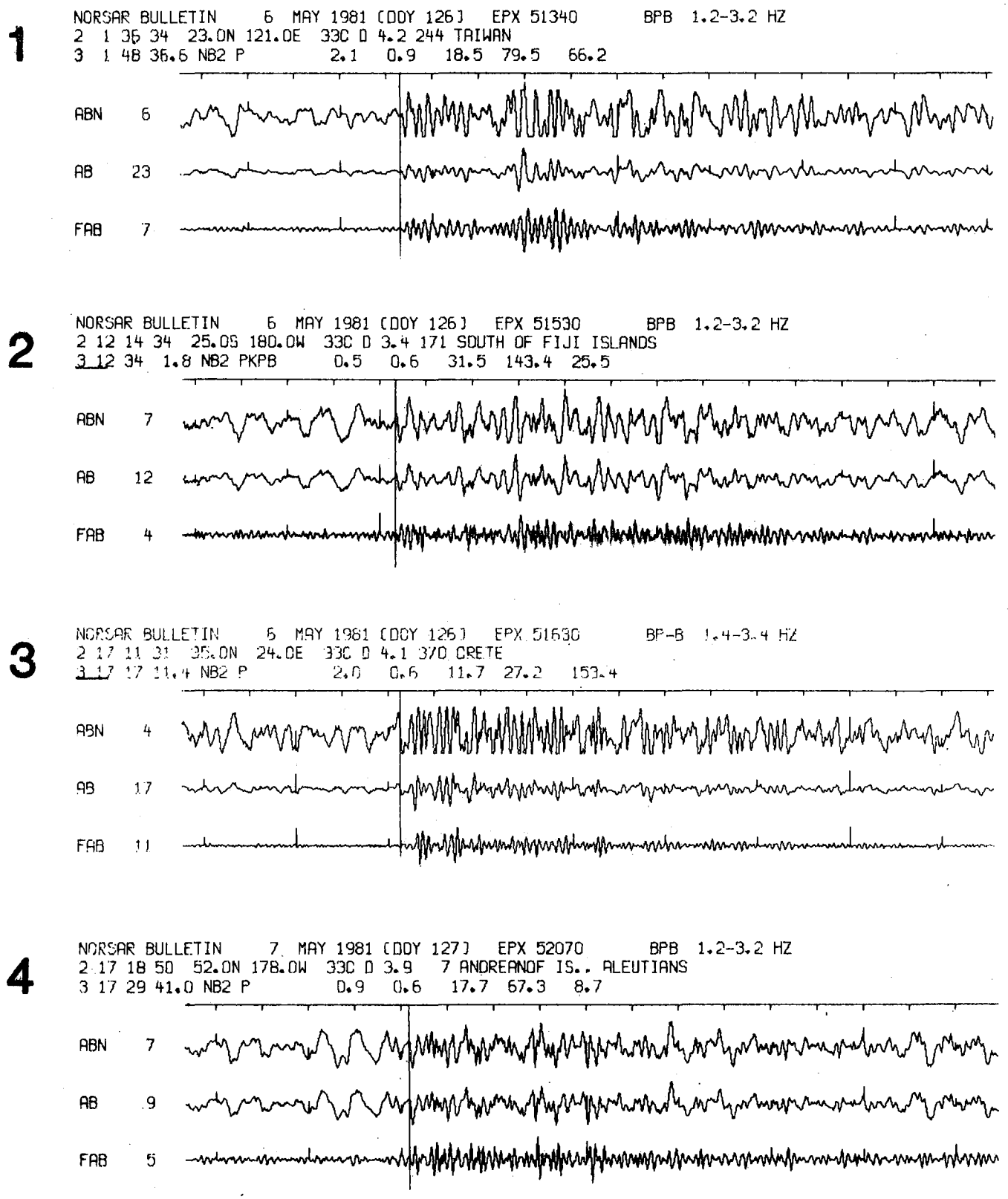

Fig. VI.4.1 Results from the automatic and routine processing of four events at NORSAR, with two unfiltered and a filtered beam for each event, and with the epicentral solution on top. The vertical lines indicate the arrival time determinations.

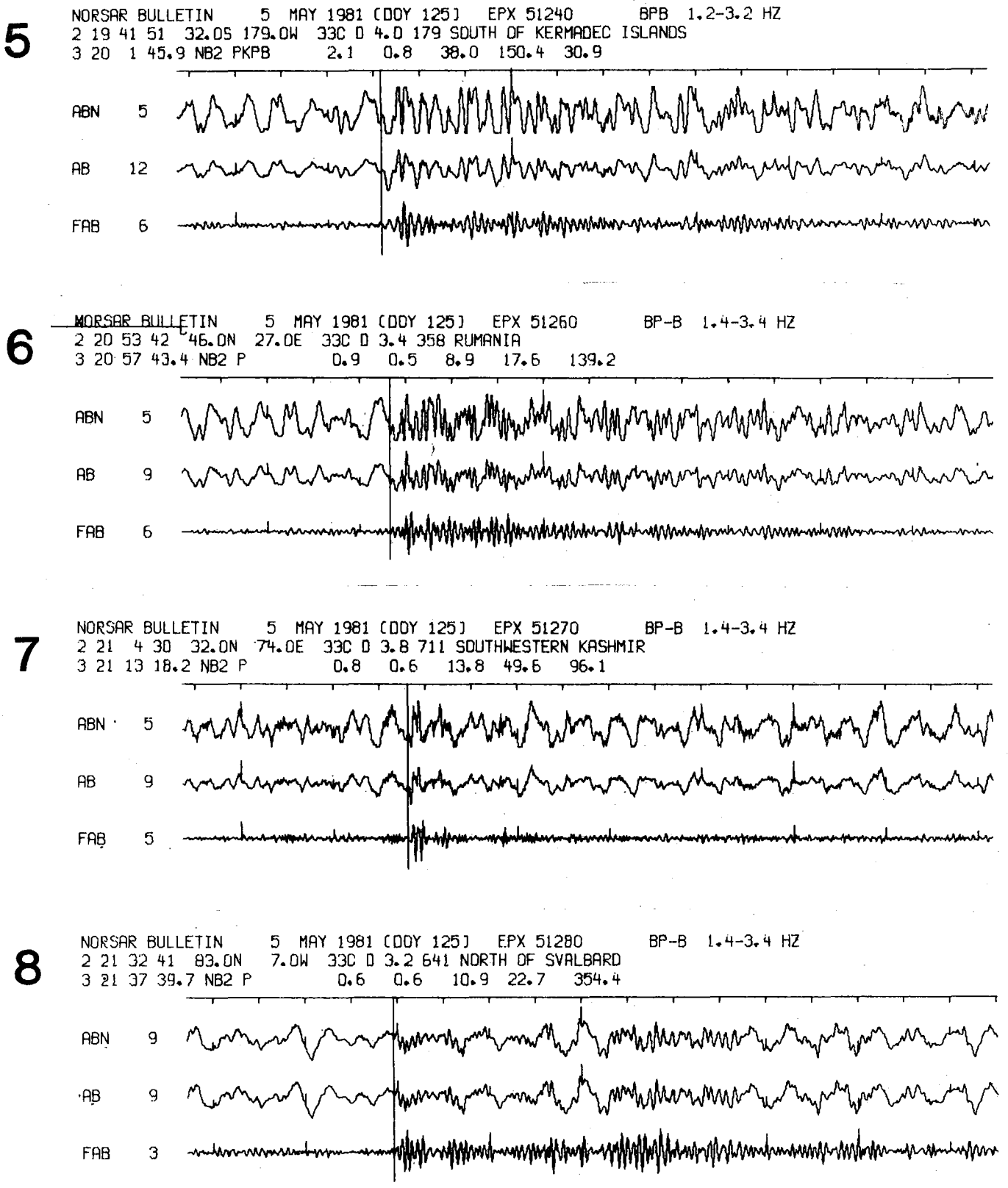

Fig. VI.4.2 Same as for Fig. VI.4.1, but with four new events.

VI.5 Seismic Moment Tensors and Kinematic Source Parameters

Parameters pertaining to the kinematics of a finite source are usually estimated by fitting specific models to the data. On the other hand, these parameters, including source location, are also contained in the moment tensors of higher degree. The source can always be represented by a generalized function, the moment tensor density. In an explosion it represents an imposed stress pulse, but in an earthquake it is the difference between the true physical stress and the model stress which satisfies Hooke's law. If the source region is 'reasonably' small (compared to the wavelengths), it is possible to approximate the effect of a moment tensor density by a limited number of moment tensors of degree zero and higher. This representation was discussed by Backus (1977), but no attempts to do the inverse problem were reported, previous studies dealing almost exclusively with the moment tensor of degree zero (usually referred to as 'the moment tensor'). The zero degree tensor does not contain spatial information (including source location), and parameters like fault geometry and rupture velocity are still obtained by fitting observations to specific 'classical' models like those of Haskell and Savage. These source parameters represent averages over the fault, so it is the long-wavelength part of the seismograms (relative to source dimensions) that is used to estimate them. Clearly, these parameters must be related to the moment tensors of higher degree, and it thus appears worthwhile to explore the feasibility of estimating these moment tensors. In doing so it is important to keep the number of unknown parameters small, and this consideration suggests to approximate not only the spatial extent, but also the source time function, by a few parameters. Such a procedure is not only practical, but also meaningful in the sense that, ideally, spatial and temporal source functions should be approximated in the same way. The representation in terms of spatial and temporal moment tensors up to degree two involves 90 source parameters, together with spatial and temporal derivatives of Green's functions. Under fairly weak assumptions however (Doornbos, 1981), the number of source parameters may be reduced to 20, and spatial derivatives rewritten in terms of temporal derivatives of asymptotic wave functions which are easy to evaluate. The 20 source parameters are

$$M_{jk},\quad \Delta\tau,\quad \Delta\xi_\ell,\quad \Delta(\tau^2),\quad \Delta(\tau\xi_\ell),\quad \Delta(\xi_\ell\xi_m)\ ;\ j,k,\ell,m = 1,2,3$$

and the tensors M_{jk}, $\Delta(\xi_\ell\xi_m)$ are symmetric. Here M_{jk} determines the final static moment, $\Delta\tau$, $\Delta\xi_\ell$ determine the source 'center' in time and space, $\Delta(\tau^2)$ represents source 'rise time', $\Delta(\tau\xi_\ell)$ involves average rupture velocity, and $\Delta(\xi_\ell\xi_m)$ represents the spatial geometry. The equation relating these source parameters to the seismic response is nonlinear (unlike the moment tensor representation of degree zero), but for inversion purposes it can be efficiently linearized. Fig. VI.5.1 shows long-period SRO and ASRO records of a deep event in the Bali Sea, with P, SH and SV phases. Of these, SV was not used because of suspected interference with SP. With two components of P, one of SH, and record lengths 40 seconds, we have in the time domain, after resampling to a 4 sec interval, 240 equations for the 20 unknowns. Although these equations will not all be independent, there is reason to expect that the problem is sufficiently overdetermined for the source inversion to be feasible. This is one of the principle advantages of inversion in the time domain.

In Figs. VI.5.2-4, results are shown from experiments involving different options and conditions (denoted by case numbers in the figures). Some features of the source relocation (Fig. VI.5.2) deserve further investigation. In particular, the relocations in time and space seem to be too large to be explained by finite source effects alone; these results were essentially unchanged after including depth phases (case number 7,8). The use of an earth model different from that used in PDE determinations might be a factor. In some cases we allowed an isotropic component to develop. The moment of this component is illustrated in Fig. VI.5.3 for two cases. The event location was fixed in case 2; in case 5 the event was relocated, and it appears that the inferred isotropic component can be made to essentially disappear by relocating the source. In Fig. VI.5.3, the deviatoric part of the moment tensor was decomposed into a major and minor double couple; this decomposition, though non-unique, serves to illustrate the deviation from a representation by one double couple only, and the major double couple can be used to construct conventional fault plane solutions (Fig. VI.5.4). It appears that differences among the various solutions are small, and the solutions are consistent with observed polarities and amplitudes (corrected for path effects). In one of these cases, moments of degree

two have been estimated. The RMS error of fit (not shown) is smaller than in all other cases, as expected with the larger number of degrees of freedom. However, the solution does not satisfy some of the physical criteria (including positivity of some of the parameters), and it appears necessary to incorporate these criteria as constraints in the inversion. The reasons for this are now being explored, and methods for constrained inversion are evaluated. The constraints are precisely those appearing as a priori assumptions in the conventional methods of source anlaysis; thus it will also be possible to investigate the impact of these assumptions.

D.J. Doornbos

References

Backus, G.E., 1977. Interpreting the seismic glut moments of total degree two or less, Geophys. J.R. astr. Soc., 51, 1-25.

Doornbos, D.J., 1981. Seismic moment tensors, in 'Identification of Seismic Sources', eds. E.S. Husebye and S. Mykkeltveit, D. Reidel Publ. Co., in press.

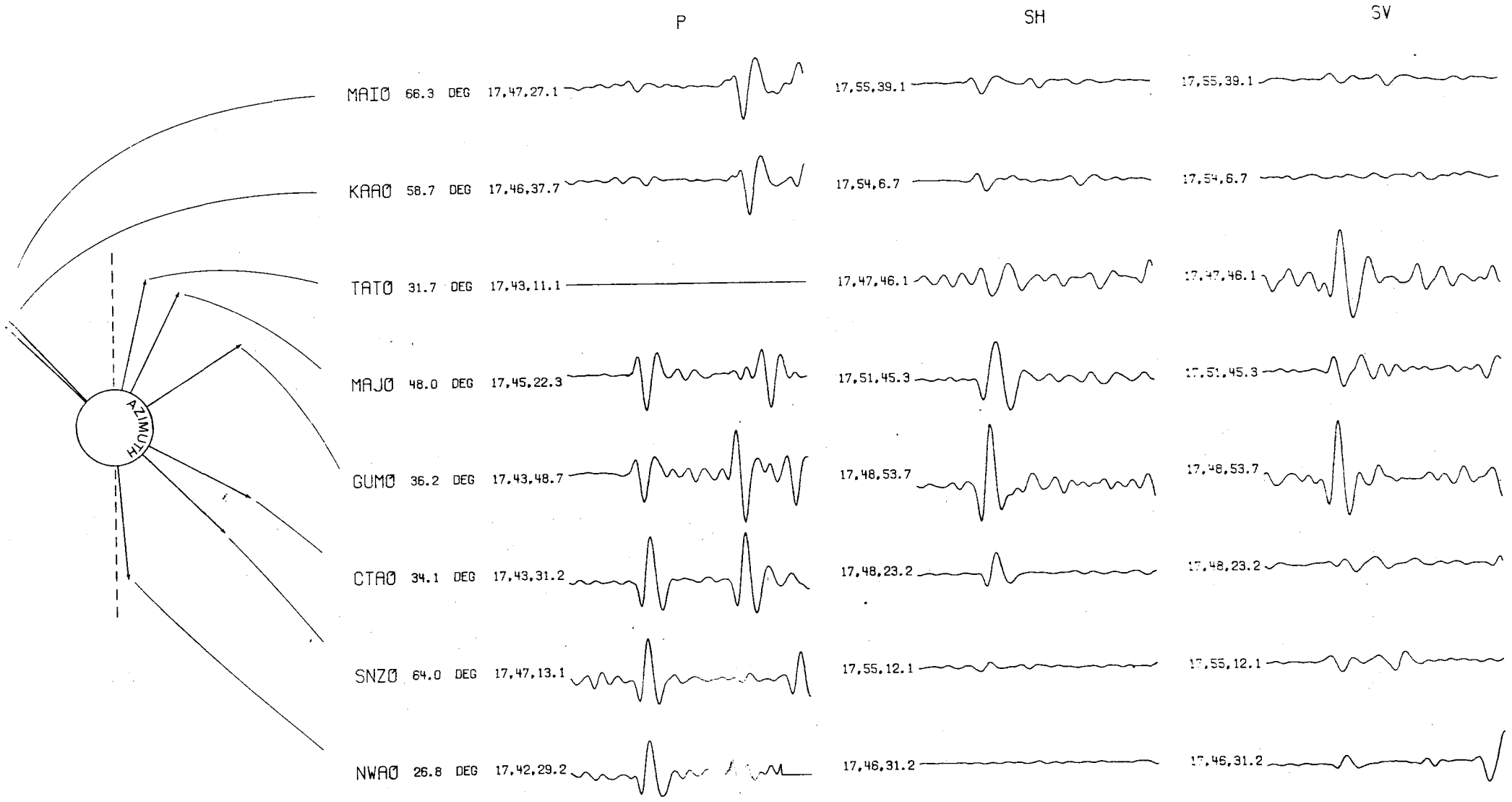

Fig. VI.5.1 SRO and ASRO records from Bali Sea event of 1978, June 10. Vertical component with P, horizontal components rotated into transverse and radial, with SH and SV. Record length is 4 minutes. Different amplitude scale for different components. The P vertical component of TATO was not used because of presumed nonlinearity effects.

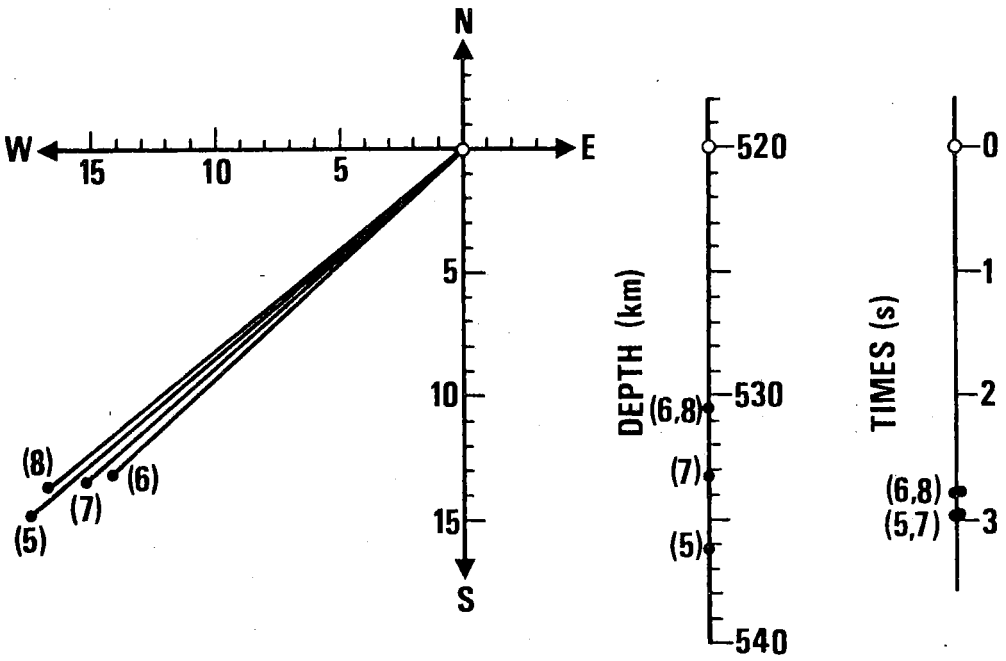

Fig. VI.5.2 Results of source relocation in space and time. Case numbers refer to different conditions and options in the inversion.

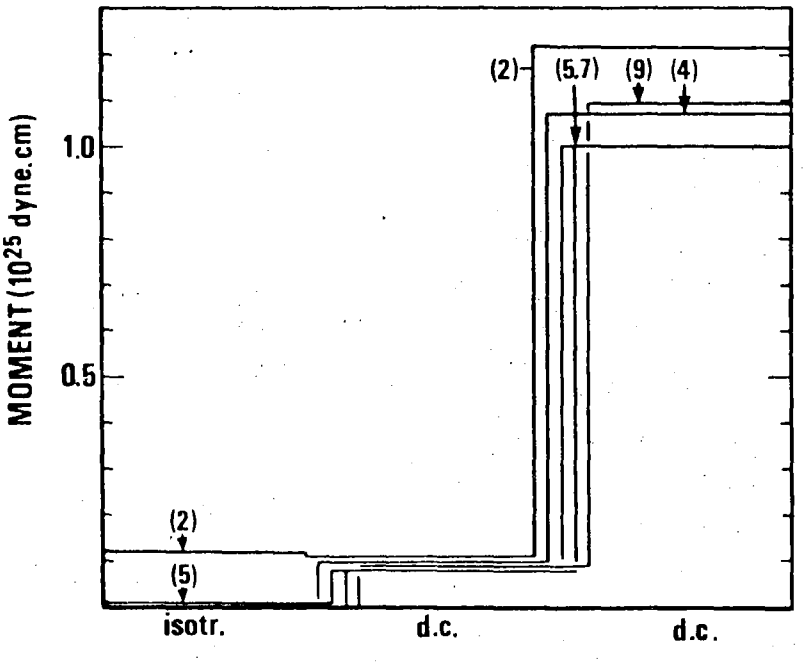

Fig. VI.5.3 Scalar moments of decomposed source, for different inversions. Decomposition in isotropic part and major and minor double couple.

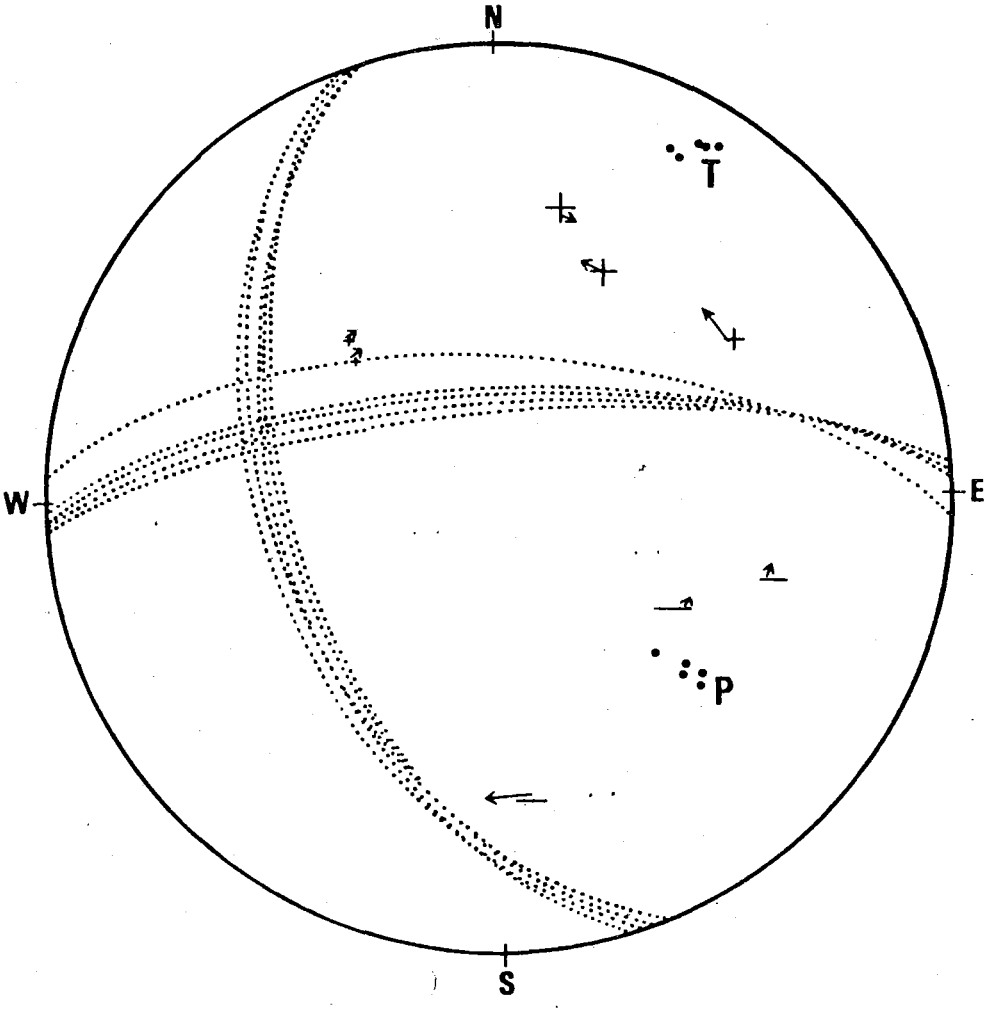

Fig. VI.5.4 Fault plane solutions in equal area projections, for different inversions. Also shown are observed polarities and amplitudes of P($\pm$) and SH($\rightarrow$).

VI.6 Location of Regional Events using Travel Time Differentials between P Arrival Branches

This study was undertaken to investigate the potential of obtaining very precise relative epicentral distance estimates of events in the range 15-30°, using information from the strong secondary P arrival branches observed on NORSAR recordings of Eurasian events at these distances. The present paper discusses the application of such techniques to a limited epicentral region north of the Caspian Sea, from which several presumed explosions have been recorded.

Earlier studies (Massé and Alexander (1974), King and Calcagnile (1975)) have discussed the strong secondary P phases that are observed on NORSAR recordings of presumed explosions in the distance range 15-30°. These can be associated with discontinuities in the upper mantle underneath Eurasia at depths near 420 and 690 km. Massé (1974) showed that arrival time differentials between such phases may give potentially very accurate constraints on epicentral distance estimates.

In this study, we examine the use of regional phases to obtain precise relative distance estimates within a limited epicentral region. We have chosen to study the area north of the Caspian Sea, from where several presumed explosions have been recorded by NORSAR (Table VI.6.1). NORSAR's detection capability for this region is very good, partly as a result of signal focusing effects which give a significant positive magnitude (m_b) bias at NORSAR relative to NEIS m_b. From Table VI.6.1, it is seen that the bias is about 0.5 m_b units on the average. Fig. VI.6.1 shows the NORSAR array deployment, and in Fig. VI.6.2, filtered traces from subarray 02B are displayed for the lowest magnitude event in the data set. This event, 12 September 1978, had a NORSAR m_b of 4.0, corresponding to a NEIS equivalent m_b of 3.5. The signal-to-noise ratio at the best sensor (02B05) is about 1.0 m_b units above the detection threshold, thus indicating that NORSAR is able to detect events down to about m_b=2.5 for this region. The large variation in signal strength across 02B is noteworthy, and shows the importance of taking advantage of signal focusing effects for detection purposes.

A subset of the single sensor traces for event 4 is displayed in Fig. VI.6.3. The relative strength of the first P phase and the second one (with onset some 7 seconds later) is highly variable between sensors. This is again due to signal focusing effects, and shows that an array of wide aperture is necessary to ensure that both phases are detected on at least some sensors.

Fig. VI.6.4 shows measured phase differentials for two events (nos. 4 and 5). The six subarrays with the clearest secondary phase have been selected for this figure, thus providing 48 measurements per event. For both events, the distances refer to a nominal event location of 48.0°N, 48.0°E. The distances are of importance mainly to indicate relative distances between sensors. (If a different location within the test region had been chosen, it would have resulted in essentially unchanged relative distances).

Several observations are made from Fig. VI.6.4:

- Event 5 has consistently greater phase differentials than event 4. Therefore event 5 is located further away from NORSAR than event 4.

- There are significant deviations from a straight-line fit to the data for both events.

- These deviations are apparently not due to inaccurate measurements, since they are very similar for both events. The similarity of the patterns is high both between subarrays and within subarrays.

The measurements of Fig. VI.6.4 were made by cross-correlating each sensor trace with portions of a reference trace. The reference trace was chosen as the record of instrument 03B01 for event 4. Both the reference trace and the other traces were bandpass filtered in the band 1.0-3.0 Hz prior to cross-correlation. The peak of the correlation function was determined by a cubic spline fit in order to obtain a higher precision than the sampling interval (0.05 seconds) of the raw data.

Table VI.6.2 summarizes the measured differences between the two events, averaged over each subarray. The averages range from 0.26 to 0.33 seconds, with a standard deviation of the mean of less than 0.01 seconds within each subarray. Average difference over all 48 instruments is 0.30 seconds.

To transform such time differences into distance differences, one may, as a first approximation, use the time-distance slope in Fig. VI.6.4. Thus 0.30 seconds corresponds to 12.5 km, which would then be the estimated distance difference between event 4 and event 5, in the azimuthal direction of NORSAR. The accuracy is difficult to assess, but appears to be on the order of ± 1-2 km based upon the consistency observed between subarrays.

In order to apply the method to low magnitude events, it is necessary to consider the traces with the best signal-to-noise ratio. Accordingly, we measured the phase differentials at the 'best' sensor 02B05 for all the events in the data set, and the results are given in Table VI.6.4. Note that the results from the largest events are uncertain due to the 'clipping' problem. It is seen that four of the low magnitude events have essentially identical time differences, indicating that their epicentral distance from NORSAR is similar. All of the other measured events appear to be located 10-20 km further away from NORSAR than this group.

There are some differences in the signal spectral contents between the high and low magnitude events in the data set. As an example, Fig. VI.6.5 shows the amplitude spectra at 01A04 for the events 12 and 14. The dominant frequency is around 2 Hz for the high magnitude event (14) and around 3 Hz for the low magnitude event (12). The latter spectrum is typical for all the low magnitude events (No. 4,5,7,8,9,12) while the former is representative for those high magnitude events for which we have been able to estimate the spectrum (No. 10,13,14,15).

In conclusion, the main advantage of the method is to obtain precise relative distance estimates (probably accurate to within 2 km) even for low magnitude events. To assess the accuracy and achieve further improvement, calibration

of the delay/distance relation is necessary. This would require knowledge of the accurate location of a subset of events, distributed across the epicentral region in question.

F. Ringdal

References

Massé, R.P. (1974): A technique for reducing epicenter coverage regions for explosions, Earthquake Notes Vol XLV, No. 4, 3-12.

Massé, R.P. and S.S. Alexander (1974): Compressional velocity distribution beneath Scandinavia and western Russia, Geophys. J.R. astr. Soc., 39, 587-602.

King, D.W. and G. Calcagnile (1975): P-wave velocities in the upper mantle beneath Fenoscandia and western Russia, Geophys. J.R. astr. Soc., 46, 407-432.

NO	DATE YEAR	MM	DD	ORIGIN TIME H	MM	SS.D	EPICENTER **LAT**	**LON**	NST	MAGNITUDE(MB) NEIS	NAO	SOURCE	COMMENTS
1	1966	04/22		2	58	03.6	47.900N	47.700E	28	4.7	-	NEIS	NO NORSAR DATA
2	1968	07/01		4	02	01.7	47.900N	47.900E	62	5.5	-	NEIS	NO NORSAR DATA
3	1971	12/22		6	59	56.3	47.900N	48.200E	81	6.0	-	NEIS	CLIPPED (ALL CHANNELS)
4	1975	04/25		5	00	00.0	48.000N	48.000E	0	-	4.7	NORSAR	
5	1976	03/29		7	00	00.0	48.000N	48.000E	0	-	4.5	NORSAR	
6	1976	07/29		4	59	57.7	47.782N	48.120E	203	5.9	-	NEIS	CLIPPED (ALL EXCEPT 14C03)
7	1977	09/30		6	59	55.6	47.800N	48.145E	99	5.1	5.5	NEIS	CLIPPED (SOME CHANNELS)
8	1977	10/14		7	00	00.0	48.000N	48.000E	0	-	4.1	NORSAR	
9	1978	09/12		5	00	00.0	48.000N	48.000E	0	-	4.0	NORSAR	
10	1978	10/17		4	59	56.5	47.818N	48.114E	257	5.8	6.4	NEIS	CLIPPED (ALL EXCEPT 01A04)
11	1978	12/18		7	59	56.3	47.787N	48.192E	254	6.0	6.3	NEIS	NO DIGITAL NORSAR DATA
12	1979	01/10		8	00	00.0	48.000N	48.000E	0	-	4.7	NORSAR	
13	1979	01/17		7	59	55.7	47.883N	48.128E	225	6.0	6.6	NEIS	CLIPPED (ALL EXCEPT 01A04)
14	1979	07/14		4	59	55.1	47.813N	48.097E	227	5.6	6.3	NEIS	CLIPPED (ALL EXCEPT 01A04)
15	1979	10/24		5	59	56.6	47.806N	48.158E	220	5.8	6.4	NEIS	CLIPPED (ALL EXCEPT 01A04)

NOTE:
ALL THE EVENTS OF MB ABOVE 5.5 EXCEED THE DYNAMIC RANGE OF THE NORSAR DIGITAL RECORDING SYSTEM, WITH THE EXCEPTION THAT ONE LOW GAIN CHANNEL HAS BEEN AVAILABLE SINCE 1976.

TABLE VI.6.1

List of events from the area north of the Caspian Sea.

SUBARRAY	NOBS	MEAN DIFF. (S)	ST.DEV	ST.DEV OF MEAN
01B	6	0.3307	0.0210	0.0086
02B	6	0.3018	0.0144	0.0059
03B	6	0.3132	0.0084	0.0034
06B	6	0.3197	0.0116	0.0048
04C	6	0.2563	0.0163	0.0067
05C	6	0.2608	0.0102	0.0042
12C	6	0.3158	0.0157	0.0064
13C	6	0.3090	0.0241	0.0099

TABLE VI.6.2

Time differentials between events 4 and 5, averaged over the 8 subarrays shown in Fig. VI.6.4.

EVENT NO	TIME DIFF SECONDS	DISTANCE(KM) (NEIS LOCATION)
1	-	2729.9
2	-	2740.3
3	-	2755.9
4	7.54	-
5	7.85	-
6	8.0 *	2761.2
7	7.93	2761.0
8	7.53	-
9	7.54	-
10	7.95*	2758.0
11	-	2764.5
12	7.53	-
13	7.8 *	2753.5
14	7.9 *	2757.5
15	8.0 *	2761.2

TABLE VI.6.3

Estimated phase differentials at instrument 02B05 between the first and second recorded P phase.
(Uncertain measurements due to clipping are marked *.)

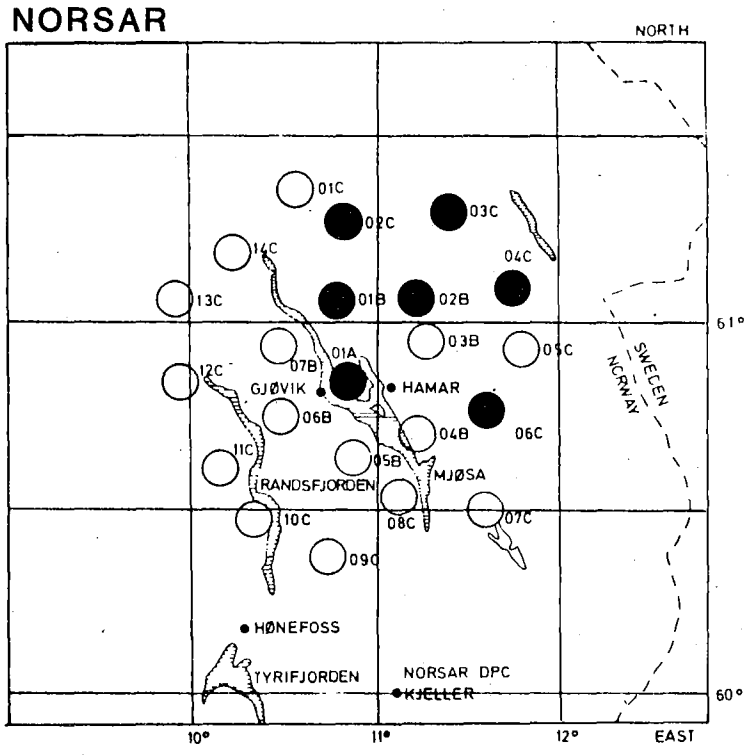

Fig. VI.6.1 Deployment of the original 22 NORSAR subarrays (from 1971 to October 1, 1976). The subset of 7 subarrays in operation since October 1, 1976, are marked as filled circles.

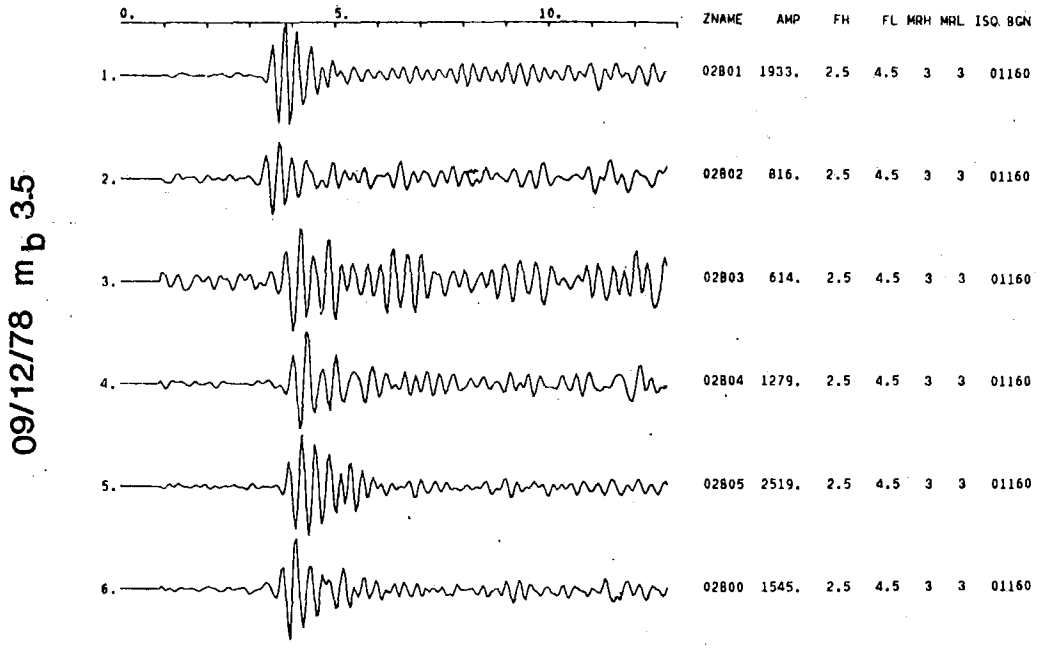

Fig. VI.6.2 NORSAR-recorded signals (at subarray 02B) for Event 9 in Table VI.6.1. The signals have been bandpass filtered (2.5-4.5 Hz) and are scaled to max. amplitude for each of the six sensors. Note the significant variation in amplitude (a factor of 4) across the subarray, from 614 q.u. at 02B03 to 2519 q.u. at 02B05.

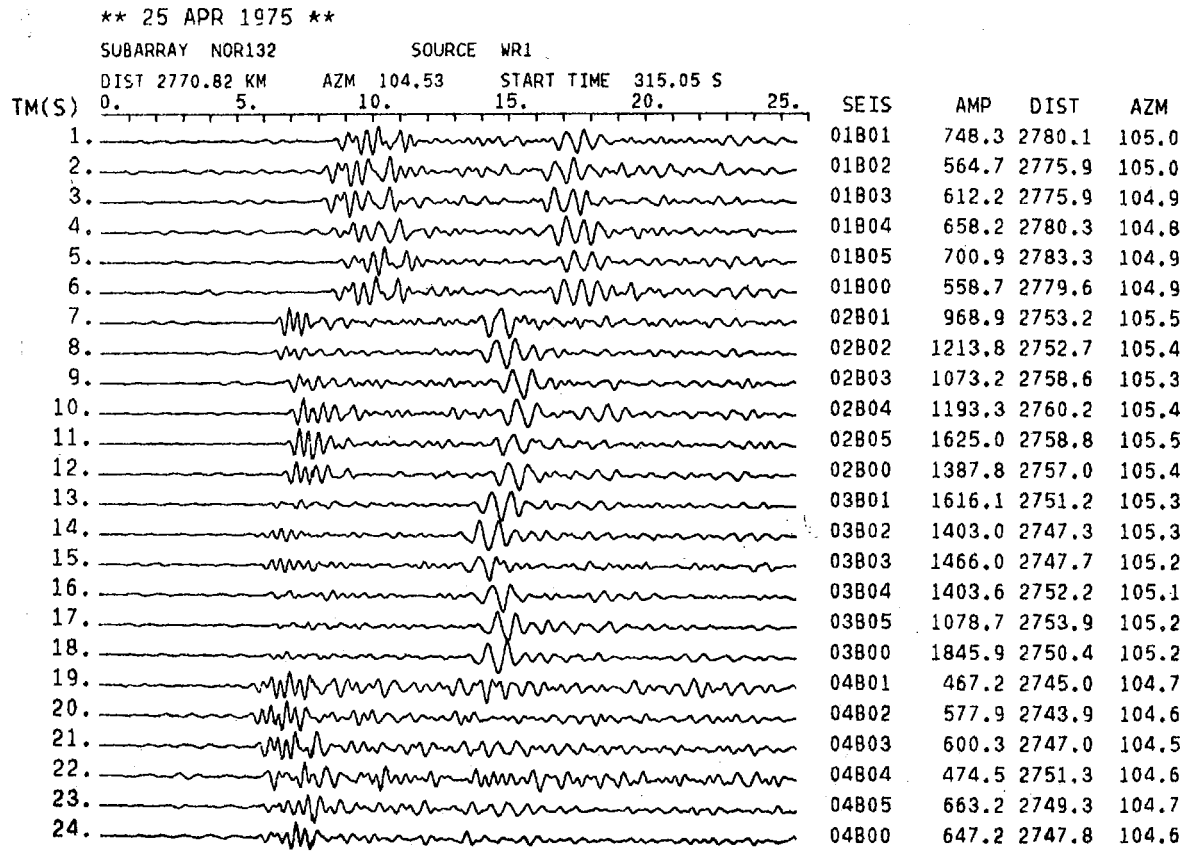

Fig. VI.6.3 Selected NORSAR recordings (subarrays 01B-04B) of event 4 in Table VI.6.1. The data have been bandpass filtered (1.0-3.0 Hz) and are scaled to max. amplitude for each sensor. (Max. amplitude is specified for each trace.) Note the strong secondary P-phase some 7 seconds after the first P-onset. Also note the strong variability in relative amplitudes between the first and secondary P phases.

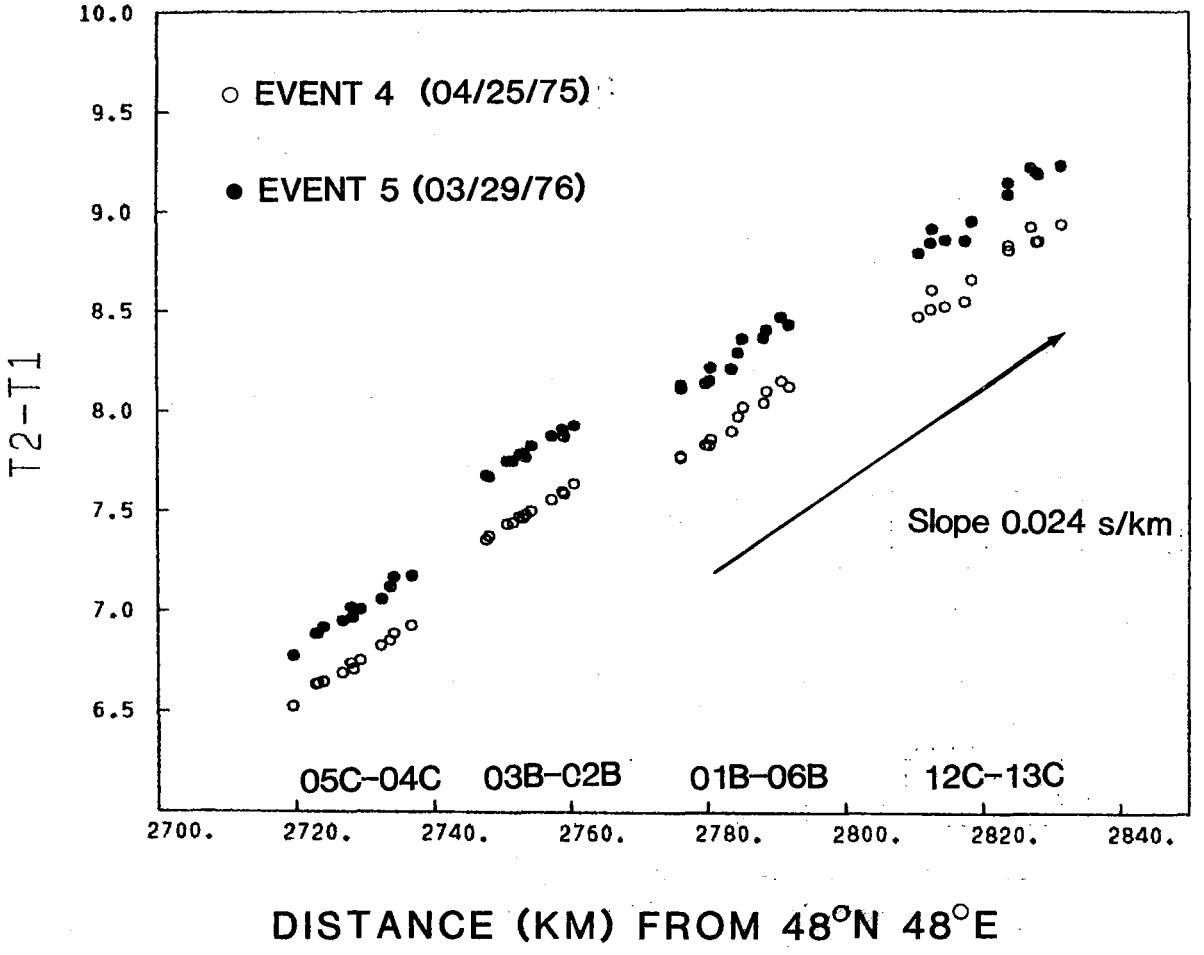

Fig. VI.6.4 Measured time delays for eight subarrays (as marked in the figure) for Event 4 (open circles) and Event 5 (filled circles). The distances are nominal as explained in the text. Note the consistency of the measurements for the two events both between subarrays and within subarrays.

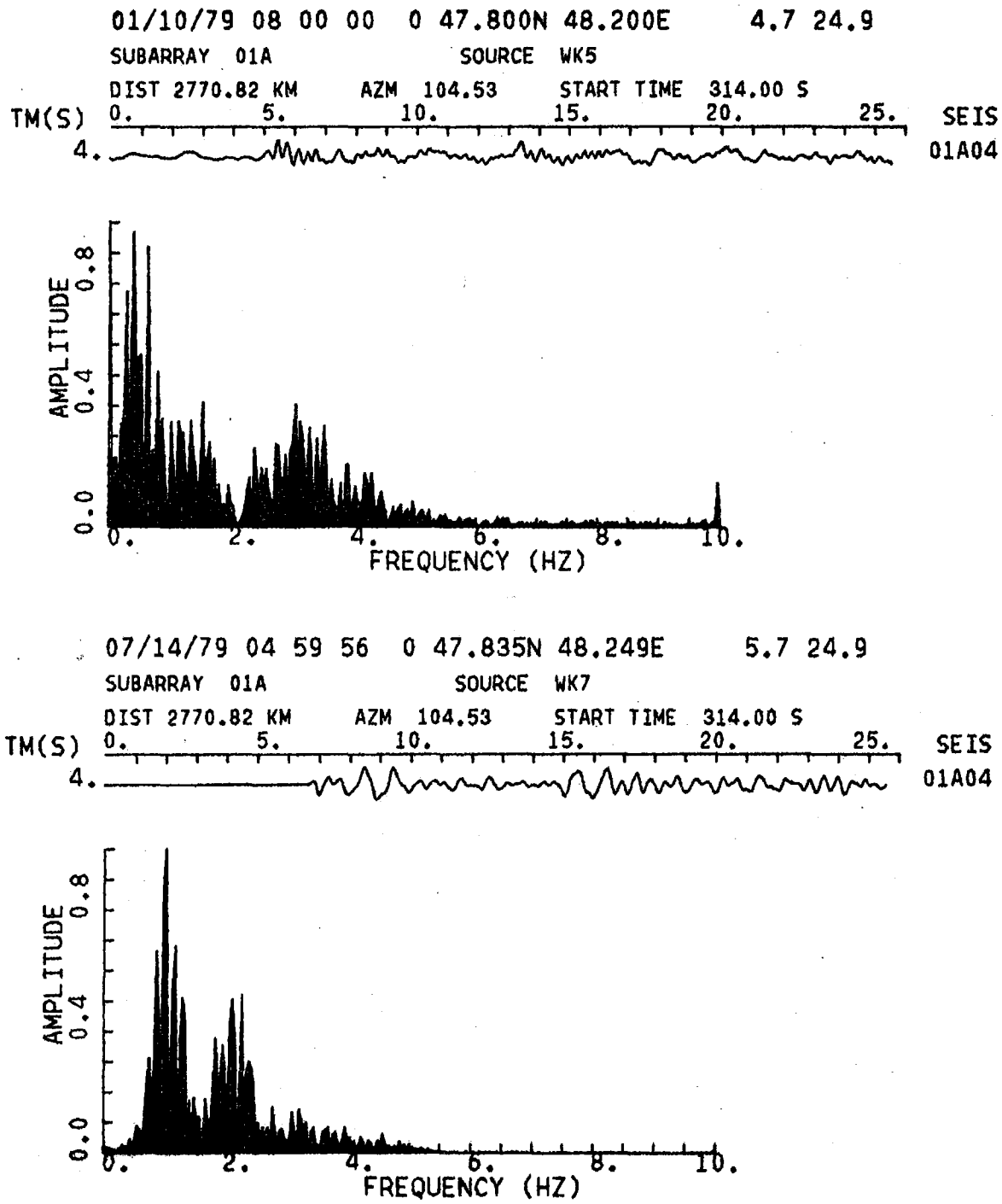

Fig. VI.6.5 Amplitude spectra at instrument 01A04 for Event 12 (top) and Event 14 (bottom). This instrument has an analog low pass filter with upper 3 dB point of 8 Hz. Note the significant difference in spectral shape above 1 Hz.

VI.7 Lg Wave Propagation in Eurasia

There is considerable interest in the potential usefulness of observations at regional distances in the context of seismic event discrimination. This is the motivation for our study of the relative propagation efficiency of phases like Pg, Pn, Sg, Sn, Lg, Li and Rg across various parts of Central Asia and Western Russia.

For obvious reasons, the choice of observational data was limited to mostly record copies from WWSSN stations in southern and western Asia and Fenno-scandia. Likewise, the events subjected to analysis are mainly presumed underground explosions in Kazakh, Caspian Sea area, Western Russia and Novaya Zemlya in addition to Central Asian earthquakes (see Fig. VI.7.1). Furthermore, the Fennoscandian observations constituted a Western Russia/ Baltic Shield population while the remainder of the data constituted a Eurasian population.

The data analysis was based on reading of all prominent onsets within the 5.0-2.7 km s^{-1} group velocity window, in addition to the main P phases, with arrival times corresponding to the wave packet onset time. Amplitudes and periods, however, were read for the maximum amplitude-to-period ratio within the same wave packet. With the data extracted fromt he WWSSN records we can calculate travel times, group velocities, event magnitudes, amplitude decays and also which component(s) are most prominent as regards higher mode surface wave recordings.

Initially, the group velocities associated with all 'local' amplitude maxima were determined both from SP and LP records. The LP observations appear to be mainly of the Sn and Rg types and at that are of the fundamental and the first few higher modes. The general SP observations are somewhat messy, exhibiting a roughly continuous distribution of group velocities in the range 4.60-3.35 km s^{-1}. This situation is much improved by considering only the most energetic arrival of each seismogram as shown in Fig. VI.7.2a for the Western Russia/Baltic Shield region.

The main results are: the Lg stands out rather clearly and with a velocity of about 3.5 km s^{-1}. In SP records it is the most likely observable phase in the phase velocity window 5.0-2.5 km s^{-1} for regional distances. Sn (and Li) is only occasionally the strongest phase. LP records are dominated by Rg phases with velocities around 3.0 km s^{-1}.

Similarly, the Eurasian group velocity data shown in Fig. VI.7.2b gave that the Lg (ca 3.50 km s^{-1}) and the Sn (4.20-4.50 km s^{-1}) phases dominate the SP records whereas Li is never the strongest phase. The LP records are again dominated by Rg arrivals and also slow Lg arrivals. In essence, for the Eurasian area as a whole the only two phases consistently observed were Lg on SP records and Rg on LP records.

With respect to distribution of dominant signal frequencies, the following characteristic features have been observed: i) In the SP records the peak amplitudes are associated with frequencies in the range 0.8-1.2 Hz with the highest frequencies for paths across Western Russia/ Baltic Shield. ii) In the LP records, the peak amplitudes are associated with periods in the range 3-7 sec.

Analysis of short period phase amplitudes is difficult, in particular when the data at hand are a mix of different event/receiver combinations. In our case, the problem is twofold, namely: i) average propagation efficiency of higher mode surface waves as a function of distance and ii) event detectability or how to compare Lg and Sn amplitudes with those of P. Our preference was to tie the scaling of the individual observation to estimates of the amplitude-distance factor in the magnitude formula, using ISC or NORSAR reportings for the 'true' event m_b-magnitude.

Using the ISC-reported body wave magnitude for the events in question, the corresponding estimates for the magnitude distance factor $B(\Delta)$ for both P and Lg waves are plotted in Fig. VI.7.3a, and estimates of $B(\Delta)$ for Sn in comparison

with B(Δ) for Lg are given in Fig. VI.7.3b. The analysis was restricted to max. amplitudes of wavelets in the Sn and Lg group velocity windows and all maxima were read on the vertical short period component. In Fig. VI.7.3a, we clearly see that P is the strongest phase for distances beyond 10°. A notable exception here is a presumed explosion on the Kola peninsual - where Lg waves are significantly stronger than the P-waves. There is a notable scarcity of observations below 10 deg because there are few observations available and because it is hopeless to read accurately strong signals on analog WWSSN records. Finally, a comparison of vertical amplitude readings with corresponding horizontal ones gave that the latter were larger by a factor of 0.1-0.2 m_b units.

Fig. VI.7.4 shows the magnitude distance factor for P and Lg waves as a function of distance for events in the Eurasian data base. The down-pointing arrows indicate a maximum possible value for log (A/T) for Lg. In fact, for these cases there is no sign of clear wave onsets within the appropriate time interval and thus the mentioned arrows indicate the general coda or noise level.

A study of Fig. VI.7.4 reveals a very high attenuation/scattering level for the Central Asia/Himalayas region in comparison with the Western Russia/Baltic Shield area both for P and Lg waves. The average amplitude difference amounts to about half a magnitude unit for both type of waves, and the above remarks on nondetections are liable to increase this difference for Lg waves, keeping in mind that all Western Russia/Baltic Shield observations given are made for readable onsets within the specified group velocity window. For an account of this relatively high attenuation level, we are in favor of a general explanation in terms of complex tectonic and sedimentary covers.

Manual analysis of analog WWSSN station records of earthquakes/explosions in Central Asia and Western Russia gave the following results. P waves (Pg, Pb or Pn) are generally the strongest in the SP records. S waves and/or higher mode Love-Rayleigh waves have velocities around 4.5 km s^{-1} (Sn waves), and 3.35-3.60 km s^{-1} (Lg waves). In SP records Lg waves are the most prominent secondary

phase. The most efficient transmission paths for Central Asian/Western Russian events appear to be westward towards Fennoscandia, whereas propagation is less efficient towards India, Pakistan and Iran. Irrespective of source type, Sn (approx. 4.5 km s^{-1}) and fundamental mode Rayleigh waves besides occasional P phases dominate the LP records. The high frequency Lg waves should have good event discrimination power is not obvious from the data analyzed here. For example, P/Lg amplitude ratios derived from Fig. VI.7.4 for the explosion and earthquake populations, respectively, do not show any separation.

A more detailed account of the results achieved in this study is given in Mykkeltveit and Husebye (1981).

S. Mykkeltveit
E.S. Husebye

References

Mykkeltveit, S. & E.S. Husebye (1981): Lg wave propagation in Eurasia, in: Identification of Seismic Sources - Earthquake or Underground Explosion, E.S. Husebye & S. Mykkeltveit (eds.), D. Reidel Publ. Co., in press.

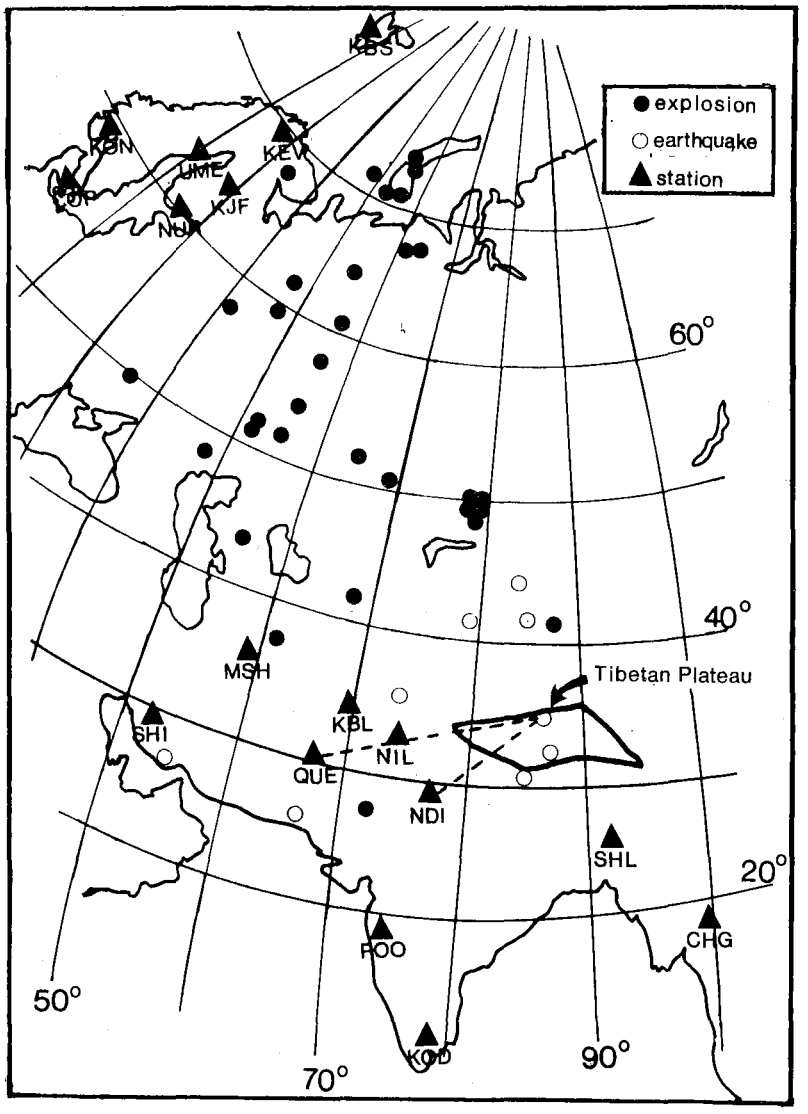

Fig. VI.7.1 Events and stations used in this analysis.

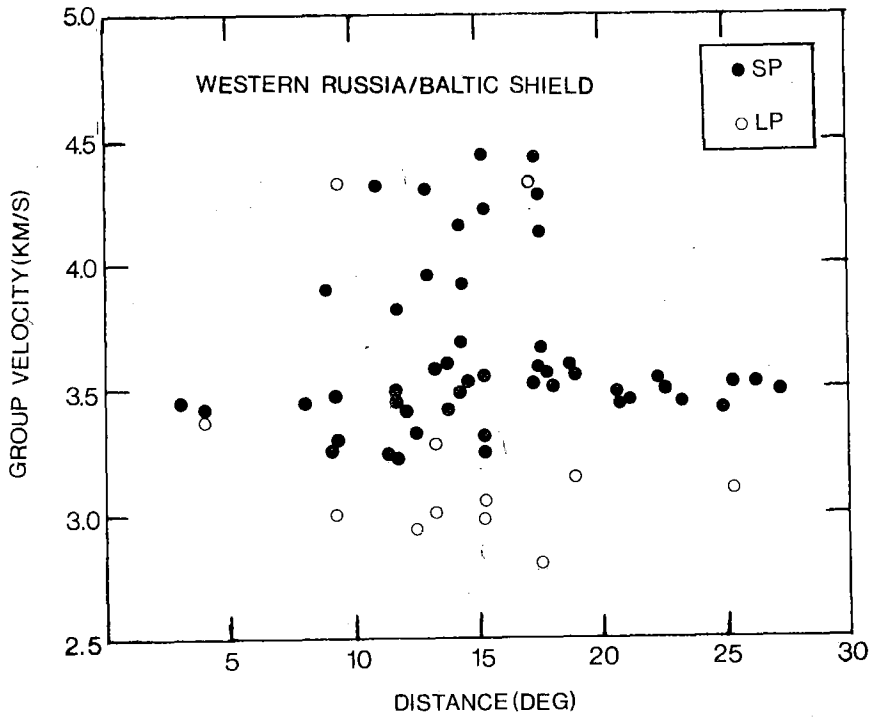

Fig. VI.7.2a Group velocity as a function of epicentral distance for the strongest phase within the group velocity window (2.7-5.0) km/s for each seismogram, as recorded by stations in Fennoscandia.

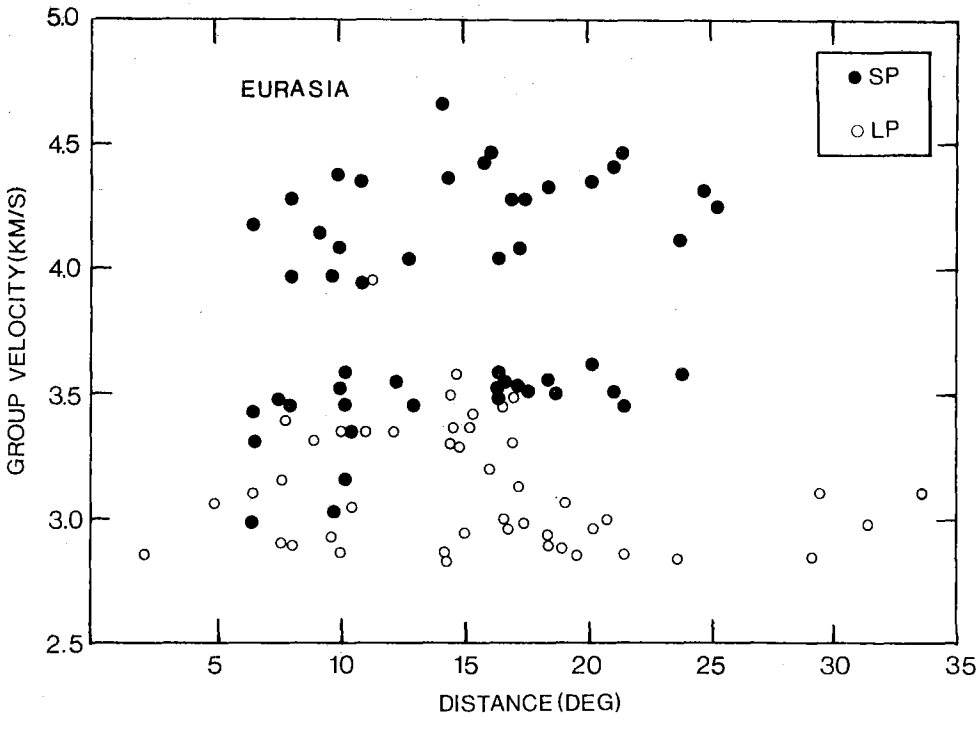

Fig. VI.7.2b Same as Fig. VI.7.2a for stations in Central Asia.

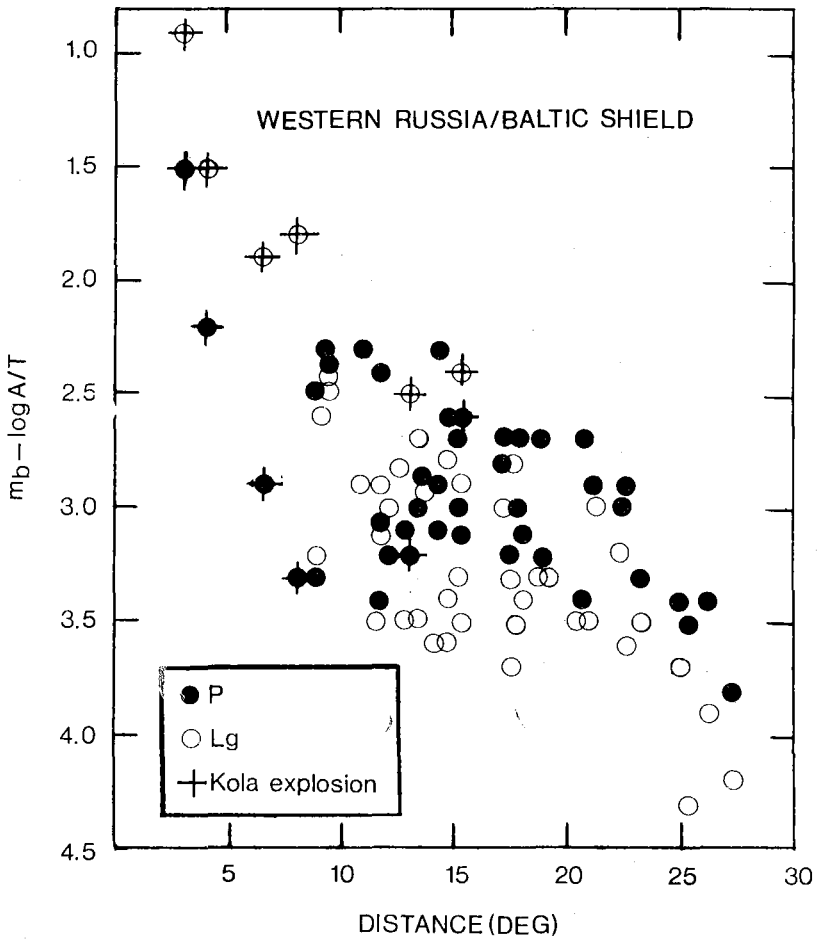

Fig. VI.7.3a Magnitude distance factor B(Δ) for P and Lg waves for Fenno-scandian stations.

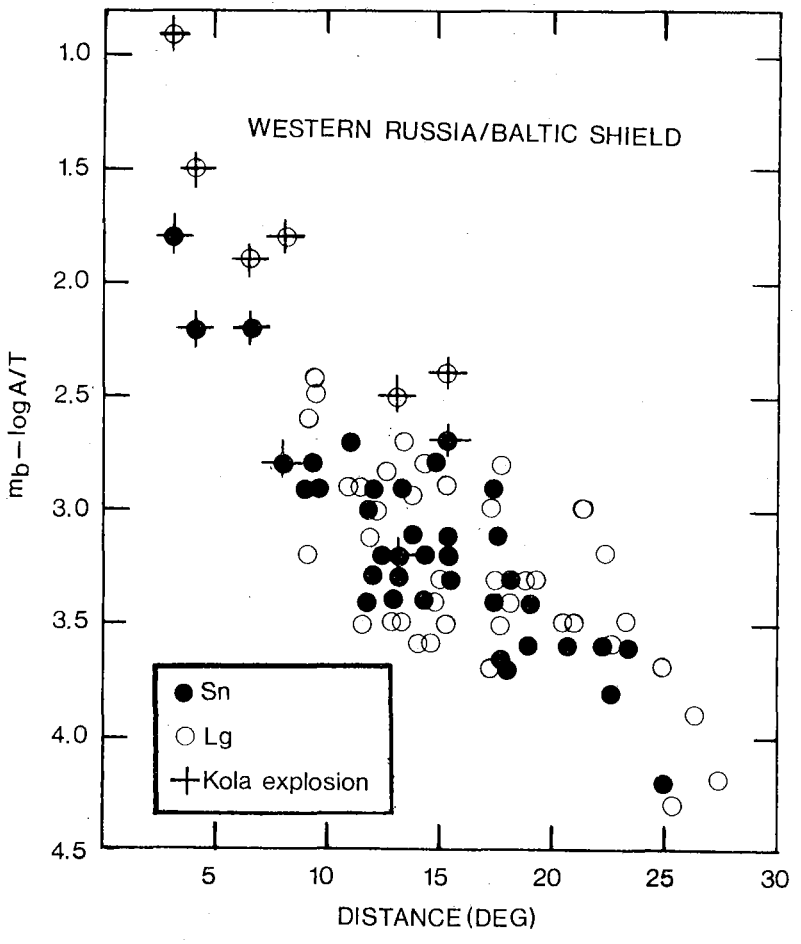

Fig. VI.7.3b Same as Fig. VI.7.3a for Lg and Sn waves.

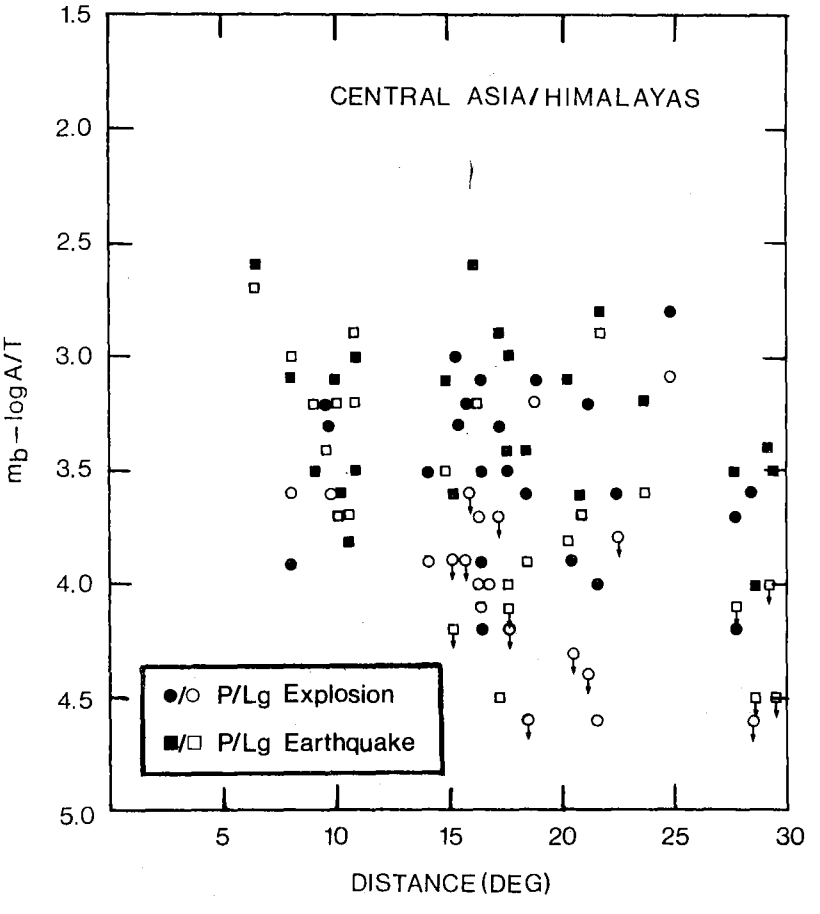

Fig. VI.7.4 Magnitude distance factor B(Δ) for P and Lg waves for stations in Central Asia.

VI.8 Three-Dimensional Seismic Velocity Image of the Upper Mantle beneath Southeastern Europe

P-wave travel time residuals for a network of stations in southeastern Europe were used in an inversion experiment to map upper mantle heterogeneities in the network region (Fig. VI.8.1). ISC data from the period 1964-1976 were used. To reduce the large data base, the minimum number of stations reporting an event was set to 50 and we also required that 30% of the network stations had detected the event. We also sorted the events in azimuth/delta intervals of 10^{o}x10^{o} to get as even distribution as possible of rays through the model. The average network time residual was subtracted from the station residuals and the resulting relative residuals are assumed to be caused by lateral variations in P velocity within a confined volume immediately beneath the receivers. The velocity structure is represented by a smooth cubic interpolation between slowness values on a three-dimensional grid of knots and the slowness/velocity perturbations at the individual knots are estimated by minimizing the quantity:

$$(\underline{\delta T}-\underline{A}\underline{m})*(\underline{\delta T}-\underline{A}\underline{m})+\theta^2\underline{m}*\underline{m}$$

where $\underline{\delta T}$ is observed travel time residuals, A is a travel path matrix, θ^2 a stochastic inverse smoothing parameter while the $\underline{m}$ vector contains the grid elements of the unknown slowness/velocity perturbations.

The network of stations covers a region from 37.0^{o} to 47.0^{o}N and from 17.5^{o} to 31.5^{o}E, a square of side approximately 1100 km. The anomalous zone has a thickness set to 600 km which includes the upper mantle, where the levels go from 0-100 km, 100-300 km, 300-500 km and 500-600 km, but the data will not discriminate too sharply between the different levels. Level 1, shown in Fig. VI.8.2, is representative of the upper 100 km and corresponds roughly to the lithosphere. The anomalies at this level correlate very well with observed heat flow. From the theoretical correlation between seismic velocity anomalies and heat flow ($\partial v_p/\partial T = 5.0 \cdot 10^{-4}$ km/s/k (Christensen, 1979)), we get about 1.2 per cent variation in P velocity for each 10 mW/m^2 change in heat flow for a 100 km thick layer. The heat flow range of 30 to 100 mW/m^2 matches the

velocity anomaly range of -5.4 to 3.4 per cent. An exception here is the velocity low of -3.6 per cent in the Ionian Sea which has a low heat flow. The velocity lows for S. Greece and SW Turkey are in agreement with high heat flow values in the same areas, and also with the extensional tectonics proposed by McKenzie for the Aegean Sea. Low velocity and high heat flow are also found in the southeastern part of the Pannonian basin, while high velocities and low heat flow are found over Bulgaria and the thermally cold Black Sea and also in southwest Yugoslavia.

The dramatic change in the anomaly picture from level 1 to level 2 agrees with the plate tectonic axiom of general decoupling between the lithosphere and the aesthenosphere. The high velocity zone north of Crete coincides with the earthquake zone which goes down to 150 km depth and clearly indicates the northern extension of a relatively cool, high velocity subducting slab (Gregersen, 1977). The high velocity extends far below southwest Greece but cannot be associated with present day subduction, although the hypothesis of a remnant slab prior to 15 m.y. ago cannot be ruled out. The low velocities beneath the northern Aegean Sea and Bulgaria are interpreted as supporting McKenzie's hypothesis of convective upwelling in the aesthenosphere as part of his extensional tectonic model for the Aegean Sea. The low velocities to the north indicate that the Pannonian basin is possibly deeply rooted in the aesthenosphere.

The levels 3 and 4 are not mapped here but the anomalies can be accounted for by variations in the depth to phase changes associated with the '400 km' discontinuity and possibly also the '650 km' discontinuity.

For further details see Hovland and Husebye (1981).

J. Hovland
E.S. Husebye

References

Cermak, V. & L. Ryback (eds.) (1979): Terrestrial Heat Flow in Europe, Springer Verlag, Berlin.

Christensen, N.I. (1979): Compressional wave velocities in rocks at high temperatures and pressures, critical thermal gradients and crustal low velocity zones, J. Geophys. Res., 84, 6849-6858.

Gregersen, S. (1977): P-wave travel time residuals caused by a dipping plate in the Aegean Arc in Greece, Tectonophysics, 37, 83-93.

Hovland, J. & E.S. Husebye (1981): Three-dimensional seismic velocity image of the upper mantle beneath southeastern Europe, in: Identification of Seismic Sources - Earthquakes or Underground Explosions, E.S. Husebye & S. Mykkeltveit (eds.), D. Reidel Publ. Co., in press.

McKenzie, D. (1978): Active tectonics of the Alpine-Himalayan belt: The Aegean Sea and surrounding regions, Geophys. J.R. astr. Soc., 55, 217-254.

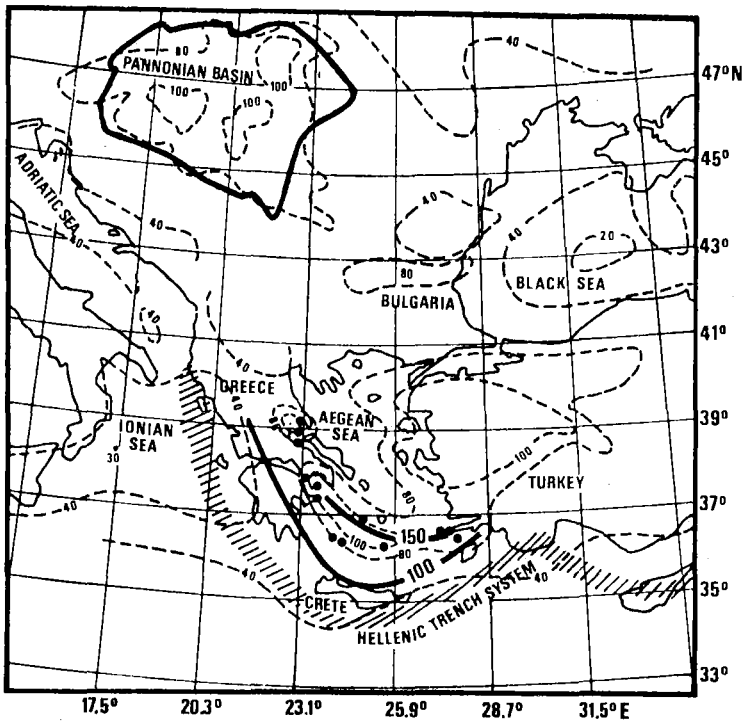

Fig. VI.8.1 Outstanding geophysical and seismological features of direct interest to this study. The heat flow data are taken from Cermak and Ryback (1979). The chain of dots north of Crete indicate volcanic activity, while the nearby two thin lines mark the 100 and 150 km iso-depth of intermediate earthquakes. To the north the intra-Carpathian basins are 'lumped' together under the notation Pannonian Basin.

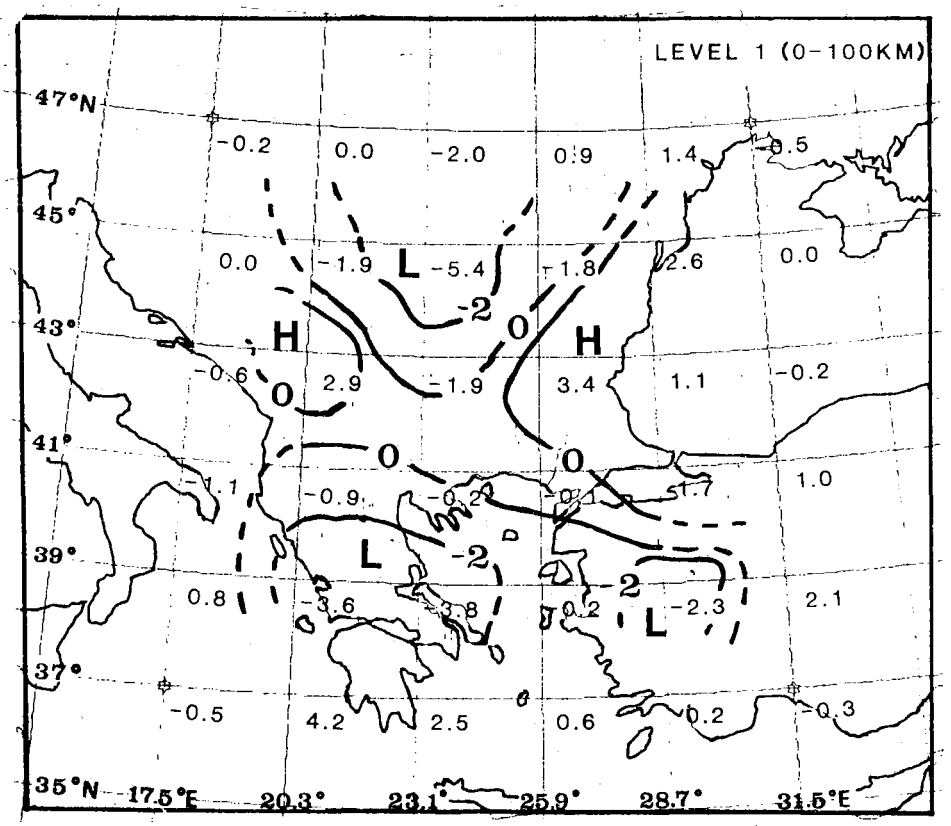

Fig. VI.8.2 Velocity perturbations (in per cent) for Level 1. Areas of high and low velocities are indicated by capital letters H and L. Resolution and standard errors for all knots are below 0.8 and 1.2, respectively.

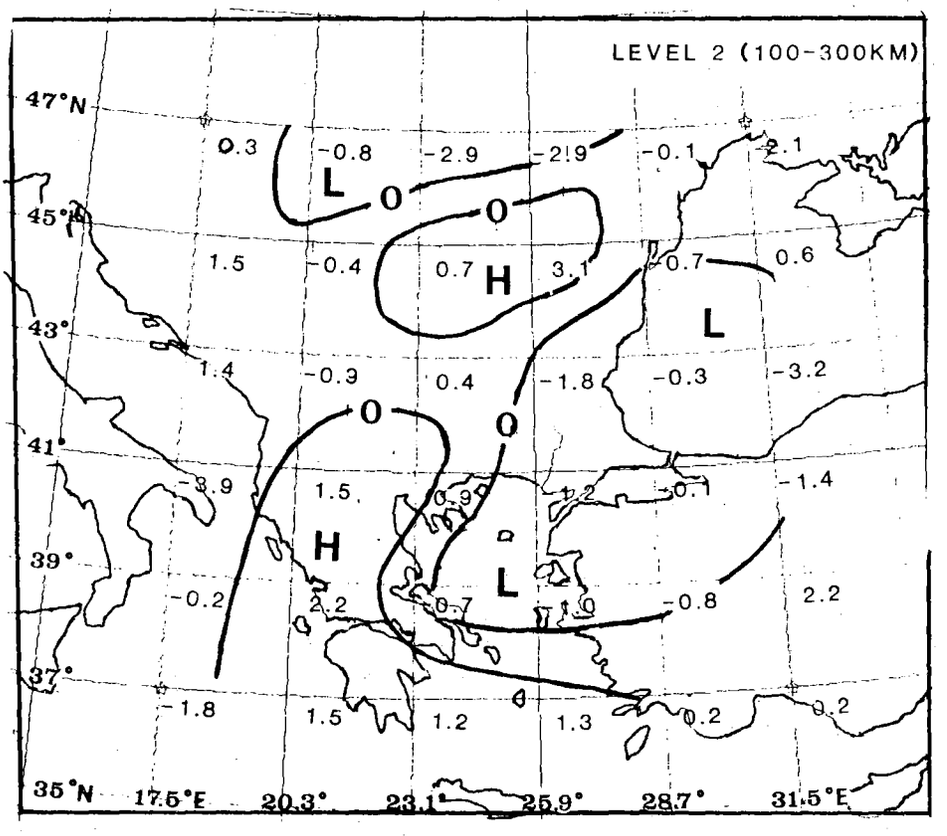

Fig. VI.8.3 Velocity perturbations (in per cent) for Level 2. Otherwise caption as for Fig. VI.8.2.

VI.9 Lithospheric Studies Based on the Principles of Holography

Concerning the possibility of using NORSAR short period data for wave field reconstruction procedures the main doubts were towards the gross undersampling of the wave field. Actually, the results obtained in the framework of random scattering and 'blocky' models (Berteussen et al, 1975; Aki et al, 1977) could not explain all the peculiarities of observed wave fields and therefore indicated a possibility of introducing the deterministic scattering model, assuming the pressence of 'strong' discrete inhomogeneities. To test NORSAR array 'holographic' feasibilities, an ultrasonic modelling experiment (Fig. VI.9.1) was undertaken so as to simulate the relative sampling of the array. Fig. VI.9.1a shows the 'transparent' medium in form of an epoxy box (v_p=2.6 km s^{-1}) and the embedded inhomogeneity in form of an aluminium cross (v_p=5.2 km s^{-1}). The size of the box is 80 • 50 • 50λ^3 (wavelengths), while the standard length and width of the individual arms in the cross are ~12λ and ~2λ respectively. The spacing between the source (diameter 12λ) and the cross is 30λ and the sensor grid area on the surface is 15λ • 15λ, Fig. VI.9.1b) gives the two sensor configurations used, namely, i) a rectangular grid with 2025 sensors with an interspacing of $\lambda/3$ and ii) a 132-sensor geometry similar to that of the NORSAR array. Fig. VI.9.1c is image reconstruction of the cross (outlined) at its correct depth location on the basis of the regular grid network with contributions from all 2025 sensors to each reconstructed point. Relative intensity scaling is used with contour levels at 1, 2, 4 & 8 dB. Fig. VI.9.1d shows the same as 1c except that contributions are restricted to those observational points being within a radius equal to the diameter of the first Fresnel zones. Notice that for 1c and 1d the relatively high intensities observed at the center of the cross stem from a non-plane source illumination. This was actually discovered when reconstructing data for a model without inhomogeneity. Fig. VI.9.1e is image reconstruction of the cross when the observational points were limited to a simulated NORSAR array configuration of 132 sensors which in turn were extrapolated to a grid of 25 • 25 sensors with an interspacing of 0.6λ. Also, as in the case of Fig. VI.9.1d, contributions to each reconstructed point were limited to a radius equal to the diameter of the first Fresnel zone. Fig. VI.9.1f displays relative intensity as a function of image reconstruction depth for both configurations of Fig. VI.9.1b. The strongest intensity is found at the proper depth location of

the cross and this coincides with a minimum distance from the center of the reconstruction axis. The intensity estimations for depth exceeding approx. 30λ reflects reconstructions of the source itself. The intensity maximum at the depth of the cross and the coinciding center axis minimum distance both imply that depth resolution should be comparable to or even better than that of 3-D time inversion. Thus, we find the results in Fig. VI.9.1 very encouraging, indicating that a satisfactory reconstruction of essential features of an embedded body seems feasible.

For testing the earth holography concept in practice, NORSAR P-wave recordings of 3 deep earthquakes at teleseismic distances (South of Honshu, Hindu Kush and Western Brazil) were subjected to analysis. The seismogram information extraction for the first 10 sec of P waves was tied to (spectral) amplitudes and phases of harmonic component at 1.8 Hz. Also, for image reconstruction purposes the earth's crust was given a thickness of 36 km and with an average P-velocity of 6.5 km/s, while the lithosphere was considered a half space with a P-velocity of 8.2 km/s. Composite results for all 3 events analyzed and for the depths 100 km, 148 km and 212 km, exhibiting the most pronounced scattering features are shown in Fig. VI.9.2. Different shading is used to identify the 3 events and their relative intensity scaling is also given. Numbers and following arrows indicate the angle of incident and azimuth for each event, correspondingly. The contours of the various shaded areas are 4 dB down from the individual event maxima which in turn are marked by black dots. In Fig. VI.9.2a we notice a good overlap between the intensity areas for the different events. This is taken to imply that heterogeneities at this depth are most uniformly seen by the 3 events. Fig. VI.9.2b which has weaker intensities as compared to Fig. VI.9.2a also exhibits less of an overlap between the respective event intensity areas. Similar comments apply to Fig. VI.9.2c. The consistency in location of the intensity areas I, II and III between figures a, b, and c are taken to imply a significant depth extent of the heterogeneous bodies in question. For areas IV, V, and VI, the anomalies are rather weak here and are seen most clearly by the Western Brazil event. For comparison the P-residual

inversion results in terms of relative velocity perturbations in per cent for their model A, depth interval 85-135 km, are displayed in Fig. VI.9.2b (Christoffersson and Husebye, 1979). The agreement between these two types of seismic results is considered good. For more detailed information we refer to the paper of Troitskiy et al (1981).

E.S. Husebye
P. Troitskiy, Inst. of Physics of the Earth, Moscow, USSR

References

Aki, K., A. Christoffersson and E.S. Husebye (1977): Determination of the three-dimensional seismic structure of the lithosphere, J. Geophys. Res., 82, 277-295.

Berteussen, K.-A., A. Christoffersson, E.S. Husebye and A. Dahle (1975): Wave scattering theory in analysis of P-wave anomalies observed at NORSAR and LASA, Geophys. J. R. astr. Soc., 42, 403-417.

Christoffersson, A. and E.S. Husebye (1979): On three-dimensional inversion of P wave time residuals: options for geological modeling, J. Geophys. Res., 84, 6168-6176.

Troitskiy, P., E.S. Husebye and A. Nikolaev (1981): Earth holography experiment - lithospheric studies based on the principles of holography. (Submitted to 'Nature').

Fig. VI.9.1

Ultrasonic experimental set-up and results. Figure a) shows the 'transparent' medium in form of an epoxy box (v_p=2.6 km s^{-1}) and the embedded inhomogeneity in form of an aluminium cross (v_p=5.2 km s^{-1}). The size of the box is 80 50 50 (wavelengths), while the standard length and width of the individual arms in the cross are ~ 12λ and ~ 2` respectively. The spacing between the source (diameter 12λ) and the cross is 30λ and the sensor grid area on the surface is 15λ • 15λ, Figure b) gives the two sensor configurations used, namely, i) a rectangular grid with 2025 sensors with an interspacing of λ/3 and ii) a 132-sensor geometry similar to that of the NORSAR array. Figure c) is image reconstruction of the cross (outlined) at its correct depth location on the basis of the regular grid network with contributions from all 2025 sensors to each reconstructed point. Relative intensity scaling is used with contour levels at 1, 2, 4 & 8 dB. Figure d) same as for c) except that contributions are restricted to those observational points being within a radius equal to the diameter of the first Fresnel zones. Notice that for c) and d) the relatively high intensities observed at the center of the cross stem from a non-plane source illumination. This was actually discovered when reconstructing data for a model without inhomogeneity. Figure e) is image reconstruction of the cross when the observational points were limited to a simulated NORSAR array configuration of 132 sensors which in turn were extrapolated grid of 25 • 25 sensors with an interspacing of 0.6λ. Also, as in case of Figure d) contributions to each reconstructed point were limited to a radius equal to the diameter of the first Fresnel zone. Figure f) displays relative intensity as a function of image reconstruction depth for both configuration of Figure b). The strongest intensity is found at the proper depth location of the cross and this coincides with a minimum distance from center of the reconstruction axis. The intensity estimations for depth exceeding approx. 30λ reflects reconstructions of the source itself. The intensity maximum at the depth of the cross and the coinciding center axis minimum distance both imply that depth resolution should be comparable to or even better than that of 3-D time inversion[4,5].

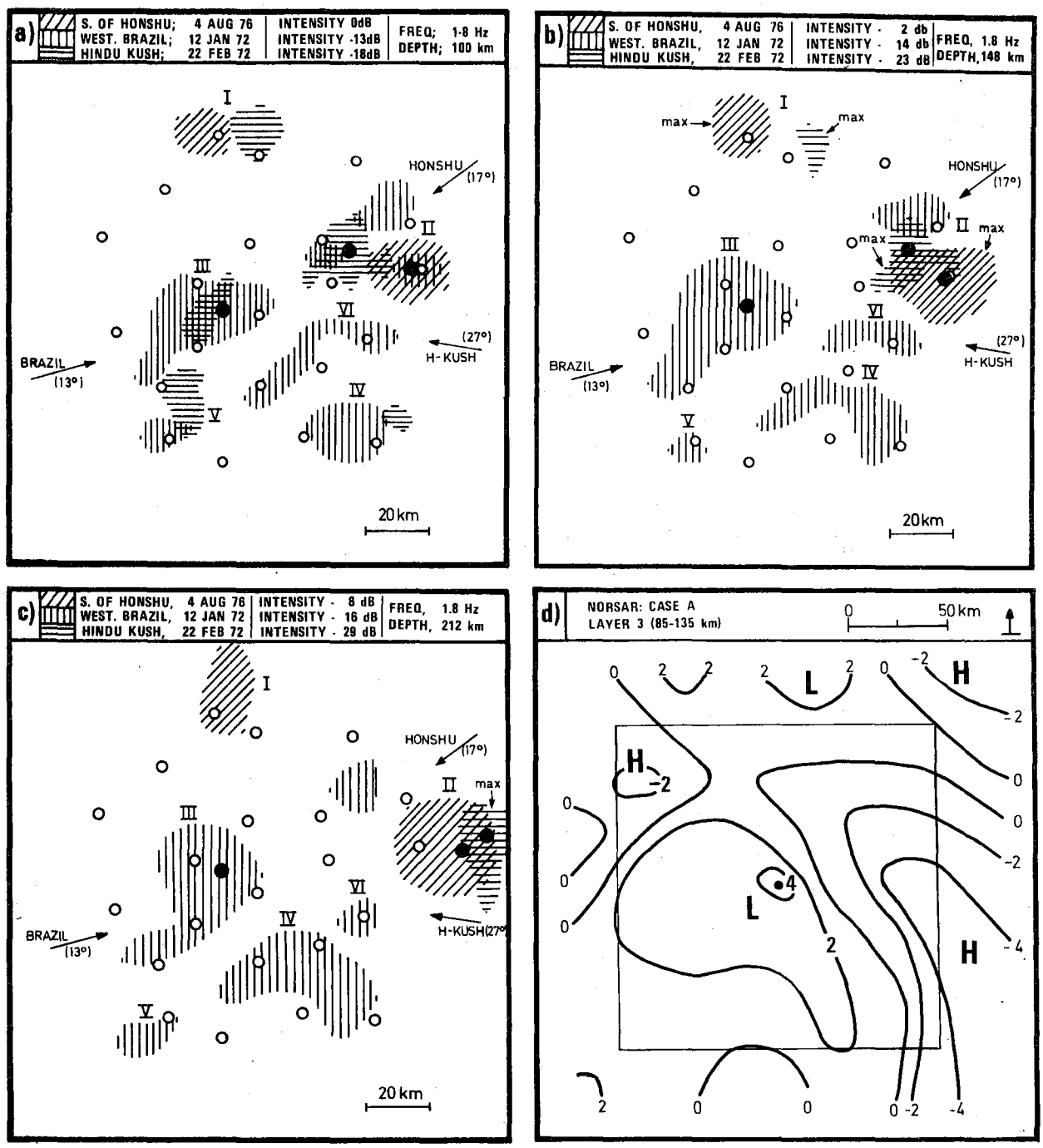
a)
S. OF HONSHU; 4 AUG 76
WEST. BRAZIL; 12 JAN 72
HINDU KUSH; 22 FEB 72
INTENSITY 0dB
INTENSITY -13dB
INTENSITY -18dB
FREQ; 1-8 Hz
DEPTH; 100 km
HONSHU (17°)
BRAZIL (13°)
(27°) H-KUSH
20 km
b)
S. OF HONSHU, 4 AUG 76
WEST. BRAZIL, 12 JAN 72
HINDU KUSH, 22 FEB 72
INTENSITY - 2 db
INTENSITY - 14 db
INTENSITY - 23 dB
FREQ, 1.8 Hz
DEPTH, 148 km
max
HONSHU (17°)
BRAZIL (13°)
(27°) H-KUSH
20km
c)
S. OF HONSHU, 4 AUG 76
WEST. BRAZIL, 12 JAN 72
HINDU KUSH, 22 FEB 72
INTENSITY - 8 dB
INTENSITY - 16 dB
INTENSITY - 29 dB
FREQ, 1.8 Hz
DEPTH, 212 km
HONSHU (17°)
BRAZIL (13°)
H-KUSH(27°)
20 km
d)
NORSAR: CASE A
LAYER 3 (85-135 km)
0 50km
L
H
-2
-4
2
0

Fig. VI.9.2

Fig. VI.9.2

Composite display of intensity maxima for the 3 depths 100, 148 and 212 km exhibiting the most pronounced scattering features. Different shading is used to identify the 3 events and their relative intensity scaling is also given. The contours of the various shaded areas are 4 dB down from the individual event maxima which in turn are marked by black dots. In figure a) we notice a good overlap between the intensity areas for the different events. This is taken to imply that heterogeneities at this depth are most uniformly seen by the 3 events. Figure b) which has weaker intensities as compared to figure a) also exhibits less of an overlap between the respective event intensity areas. Similar comments apply to figure c). The consistency in location of the intensity areas I, II and III between figures a), b) and c) are taken to imply a significant depth extent of the heterogeneous bodies in question. For comparison the P-residual inversion results[5] in terms of relative velocity pertubations in per cent for their model A, depth interval 85-135 km are displayed in figure b). The agreement between these two types of seismic results is considered good. Also notice that the time inversion results for the depth interval 185-235 km are essentially the same as those for the 85-135 km interval, implying decreasing resolution with increasing depth for this particular method.

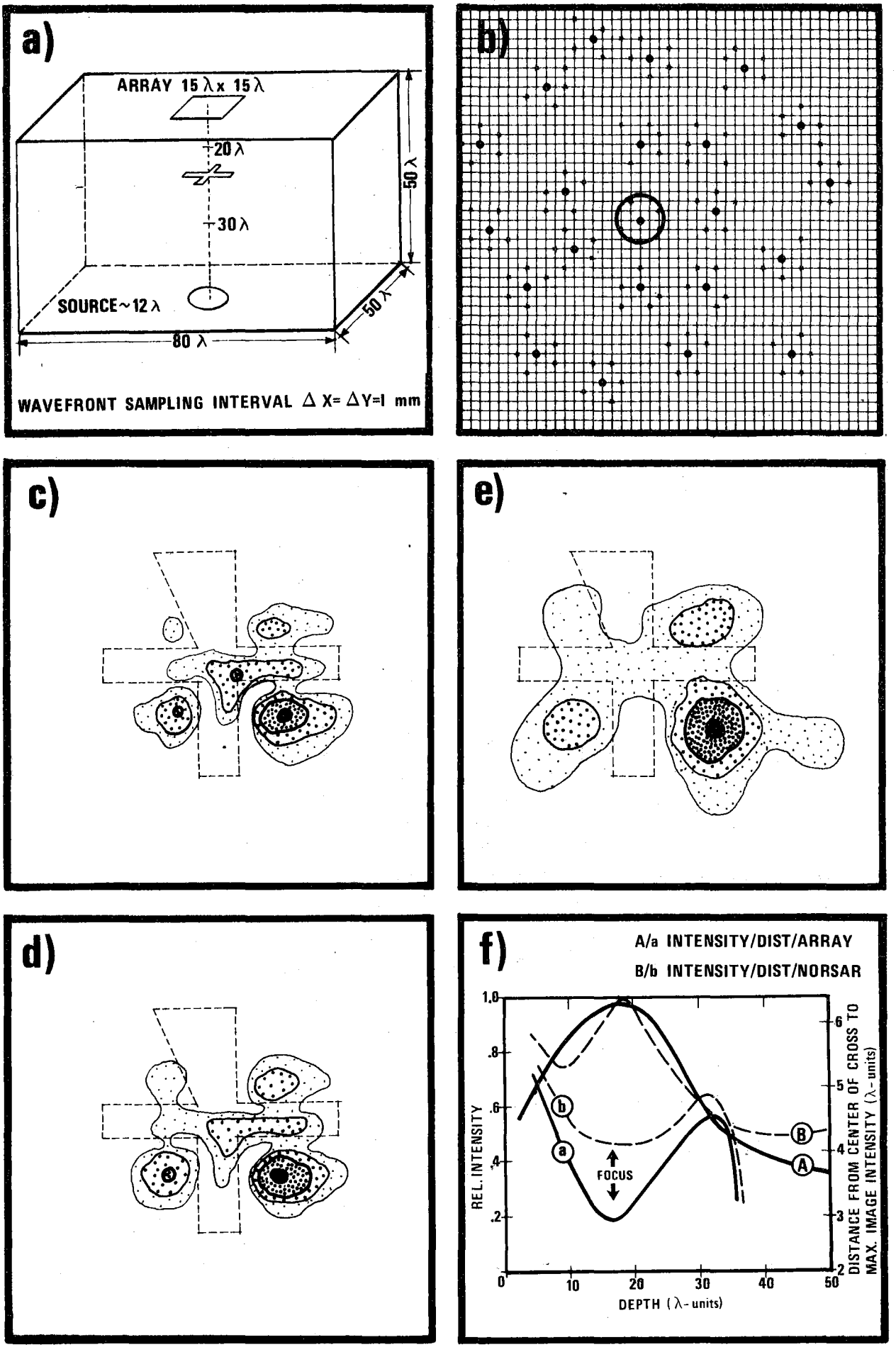
a)
ARRAY 15 λ x 15 λ
20 λ
30 λ
50 λ
SOURCE ~ 12 λ
50 λ
80 λ
WAVEFRONT SAMPLING INTERVAL Δ X = Δ Y = 1 mm
b)
c)
e)
d)
f)
A/a INTENSITY/DIST/ARRAY
B/b INTENSITY/DIST/NORSAR
REL. INTENSITY
1.0
.8
.6
.4
.2
0
10
20
30
40
50
DEPTH (λ-units)
FOCUS
a
b
A
B
DISTANCE FROM CENTER OF CROSS TO MAX. IMAGE INTENSITY (λ-units)
2
3
4
5
6

Fig. VI.9.1

VI.10 Proceedings from NATO Advanced Study Institute 'Identification of Seismic Sources - Earthquake or Underground Explosion'

A NATO Advanced Study Institute entitle 'Identification of Seismic Sources - Earthquake or Underground Explosion' was organized by NORSAR staff members and several American colleagues. The seminar took place at Voksenåsen, Oslo, Norway, 8-18 September 1980.

All key lecturers and a number of the other participants that presented talks during the seminar have now submitted their manuscripts for publication in the proceedings. A total of 45 contributions, amounting to 823 pages, has now been sent to the publisher, D. Reidel Publishing Company, and we have been informed that the proceedings will appear in September this year.

The preface as well as the list of contents for the proceedings, as submitted to the publisher, are given in the following:

"PREFACE

The subject of this NATO Advanced Study Institute was seismic monitoring under a nuclear test ban - an application of scientific knowledge and modern technology for a political purpose. The international political objective of a comprehensive nuclear test ban provided in turn the motivation for our technical and scientific discussions. In order to obtain a historical perspective on the progress of the work towards a comprehensive test-ban treaty (CTB), it is necessary to go back to 1958, when a conference of scientific experts in Geneva made the first steps toward an international seismic monitoring system. However, agreement on actual capabilities of a monitoring system for verifying compliance with such a treaty was not achieved, and thus the conference did not lead to immediate political results.

After the Partial Test Ban Treaty of 1963, which banned nuclear explosions in the atmosphere, outer space and under the seas, renewed interest in the seismological verification of a CTB took place. A number of countries initiated large-scale research efforts toward detecting and identifying underground nuclear explosions, and it was in this context that the large-aperture seismic arrays NORSAR and LASA were established. This

type of development resulted in excellent seismic data in digital form and was thus of great importance to the seismological community. These efforts have signficantly improved the technical possibilities of verifying a potential nuclear test-ban treaty, although the most efficient source discriminants still reflect observational experience and to a lesser extent a true in-depth physical understanding of the various seismic signal-generating processes.

The main theme of these proceedings is the identification of seismic sources. In this context we consider different aspects of technical methods that can be used to answer on a routine basis the question: Was a recorded seismic event an earthquake or an underground nuclear explosion?

Now, to answer this question confidently and correctly, we must have a proper understanding of the physical processes associated with both earthquakes and explosions. Therefore, an extensive review is given of the present state of the art with respect to these phenomena with due regard to the compiling of observational data and to the theoretical developments - the hallmarks of the seismological science.

The ultimate experience for any seismologist would be to have a direct, unobstructed view of the earthquake or explosion process, so the digital/analog seismometer recordings available represent a relatively poor substitute, though the only one available. Also, complexities of the earth strongly affect the seismic signal, thus presenting us with a blurred and distorted observational image of the source. To improve this image we have to remove complicating wave-propagation and recording effects, and consequently these topics are subject to extensive presentations in the proceedings. In particular, recent approaches to wave propagation modeling and also the use of observational data in constructing structural images of the earth's interior are reviewed.

These proceedings also comprise extensive contributions on the present state of the art of signal processing, seismic source identification, seismometer developments and finally seismological data center operations. These items are partly considered in the context of seismic monitoring of a possible nuclear test ban. The recent trends in this area of seismology are indeed fascinating, with the traditional, faithful seismogram anlayst being replaced by specialists screening waveform data from a network of seismograph stations, and with a battery of computers to perform any conceivable kind of seismogram analysis. The hugh data bases likely to be collected at the seismological centers of the future would undoubtedly be an excellent research tool for dedicated seismologists.

The planning of a conference such as this one calls for a considerable amount of effort, both technical and administrative, from a number of people. We would like to express our sincere thanks to all who have assisted in making this conference possible. Particular thanks go to K. Frydenlund, Foreign Minister of Norway and G.V. Bulin, DARPA, USA, who gave the opening addresses of the Institute. Also, we are most indebted to our fellow scientific directors H.C. Rodean and W. Best and organizing committee members L.B. Tronrud, G. Young and M. Shore without whose interest, work efforts and advice these conference proceedings would not have been possible."

E.S. Husebye
S. Mykkeltveit

CONTENTS

* Key Lecturer

THE EFFECT OF GREEN'S FUNCTIONS ON THE DETERMINATION OF SOURCE MECHANISMS BY THE LINEAR INVERSION OF SEISMOGRAMS
B.W. Stump and L.R. Johnson

SIMPLIFIED BODYWAVE SOURCE TERMS WITH ONE APPLICATION IN MOMENT TENSOR RECOVERY
S.N. Ward

THE INTERPRETATION OF MOMENT TENSOR INVERSIONS
R.A. Strelitz

SEISMIC WAVEFIELD SYNTHESIS

COUPLING NEAR SOURCE PHENOMENA INTO SURFACE WAVE GENERATION
D.G. Harkrider*

ON SEISMIC SYNTHESIS
B.L.N. Kennett*

SOME RECENT EXTENSIONS OF THE REFLECTIVITY METHOD
G. Müller* and W. Schott

ISOCHRONAL FORMULATION OF SEISMIC DIFFRACTION
P.W. Buchen and R.A.W. Haddon

HIGH FREQUENCY TOROIDAL MODES
T.J. Clarke

ELASTIC AND ELECTROMAGNETIC WAVE PROPAGATION IN HORIZONTALLY LAYERED MEDIA
B. Ursin

CALCULATION OF WAVE FIELDS IN MANTLE VELOCITY MODELS
M.R. Illingworth and B.L.N. Kennett

THE EFFECT OF FOCAL DEPTH AND SOURCE TYPE ON SYNTHETIC SEISMOGRAMS
K.K. Nakanishi

SEISMIC WAVE ANALYSIS

SURFACE WAVE PROPAGATION ACROSS DIFFERENT TECTONIC REGIONS
M. Cara*

Lg WAVE PROPAGATION IN EURASIA
S. Mykkeltveit and E.S. Husebye

SEISMOGRAMS OF EXPLOSIONS AT REGIONAL DISTANCES IN THE WESTERN UNITED STATES: OBSERVATIONS AND REFLECTIVITY METHOD MODELING
K.H. Olsen and L.W. Braile

PHASE IDENTIFICATION AND EVENT LOCATION AT REGIONAL DISTANCE USING SMALL-APERTURE ARRAY DATA
S. Mykkeltveit and F. Ringdal

P AND S-VELOCITY JUMP AT THE INNER-CORE BOUNDARY FROM PKP AMPLITUDES
H. Häge

CONVERSION PHASES FROM MANTLE TRANSITION ZONES
S. Faber

THE EXCITATION AND ATTENUATION OF SEISMIC CRUSTAL PHASES IN TURKEY
B. Maddison, A. Necioglu and N. Turkelli

COMPARISON OF WAVEFORM INVERSION SCHEMES FOR HORIZONTALLY STRATIFIED MEDIA
K.-A. Berteussen and B. Ursin

SCATTERING AND EARTH HETEROGENEITIES

ATTENUATION AND SCATTERING OF SHORT-PERIOD SEISMIC WAVES IN THE LITHOSPHERE
K. Aki*

SOURCE LOCATION IN LATERALLY VARYING MEDIA
D. Gubbins*

OPTIMUM APPROACHES TO MAGNITUDE MEASUREMENTS
A. Christoffersson* and F. Ringdal

THREE-DIMENSIONAL SEISMIC VELOCITY IMAGE OF THE UPPER MANTLE BENEATH SOUTHEASTERN EUROPE
J. Hovland and E.S. Husebye

TAU INVERSION OF UPPER MANTLE ARRAY DATA WITH APPLICATION TO THE PROBLEM OF THE SCATTERING OF SEISMIC WAVES IN THE LITHOSPHERE
R.F. Mereu

OBSERVATION OF SCATTERING IN THE LITHOSPHERE
A.M. Dainty

LATERAL VARIATIONS IN THE EARTH'S CRUST AND THEIR EFFECT ON SEISMIC WAVE PROPAGATION
R.F. Mereu and S. Ojo

SIGNAL ANALYSIS

FUNDAMENTALS OF MULTIDIMENSIONAL TIME SERIES ANALYSIS
M.P. Ekstrom and T.L. Marzetta*

THE INSTANTANEOUS AMPLITUDE, PHASE AND FREQUENCY IN SEISMIC EVENT DETECTION, TIMING AND IDENTIFICATION
R. Unger

SEISMIC SOURCE DISCRIMINATION

MULTIDIMENSIONAL DISCRIMINATION TECHNIQUES - THEORY AND APPLICATION
D. Tjøstheim*

SEISMIC DISCRIMINATION PROBLEMS AT REGIONAL DISTANCES
R.R. Blandford*

LINEAR DISCRIMINATION FOR SAMPLES OF LIMITED SIZE
V.F. Pisarenko, A.F. Kushnir, F.M. Pruchinka and S.L. Zvang

DEVELOPMENTS IN SEISMIC INSTRUMENTATION

THE GLOBAL DIGITAL SEISMOGRAPH NETWORK: A STATUS REPORT
J. Peterson*

BROAD-BAND SEISMOMETRY - A UNIFIED APPROACH TOWARDS A KINEMATIC AND DYNAMIC INTERPRETATION OF SEISMOGRAMS
H.-P. Harjes*

SEISMIC DATA CENTERS